

6.03 Plate Rheology and Mechanics

EB Burov, Université Pierre et Marie Curie, Paris, France; Centre National de la Recherche Scientifique, Paris, France

© 2015 Elsevier B.V. All rights reserved.

6.03.1	Introduction: Plate Rheology and Mechanics	95
6.03.2	Rock Mechanics Data and Conventional Rheology Models	99
6.03.2.1	Elastic Properties	100
6.03.2.2	Brittle or Plastic Properties	101
6.03.2.3	Ductile (Viscous) Properties	103
6.03.2.3.1	Diffusion and dislocation creep	103
6.03.2.3.2	Pressure solution, cataclastic flow, Peierls plasticity, GBS flow, and other mechanisms	103
6.03.2.4	Yield Stress Envelopes	105
6.03.3	Constitutive Models	106
6.03.3.1	Maxwell Model	106
6.03.3.2	Kelvin Model	109
6.03.3.3	Mixed Models	109
6.03.4	Uncertainties in the Experimental Rheology Laws	109
6.03.4.1	Uncertainties of Rock Mechanics Data	109
6.03.4.2	Uncertainties in the Synthetic Yield Stress Envelopes	110
6.03.4.3	Uncertainties in Deformation Mechanisms in Nature	110
6.03.4.4	Role of Secondary Factors: Frictional Heating, Pressure, Fluid Content, Partial Melting, and Metamorphic Phase Changes	111
6.03.4.5	Possible Ways to Parameterize Rheology Data for Geologic Timescales	114
6.03.5	Rheology and Structure of the Oceanic Lithosphere	115
6.03.5.1	Goetze and Evans Yield Stress Envelopes: Age Dependence of the Integrated Strength	115
6.03.5.2	Rheology and Observations of Flexure (T_e Data)	116
6.03.5.3	Flexural Strength and Initiation of Oceanic Subduction	117
6.03.5.4	Intraplate Seismicity (T_s), T_e , and Brittle–Ductile Interactions	117
6.03.5.5	Intraplate Seismicity and Ductile Creep	121
6.03.5.6	Constraints on the Long-Term Viscosity from Subsidence Data	122
6.03.5.7	Large-Scale Lithospheric Folding	122
6.03.6	Rheology and Structure of the Continental Lithosphere and Continental Margins	122
6.03.6.1	Common Goetze and Evans Yield Stress Envelopes	122
6.03.6.2	Age Dependence and Other Dependences of the Integrated Strength of the Lithosphere	123
6.03.6.3	Seismicity, T_s , BDT, and Long-Term Strength	130
6.03.6.4	Physical Considerations Beyond the Observations of Flexure, Gravity Potential Theory, Intraplate Stresses	133
6.03.6.5	Gravitational Stability Analysis: Rayleigh–Taylor Instabilities or Survival of Cratons, Continental Margins, and Mountain Roots	133
6.03.6.6	Dynamic Stability Analysis Using Direct Numerical Thermomechanical Models	138
6.03.6.7	Resistance to Stable Deformation Under Compressional Tectonic Forces ('Simple Shear' Subduction versus 'Pure Shear' Collision)	138
6.03.6.8	Response to Large-Scale Compressional Instabilities (Folding)	141
6.03.6.9	Response to Extensional Tectonic Loading (Rifting)	143
6.03.7	Relations Between Short-Term and Long-Term Properties	143
6.03.7.1	Seismicity and Long-Term Deformation	143
6.03.7.2	Postseismic Relaxation Data and Long-Term Deformation	145
6.03.7.3	Field Observations and Geophysical Data	146
6.03.8	Conclusions and Future Perspectives	146
Appendix A	Flexure of Continental Lithosphere with Multilayered Nonlinear Rheology	147
Appendix B	Thermal Model of the Lithosphere	148
Acknowledgments		148
References		148

6.03.1 Introduction: Plate Rheology and Mechanics

The rheology and strength of the Earth's lithosphere has been a topic of debate since the beginning of the twentieth century when Joseph Barrell introduced the concept of a strong lithosphere overlying a fluid asthenosphere (Barrell, 1914), after the formulation of the continental drift theory by Wegener and first interpretations of regional isostasy by J. Barrell and Vening-Meinesz (Barrell, 1914; Watts, 2001; Watts, this volume). This concept constitutes an integral part of plate tectonics (e.g., Le Pichon et al., 1973; Turcotte and Schubert, 2002; Watts, 2001) and the question of how the strength of the plates varies spatially and temporally is fundamental to geology and geodynamics (e.g., Burov, 2007, 2010; Burov and Watts, 2006; Cochran, 1980; Jackson, 2002). As suggested on the basis of recent mantle–lithosphere interaction models (e.g., Schmeling et al., 2008), the elastic and plastic properties of the lithosphere essentially determine the geometry of lithospheric plates and the mechanisms of formation of constructive, destructive, and transform plate boundaries at a global scale. At smaller scales, the mechanical properties of the lithosphere condition formation and evolution of major geologic structures such as spreading centers, transform/strike-slip faults, rift and foreland basins, passive margins, mountain ranges, or plateaus. They also control short-term processes such as seismicity (Watts and Burov, 2003).

The fact that the lithosphere has finite measurable strength has been first demonstrated from observations and models of regional isostatic compensation of considerable topographic loads such as oceanic islands or continental mountain belts. Before that, the lithosphere was considered as either a very strong solid layer (Pratt's model) or, in turn, a weak fractured layer (Airy's model). Postglacial rebound studies of the early twentieth century have contributed to the definition of the 'mechanical lithosphere' as the uppermost layer of the solid Earth characterized by slow viscoelastic relaxation, in contrast to the underlying, relatively low-viscosity asthenosphere. The long-term mechanical base of the lithosphere, h_m , is limited by the depth to the 500–600 °C isotherm in oceans and the 700–800 °C isotherm in continents, while the base of the thermal lithosphere is almost twice as deep at the 1330 °C isotherm.

The strength of lithospheric plates depends on their structure and rheological properties exhibited in the particular geodynamic context. For a rock of given mineralogical composition and microstructure, the most important controlling parameters are pressure, temperature, strain, strain rate, strain history, fluid content and pore fluid pressure, grain size, fugacities of volatiles, and chemical activities of mineral components (Evans and Kohlstedt, 1995; Keefner et al., 2011).

Goetze and Evans (1979) were the first to combine the data of experimental rock mechanics and extrapolate them to geologic timescales and spatial scales. They introduced the yield strength envelope (YSE) for the oceanic lithosphere, that is, a vertical profile that predicts the maximum differential stress supported by rock as a function of depth. In YSE rheology models, the depth dependence of rock strength integrates multiple factors such as the increase of both brittle and ductile strength with pressure and the decrease of ductile strength with depth-increasing temperature, lithologic structure, and fluid content. YSEs are used both to validate rock mechanics data and to explain the mechanical behavior of lithospheric

plates. The YSE concept has been proven to work fairly well for oceans where it explains the observed age and temperature dependence of plate responses to surface and subsurface loads. Yet, the same concept faces a number of difficulties in continents and at continental margins (Afonso and Ranalli, 2004; Burov, 2010, 2011; Burov and Diament, 1995; Burov and Watts, 2006; Handy and Brun, 2004; Jackson, 2002). However, a complete understanding of oceanic lithosphere dynamics requires a thorough account for thermomechanical response of its continental boundaries, as well as a study of continental dynamics itself.

One of the major experimental rheology laws used for construction of YSEs is Byerlee's law of brittle failure (Byerlee, 1978). Byerlee's law demonstrates that brittle rock strength is above all a function of pressure–depth and is almost independent of rock type (Figure 1). Byerlee's law shows that most common rocks exhibit a similar relationship between yield stress and normal stress and that this relationship resembles Mohr–Coulomb plasticity. That is, it refers to the classical Amonton's law of friction (e.g., Nadai, 1963). Byerlee's law has been confirmed by multiple studies, which show that most rocks have similar angles of internal friction (30–33°) and similar (small) dilatation angles (~10°). This explains why even highly stratified volumes of brittle rocks often behave as a mechanically uniform media: tectonic faults can propagate large distances at depth or horizontally, ignoring lithologic stratification and inherited structures. The fault dip or the angle between conjugate faults is a function of the internal friction angle; it is thus possible to constrain the properties of brittle rocks from direct observations of fault/fracture geometries. These properties do not depend on timescale. Hence, brittle failure parameters derived from laboratory experiments can be applied on geologic spatial and temporal scales. Of course, rheologically anomalous inclusions, variations in porous pressure, or stress concentrations can change fault geometries (e.g., Huismans et al., 2005; Lavier et al., 2000; Le Pourhiet et al., 2004; Melosh, 1990; Tirel et al., 2004). In particular, the formation of low-angle faults observed in a number of geologic contexts presents one of specific problem (e.g., Buck, 2007; Huet et al., 2011; Melosh, 1990; Cloetingh et al., this volume; Buck, this volume). Yet, in most cases, observations of 'abnormal' fault dips can be explained within Byerlee's law. For example, common interpretations of low-angle faulting compatible with Byerlee's law refer to local rotation of principal stress axis due to shear flow in the ductile crust (e.g., Melosh, 1990) or due to flexural rotation of originally steep faults (e.g., Buck, 1988). Other explanations refer to various special mechanisms of friction or cohesion softening applied to Byerlee's law (e.g., Huismans et al., 2005).

In contrast with brittle properties, ductile rock strength strongly depends on rock type and a large number of specific conditions such as grain size, macro- and microstructure, temperature, strain rate, fluid content, and many other factors. In particular, ductile behavior depends nonlinearly on strain rate and thus on the timescale of the deformation process. Laboratory experiments are conducted on human timescale (5–10 years). Their results are then extrapolated to geologic timescales (>10⁶ years). From a mathematical point of view, such huge extrapolation cannot be justified, specifically because of the non-linear character of ductile deformation. From a physical point of view, one also cannot be certain that the same mechanisms of ductile deformation act at both slow and high strain rates or at

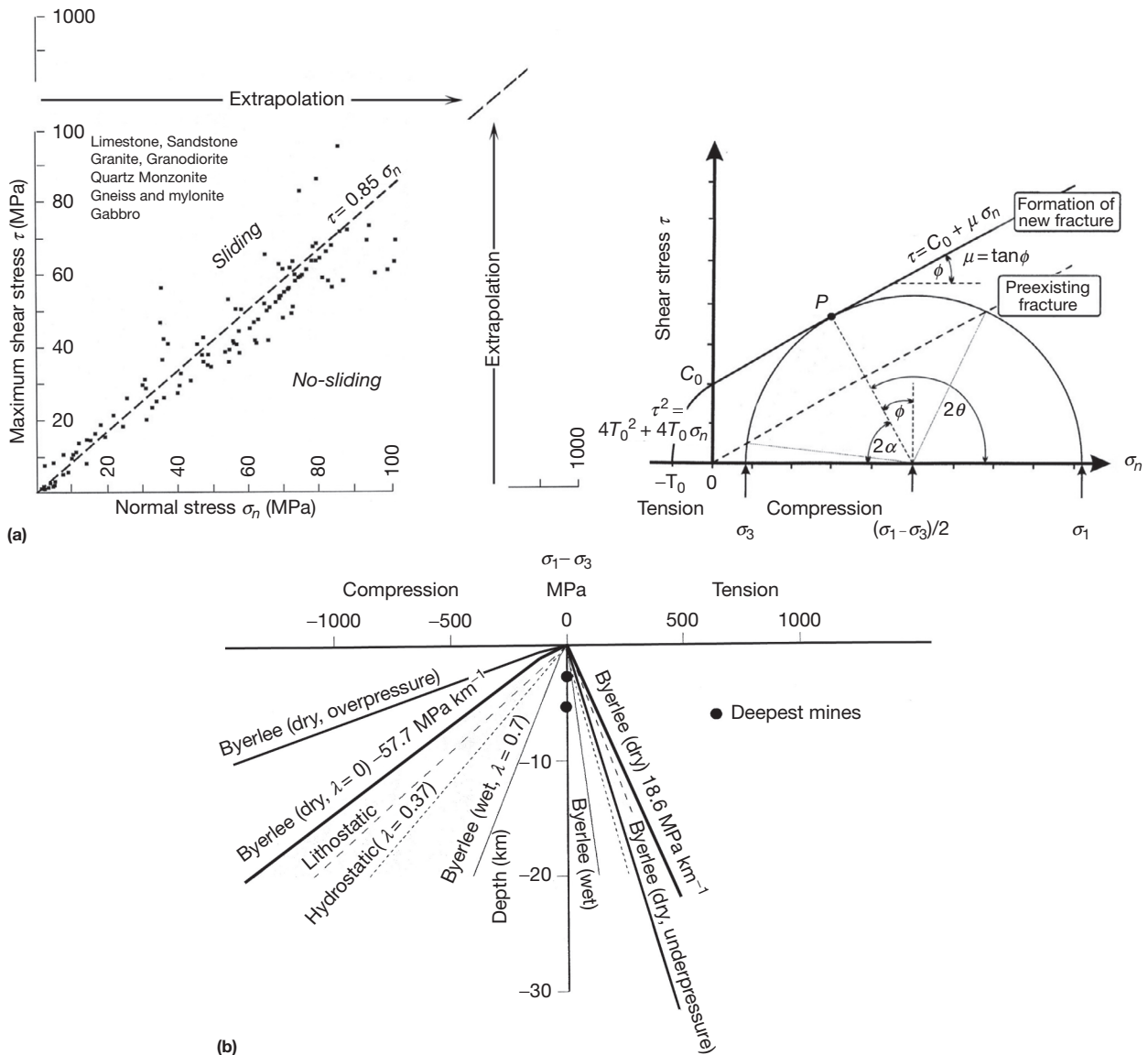


Figure 1 (a) (right) Experimentally established linear dependence between normal stress and shear stress for compressional failure of various rocks (modified from Byerlee JD (1978) Friction of rocks. *Pure and Applied Geophysics* 116: 615–626). These data demonstrate the applicability of Coulomb–Navier failure criterion $\tau = C_0 + \mu \sigma_n$ and relative independence of Byerlee's law on rock type. This law has been validated only for the first several kilometers of the upper crust (pressures of few MPa). However, it is commonly extrapolated to more important depth/pressure conditions (up to 40–50 km depth or 1–1.5 GPa), where other stress-limiting mechanisms such as Peierls law are likely to operate. (left) Two principal failure criteria (Coulomb–Navier and Griffith). Under general compression (here, $\sigma_n > 0$), Coulomb criterion predicts linear relation between normal stress σ_n and shear stress τ . Under general extension (here, $\sigma_n < 0$), parabolic Griffith criterion applies. C_0 is cohesion, T_0 is tension cutoff, μ is friction coefficient, β is friction angle, and σ_1 and σ_3 are principal stresses. 2α is angle between two conjugated faults forming under stress σ_1 , and $\phi = \pi/2 - 2\alpha$ is friction angle ($\mu = \tan \phi$). For most dry rocks, $\phi = 30^\circ$ (modified from Price NJ and Cosgrove JW (1990) *Analysis of Geological Structures*. Cambridge: Cambridge University Press). It can be seen that Byerlee's law corresponds to Mohr–Coulomb plasticity with preexisting fractures. (b) Dependence of brittle strength on depth/pressure: lithostatic pressure (if not stated otherwise), fluid pressure, and tectonically induced over- or underpressure. Note that rocks are weaker under extension than under compression, which explains frequent deep seismicity in overall weak rift zones. Tectonic extension or compression may change total pressure and, consequently, brittle strength, by a factor of, respectively, 0.5–2. Combined from Watts (2001) and Petrini and Podladchikov (2000). λ is pore pressure factor.

both low and high temperatures (exaggerated temperatures are commonly used in experiments to accelerate deformation and to avoid brittle failure). Solid-state theory successfully reproduces some creep mechanisms such as diffusion creep or pressure solution (e.g., Poirier, 1985). However, this is not the case for

major creep mechanisms such as dislocation creep (e.g., Hull and Bacon, 1984). Most of the Arrhenius-type constitutive laws proposed for ductile rocks are approximations of experimental data and are not physically formulated dependencies (e.g., Brace and Kohlstedt, 1980; Rutter and Brodie, 1991). The YSEs derived

for oceanic and continental lithosphere under the assumption of dry olivine rheology predict important strength in the mantle part, down to 50–60 km depth in oceans and to 100–120 km depth in cratons. However, some studies (e.g., Jackson, 2002) suggest that lithosphere mantle is mechanically weak below 40 km depth, or, more exactly, below the 500 °C isotherm. According to this hypothesis, the cratons are thin and hot (equilibrium thermal thickness $a=z(1330^\circ)\sim 100$ km) and the continental plate strength is concentrated in the crust. These propositions arrive from conflicting interpretations of rock mechanics and intraplate seismicity data. Plate seismicity is detected mainly above 40 km depth (Jackson, 2002) in both continents and oceans. Jackson (2002) found that all continental microseismicity originates in the crust. Yet, reassessment of same data sets by Monsalve et al. (2006) shows earthquake locations as deep as 100 km, that is, well below the Moho depth. Nevertheless, most microseismic events do indeed occur above 40 km depth. In continents, the depth interval 0–40 km corresponds to diversely composed granite–diorite–feldspar–diabase–granulite crust, but in the oceans, it comprises 30 km of olivine-based uppermost mantle lithosphere and 7–10 km of basaltic crust. Hence, it can be logically concluded that in the 0–40 km depth interval, the maximum earthquake depth cannot be strongly related to rock type. The only rheological property that is largely rock type-independent is brittle strength (Byerlee, 1978), which is a linear function of pressure for all magmatic rocks. In contrast, ductile strength is strongly dependent on rock type and temperature and is expected to vary considerably at 40 km depth or 500 °C isotherm in different plates. Consequently, it is reasonable to assume that maximum earthquake depth is linked to depth-dependent brittle strength and should be conditioned by intraplate stress levels. Indeed, brittle strength is expected to be similar at the same depth in both oceans and continents. For this reason, a large number of studies (e.g., Handy and Brun, 2004; Watts and Burov, 2003) do not find any significant correlation between seismic depth and the long-term ductile strength of the lithosphere. It is pointed out that if a direct link between the two properties could exist, it would have to be an anticorrelation. According to this point of view, depth-dependent confining pressure precludes brittle failure explaining the scarcity of deep earthquakes. Hence, it is suggested that seismic deformation is a sign of mechanical weakness of shallow levels of the lithosphere. In addition, in continents, mechanical crust–mantle decoupling results in a stress drop at the Moho boundary making mantle earthquakes even less possible. The other part of this reasoning refers to the fact that seismicity is characteristic of short timescale behavior, which is physically unrelated to long-term rheology because at this short timescale, viscous–elastic–plastic lithosphere is expected to deform only in brittle–elastic mode.

Consequently, there may be no direct correlation between seismic behavior and long-term ductile behavior. Indeed, the observations of plate flexure below orogens (Watts, 2001) suggest that many continental plates have strong elastic cores (T_e), which are 2–2.5 times thicker than the seismogenic layer thickness, T_s . However, a number of points still need to be explained. In particular, maximum earthquake depth apparently correlates with the long-term brittle layer thickness, which vanishes, together with T_e , in the vicinity of oceanic spreading centers. The long-term thickness of the brittle layer

is controlled by the depth to the brittle–ductile transition (BDT) and hence is temperature-dependent. Thermal gradients in hot lithosphere near spreading centers are much steeper than in normal lithosphere. As result, due the exponential dependency of the ductile strength on temperature, the BDT depth near ridges is close to the depth of 500–700 °C that defines the bottom of the mechanical lithosphere. Hence, near the ridges, plate strength is concentrated in the uppermost brittle layer; the YSE is saturated, that is, the deformation is largely nonflexural. In these specific conditions, integrated plate strength may correlate with T_s . With distance from spreading centers, BDT depth becomes shallower than the depth to 500–600 °C, an elastic core forms within the lithosphere, and the correlation rapidly breaks down. In particular, there is a large difference between the depths of extensional and compressional earthquakes (Watts and Burov, 2003).

However, driven by the idea of correlation between the seismogenic layer thickness and long-term strength of the lithosphere, a number of authors (Jackson, 2002; McKenzie and Fairhead, 1997; Zoback and Townend, 2001) challenge conventional rheology models for the lithosphere where ductile mantle provides an important contribution to the integrated plate strength. In continents, the conventional model is known as the ‘jelly sandwich’ because the assumption of strong mantle implies a stratified rheology profile with strong upper/lower crust and mantle layers separated by a weak ‘jelly-like’ ductile layer at the base of the lower crust. The previously mentioned authors stated that the ‘jelly sandwich’ model is incorrect, proposing instead a model in which all long-term strength is concentrated in the brittle layer. For continents, they have chosen a rheology envelope originally developed for Venus (Mackwell et al., 1998), in which the crust is strong, but the mantle is weak. This model (that I dubbed ‘crème brûlée’ model) suggests that continents are thin and hot (>800 °C at 60 km depth) and have a water-saturated mantle.

Historically, the ‘crème brûlée’ model has arisen because of conflicting results from rock mechanics, earthquake, and elastic thickness (T_e) data. Even if its validity is largely debated, its appearance illustrates the lack of reliable constraints on long-term rheology. Indeed, while one can systematically improve the precision and inherent consistence of rock mechanics experiments, it is difficult to prove, on the basis of laboratory experiments alone, that these data are relevant to long-term deformation (Kohlstedt et al., 1995). There is actually much confusion concerning the interpretation of brittle–elastic–ductile YSEs derived for the continental lithosphere. Even if the underlying rheology laws were robust, the common YSE profiles introduce additional uncertainties, because they are derived using strong assumptions regarding the shape of the geotherm, pressure, strain, and strain rate distribution at depth. For example, Jackson’s (2002) suggestion that the depth of seismicity is limited by the depth of the BDT is based on interpretation of YSEs derived for geologic strain rates ($\sim 10^{-17}\text{--}10^{-15}\text{ s}^{-1}$). Yet, long-term YSEs are not valid for seismic timescale deformation: when recomputed for seismic strain rates ($10^3\text{--}10^6\text{ s}^{-1}$), YSEs predict that at this timescale, the lithosphere is entirely brittle–elastic, with BDT depth well below its bottom. Indeed, as revealed by postglacial rebound data (e.g., Peltier, 1974; Peltier and Andrews, 1976), the shortest ductile timescales in the lithosphere–asthenosphere system are on the order of thousands of years. Consequently, the

long-term BDT depth is not a direct proxy to maximum seismic depth. It can be only argued that since brittle earthquakes take place on the preexisting fractures or faults forming by coalescence of smaller fractures, they will more likely happen within a permanently brittle layer.

It becomes evident that independent large-scale constraints are needed to assess the long-term rheology of the lithosphere. In the following chapter, we summarize available experimental and observational data on lithosphere rheology and discuss possible approaches for parameterization and the application of data from experimental rock mechanics at geologic temporal and spatial scales.

6.03.2 Rock Mechanics Data and Conventional Rheology Models

For very small strains and/or short timescales (e.g., seismic), rocks deform elastically (Tables 1–4). Under stress, atomic bonds can be broken at quite small strains leading to inelastic deformation. Inelastic ductile deformation results from thermally activated creeping flow at long timescales. The most common mechanisms of ductile flow refer to atomic diffusion under pressure, sliding along intracrystalline dislocations, point or planar defects, or sliding at grain boundaries. Inelastic brittle deformation results from coalescence of

Table 1 Commonly inferred parameters for diffusion creep in the mantle lithosphere, $n=1$ (Hirth and Kohlstedt, 2003; Karato et al., 1986)

Rock/mineral	A ($s^{-1} Pa^{-1} \mu m^m$)	m	Q (kJ mol $^{-1}$)	Comments
Dry olivine	7.7×10^{-8}	1–3	536	Karato et al. (1986)
Dry olivine	1.5×10^3	3	375 ± 50	Hirth and Kohlstedt (2003)
Wet olivine	1.5×10^{-9}	1–3	498	Karato et al. (1986)
Wet olivine	2.5×10^1	3	375 ± 75	Hirth and Kohlstedt (2003)

These data are provided with primary goal to demonstrate characteristic values of parameters and to illustrate the scatter in experimental parameters.

Table 2 Commonly inferred parameters of dislocation creep

Rock/mineral	A ($MPa^{-n} s^{-1}$)	n	Q (kJ mol $^{-1}$)	Comments
Wet quartzite	10^{-4}	2.4	160	Brace and Kohlstedt (1980), Kirby and Kronenberg (1987), and Kohlstedt et al. (1995)
Wet quartzite	1.1×10^{-4}	4	223	Gleason and Tullis (1995), Figure 4(b)
Wet quartzite	1.25×10^{-5}	3 ± 0.2	242 ± 24	Rutter and Brodie (2004)
Dry feldspar (anorthite)	5.01×10^{12}	3	641	Rybacki et al. (2006)
Wet feldspar (anorthite)	1.58	3	345	Rybacki et al. (2006)
Dry diabase	$10^{-3.7}$	3.4	260	Kirby (1983)
Dry diabase	2.0×10^{-4}	3.4	260	Kirby (1983)
Columbia diabase (weak)	190 ± 110	4.7 ± 0.6	485 ± 30	Mackwell et al. (1998), Figure 4(b)
Maryland diabase (strong)	8 ± 4	4.7 ± 0.6	485 ± 30	Mackwell et al. (1998)
Granite(wet)	2×10^{-4}	1.9	140	Mackwell et al. (1998)
Wet diorite	3.2×10^{-2}	2.4	212	Ranalli (1995)
Dry mafic granulite	1.4×10^4	4.2	445	Wilks and Carter (1990)
Undried Adirondack granulite	3.18×10^{-4}	3.1	243	Wilks and Carter (1990)
Undried Pikwitonei granulite	1.4×10^4	4.2	445	Wilks and Carter (1990), Figure 4(b)
Dry olivine	10^4	3	520	Chopra and Paterson (1984)
Dry olivine	4.8	3.0	502	Evans and Kohlstedt (1995)
Dry olivine	5.0	3.5	530	Hirth and Kohlstedt (2003)
Dry dunite	4.85×10^4	3.5	535	Hirth and Kohlstedt (1996)
Microgabbro	5×10^9	3.4	497	Wilks and Carter (1990)
Wet olivine (dunite)	275.6	4.45	498	Chopra and Paterson (1981)
Wet olivine	4.876×10^6	3.5	515 ± 30	Hirth and Kohlstedt (1996)
Wet olivine	2.5×10^7	1.0	375 ± 75	Hirth and Kohlstedt (2003)
Wet Aheim dunite	2.6	4.5	498	Evans and Kohlstedt (1995)
Dry Anita Bay dunite	4.5	3.6	535	Chopra and Paterson (1981)
Wet synthetic San Carlos olivine	1.5×10^6	3	250	Karato et al. (1986)
Dry synthetic olivine	5.4	3.5	540	Karato et al. (1986)
Dry synthetic olivine	1.25×10^6	3.0 ± 0.1	510 ± 30	Karato and Jung (2003)
Wet synthetic olivine	3.3	3.0	420	Karato et al. (1986)
Wet synthetic olivine	794	3.0 ± 0.1	470 ± 40	Karato and Jung (2003)
Wet Anita Bay dunite	955	3.4	444	Chopra and Paterson (1984)
Wet Aheim dunite	417	4.48	498	Chopra and Paterson (1984), Figure 4(b)
Dry olivine	4.85×10^4	3.5	535	Chopra and Paterson (1981), Figure 4(b)
Olivine (Dorn's dislocation glide) at $\sigma_1 - \sigma_3 \geq 200$ MPa	$\dot{\epsilon}_0 = 5.7 \times 10^{11} s^{-1}$	$\sigma_0 = 8.5 \times 10^3$ MPa	$H^* = 535$ kJ mol $^{-1}$	

These data are provided with primary goal to demonstrate characteristic values of parameters and to illustrate the scatter in experimental parameters; for recent updates, see, for example, Kohlstedt (2007).

Table 3 Peierls plasticity

Rock/mineral	τ_0 (MPa)	$\dot{\varepsilon}$ (s^{-1})	Q ($kJ mol^{-1}$)	Comments
Synthetic olivine	8500	5.7×10^{-11}	536	Karato et al. (1998)
San Carlos peridotite	9100	1.3×10^{-12}	498	Goetze and Evans (1979)

Table 4 Summary of most common thermal and mechanical parameters of the lithosphere (also used in various model simulations shown in this paper)

Type	Parameter	Value
Thermal	T_{z0} , surface temperature	0 °C
	T_m , temperature at base of thermal lithosphere	1330 °C
	k_c , thermal conductivity of the upper crust	$2.5 \text{ W m}^{-1} \text{ °C}^{-1}$
	k_{c2} , thermal conductivity of the lower crust	$2.0 \text{ W m}^{-1} \text{ °C}^{-1}$
	k_m , thermal conductivity of mantle	$3.5 \text{ W m}^{-1} \text{ °C}^{-1}$
	χ_c , thermal diffusivity of the upper crust	$8.3 \times 10^{-7} \text{ m}^2 \text{ s}^{-1}$
	χ_{c2} , thermal diffusivity of the lower crust	$6.7 \times 10^{-7} \text{ m}^2 \text{ s}^{-1}$
	χ_m , thermal diffusivity of mantle	$10^{-6} \text{ m}^2 \text{ s}^{-1}$
	H_s , radiogenic heat production at surface	$9.5 \times 10^{-10} \text{ W kg}^{-1}$
	h_r , radiogenic heat production decay depth constant	10 km
	H_{c2}/C_{c2} , heat source term, lower crust	$1.7 \times 10^{-13} \text{ °K s}^{-1}$
	a , equilibrium thermal thickness of the lithosphere	125–350 km
	t , thermotectonic age of the lithosphere	0–1000 My
	ρ_c , density of upper crust	2700 kg m^{-3}
Mechanical	ρ_{c2} , density of lower crust	2900 kg m^{-3}
	ρ_m , density of mantle (undepleted)	3330 kg m^{-3}
	ρ_a , density of asthenosphere	3310 kg m^{-3}
	Lamé elastic constants λ, G (here, $\lambda = G$)	30 GPa
	ϕ , Byerlee's law/Mohr–Coulomb criterion – friction angle	30°
	C_0 , Byerlee's law /Mohr–Coulomb criterion – cohesion	20 MPa
	A, m, n, Q, H , ductile flow law parameters	Tables 1–3
	T_e , equivalent elastic thickness	0–110 km
	h_{1c}, h_{2c}, h_m , mechanical bottoms of the upper crust, lower crust, and mantle, respectively	<20; <40; <125 km, respectively
	T_c , crustal thickness	7–70 km, 36–40 km (average in continents)
Divers	T_s , seismogenic layer thickness	15–20 km; <50 km

preexisting microcracks and fractures into a single frictional shear band (fault) at sufficiently high strains (Byerlee, 1978; Lokhner, 1995). In nature, there is no pure elastic, viscous, or plastic deformation; all types of deformation take place simultaneously but in different proportions.

6.03.2.1 Elastic Properties

Elasticity arises from short-range interatomic forces that, when the material is unstressed, maintain the atoms in regular patterns. Stresses resulting from elastic deformation are linear function of strain, and the initial geometry of the material is fully recoverable after stress/strain relief. The elastic strain propagates with a speed of sound and goes ahead of viscous or plastic strain. This behavior is described by linear Hooke's law:

$$\sigma_{ij} = \lambda \varepsilon_{ii} \delta_{ij} + 2G \varepsilon_{ij} \quad [1]$$

where λ and G are Lame's constants. Repeating indexes mean summation and δ is Kronecker's operator. λ and G are related to the incompressibility (bulk) modulus K_e :

$$K_e = \frac{1}{3}(3\lambda + 2G) \quad [2]$$

An equivalent form of eqn [1] is

$$\begin{aligned} \varepsilon_{ij} &= E^{-1} \sigma_{ii} \delta_{ij} - E^{-1} v \sigma_{ij} \\ G &= E/2(1+v); \lambda = Ev/((1+v)(1-2v)) \end{aligned} \quad [3]$$

where E is Young's modulus and v is Poisson's ratio. A number of direct observations suggest that the lithosphere maintains elastic stresses over long periods of time. These observations demonstrate that lithospheric plates behave as rigid blocks or shells for tens and hundreds My. Plate tectonics is the most evident demonstration of this phenomenon (DeMets et al., 1990). For normal loading, plate flexure, or regional isostasy, studies demonstrate that plates behave as thin rigid plates of finite thickness called equivalent elastic thickness of the lithosphere (T_e ; Figure 2(a)). T_e varies from 0 km for very young areas (spreading centers) to 110 km for cratons (Audet and Burgmann, 2011; Forsyth, 1985; Watts, 2001). The continent average T_e is 30–50 km. For oceans, T_e is proportional to the square root of their age t (in My) (Le Pichon et al., 1973) and is generally smaller than 50 km:

$$T_{e \text{ oceans}} \sim 5t^{1/2} \quad [4]$$

The age t of the oceanic lithosphere is a proxy of its thermal state and thus of its ductile strength. The integrated strength of the oceanic lithosphere is largely controlled by its ductile

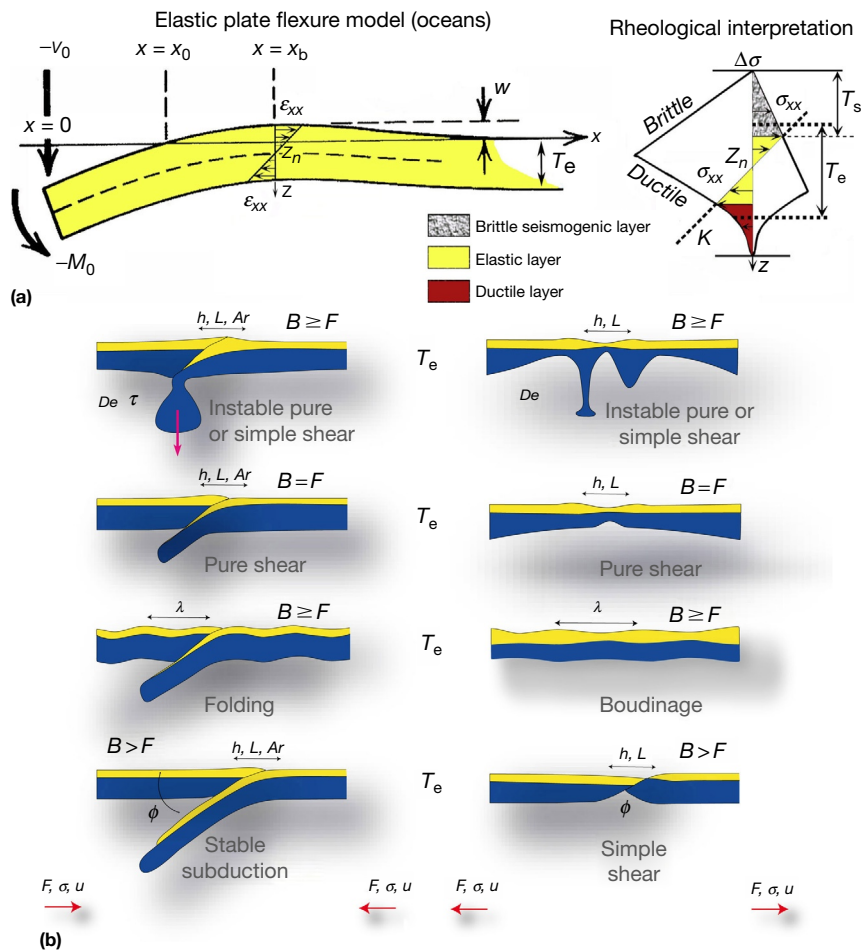


Figure 2 (a) Lithospheric flexure is the most widespread mode of deformation of the lithosphere since it is primarily related to the response of the lithosphere to permanently present vertical gravitational forces (and also boundary moments and vertical and horizontal boundary forces acting at plate boundaries). The figure shows a stress-strain distribution ($\sigma_{xx}, \epsilon_{xx}$) in the classical elastic model of lithospheric flexure. w is vertical deflection of the plate, V_0 is cutting force, and M_0 is the boundary moment (both are associated with plate boundary conditions such as slab pull, loading from the upper plate, mantle drag, and other forces). Z_n is the neutral plane. T_e is the equivalent elastic thickness of the plate, that is, the thickness of an ideal monolayer elastic plate that provides same observed geometry of bending $w(x)$ as the real lithosphere. Thickness of the real lithosphere may be essentially larger than T_e (modified from Turcotte DL and Schubert G (2002) *Geodynamics*, 2nd edn., p. 456. Cambridge: Cambridge University Press). (b) Observed modes of lithospheric deformation under horizontal forcing and related large-scale parameters used for estimation of lithospheric strength and rheology: T_e , F , σ , u , De , τ , h , L , λ , ϕ . T_e is equivalent elastic thickness. F , σ , u are, respectively, horizontal force, stress, and convergence/extinction velocity that are linked to the lithospheric strength and possible deformation styles. De and τ are, respectively, Deborah number and relaxation/growth time related to viscosity contrasts in the lithosphere. λ is the characteristic wavelength of unstable deformation related to the thickness of the competent layers in the lithosphere. h , L are, respectively, the vertical and horizontal scales for process-induced topography supported by lithospheric strength, Argand number $Ar = \rho ghL/F$. ϕ is subduction or major fault angle that can be indicative of the brittle properties and of overall plate strength. In oceans, subduction and folding prevail at destructive boundaries and pure shear – at constructive boundaries (ridges). Compressive pure shear, boudinage, and RT instabilities are basically observed only in continents. In all cases, flexural deformation interferes with the other modes of deformation.

strength. In the continental domain, T_e is controlled by several factors and cannot be estimated from simple relations (Burov and Diament, 1995).

6.03.2.2 Brittle or Plastic Properties

Brittle failure occurs in different modes. One of them refers to tensile failure that results in fractures parallel to one of the axis of the principal stresses (σ_1, σ_3) and does not depend on confining pressure (Jaeger and Cook, 1976). However, tectonic fracturing is mostly related to shear failure, which is pressure-dependent plastic behavior (Figure 1; Nadai, 1963). Brittle

deformation in shear described by Byerlee's law refers to frictional sliding on preexisting microfractures with either one or two fault planes forming an angle of $<45^\circ$ with the direction of the maximum compression. Several empirical plastic yielding criteria exist that predict activation of brittle–plastic deformation for given conditions (Von Mises, Tresca, Mohr–Coulomb, Drucker–Prager, etc.). The Coulomb–Navier failure criterion (referred to as Mohr–Coulomb criterion when expressed in terms of Mohr's circle diagrams) best represents the brittle behavior of rocks in geologically relevant contexts (Byerlee, 1978). This criterion refers to Amonton's law of friction:

$$\tau = C_0 + \tan(\phi)\sigma_n \quad [5]$$

where C_0 is the cohesive strength (<20 MPa), $\tan(\phi)$ is the internal friction coefficient, ϕ is the internal friction angle (typically 30–33°), τ and σ_n are, respectively, the shear stress and normal stress on a selected surface within material. According to Cauchy's formulation for a Cartesian basis (x, y, z) (e.g., Kachanov, 1971),

$$\begin{aligned} \sigma_n = & \sigma_{xx}\cos^2(n, x) + \sigma_{yy}\cos^2(n, y) + \sigma_{zz}^2\cos(n, z) \\ & + 2(\tau_{yx}\cos(n, x)\cos(n, y) + \tau_{yz}\cos(n, y)\cos(n, z) \\ & + \tau_{xz}\cos(n, z)\cos(n, x)) \end{aligned} \quad [6]$$

where subscripts refer to the global Cartesian stress components. The shear stress on a fault plane τ_n is $\tau_n^2 = X_n^2 + Y_n^2 + Z_n^2 - \sigma_n^2$, where X_n, Y_n, Z_n refer to the x, y, z components of σ_n . Assigning the origin of the z -coordinate to Z_n , we obtain 2-D Mohr circles ($\theta = \text{angle}(n, x)$):

$$\begin{aligned} \sigma_n = & \sigma_{xx}\cos^2\theta + \sigma_{yy}\sin^2\theta, \quad \tau_n^2 = X_n^2 + Y_n^2 - \sigma_n^2, \\ \sigma_n^2 + \tau^2 - & \sigma_n(\sigma_{xx} + \sigma_{yy}) + (\sigma_{xx}\sigma_{yy}) = 0 \end{aligned} \quad [7]$$

Measurements *in situ* are referred to the (σ_1, σ_3) frame (Figure 1):

$$\begin{aligned} \sigma_n = & \frac{1}{2}(\sigma_1 + \sigma_3) + \frac{1}{2}(\sigma_1 - \sigma_3)\cos 2\theta \\ \tau = & \frac{1}{2}(\sigma_1 - \sigma_3)\sin 2\theta \end{aligned} \quad [8a]$$

σ_n and τ refer to a plane (e.g., fault plane), whose normal n forms an angle θ with the direction of σ_1 ; $\phi = 2\theta - \frac{1}{2}\pi = \frac{1}{2}\pi - 2\alpha$, where 2α is the angle between two conjugated shear planes $\alpha = \theta - \frac{1}{2}\pi$. Shear fractures are thus oblique to σ_1 and σ_3 and develop in two preferred orientations that form an angle of $\sim 60^\circ$ ($2\theta - \pi = \frac{1}{2}\pi - \phi$) to each other, constituting an 'X'-shaped conjugate set. Conjugated shear zones are bisected acutely by the maximum shortening direction and obtusely by the maximum extension direction. Their intersection is parallel to σ_2 , which is normal to (σ_1, σ_3) plane. Large-scale shear bands and faults follow the same rule and may form by coalescence of various types of smaller fractures: shear fractures parallel to the sense of displacement along the conjugate shear zones, tensile fractures striking parallel to each other in both conjugate zones, and 'Riedel' shear fractures that make an angle of $\sim 15^\circ$ (or $\sim 75^\circ$) to the bulk shear direction. These small-scale fractures may step en échelon along incipient shear zones.

The parabolic Griffith criterion extends the Mohr-Coulomb criterion to the domain of tensile stress:

$$\tau^2 = 4T_0^2 + 4T_0\sigma_n \quad [8b]$$

where $2T_0 = C_0$ is the tension cutoff (Figure 1). Tensile fractures open in normal to the maximum extension direction. They next dilate and get filled (healed) with minerals (quartz and calcite) precipitated from fluids circulating within the host rock to form extensional veins.

The point where the yield criterion function is tangent to the largest of Mohr circles (σ_1, σ_3) defines failure stress and angles θ and α . A third parameter, Ψ , dilatation angle, accounts for dilatation in shear that occurs due to sliding over interface asperities. Hence, Ψ characterizes the degree of compressibility ($\Psi = 0$ for incompressible rock). For simple shear, Ψ is defined from the ratio of volume strain rate $\dot{\varepsilon}_{ii}$ to shear strain rate $\dot{\varepsilon}_{ij}$:

$$\tan \Psi = \dot{\varepsilon}_{ii}/\dot{\varepsilon}_{ij} \quad [8c]$$

Plasticity is associative if $\Psi = \phi$ or nonassociative if $\Psi \neq \phi$. More precisely, plasticity is nonassociative if the plastic potential function differs from the plastic failure function. For Mohr-Coulomb or Drucker-Prager plasticity, this is the case when $\Psi \neq \phi$. Most rocks are nonassociative: $\Psi < 10^\circ$ and $\phi = 30^\circ - 40^\circ$ (Vermeer and de Borst, 1984). This explains localization of shear bands due to the rheological instabilities even without material softening. These instabilities occur because the nonassociative materials do not deform homogeneously in a postpeak stress regime, but bifurcate into two states: plastic deformation within a shear band and elastic unloading outside. This leads to a stress discontinuity across the shear band and, consequently, to instabilities. Normal stresses parallel to the shear band decrease in a postpeak regime, which results in a decrease in vertical stress as well. This stress drop is called 'nonassociated softening' (Vermeer, 1990), as distinct from material softening, which occurs when some intrinsic material parameters (cohesion and friction angle) decrease as a function of strain or stress.

Byerlee (1978) experimentally demonstrated that for the majority of rocks, the Coulomb failure criterion applies in the form (Figure 1)

$$\begin{aligned} \tau = & 0.85\sigma_n, \quad \sigma_n \leq 200 \text{ MPa} \\ \tau = & 50 \text{ MPa} + 0.6\sigma_n, \quad 1700 \text{ MPa} > \sigma_n > 200 \text{ MPa} \end{aligned} \quad [9]$$

or

$$\begin{aligned} \sigma_1 = & 4.7\sigma_3, \quad \sigma_3 \leq 114 \text{ MPa} \\ \sigma_1 = & 3.1\sigma_3 + 177 \text{ MPa}, \quad 1094 \text{ MPa} > \sigma_3 > 114 \text{ MPa} \end{aligned} \quad [10]$$

Byerlee (1978) had also shown that frictional properties of rocks are nearly independent of rock type. This explains why tectonic faults may intersect lithologically heterogeneous structures. However, brittle strength depends highly on pressure variations caused by tectonic stresses and fluids. The latter are described by the fluid pressure factor $\lambda = \rho_w/\rho$, where ρ_w is the density of water and ρ is rock density:

$$\Delta\sigma = \sigma_1 - \sigma_3 = \alpha\rho g z(1 - \lambda) \quad [11]$$

where $\alpha = 1 - R^{-1}$ for normal faulting, $\alpha = R - 1$ for thrusting, and $\alpha = (R - 1)/(1 + \beta(R - 1))$ for strike-slip faulting, with $R = ((1 + \phi^2)^{1/2} - \phi)^{-2}$ and $\tan\beta = (\sigma_2 - \sigma_3)/(\sigma_1 - \sigma_3) < 1$.

It is noteworthy that Byerlee's data can also correspond to a weak power law (Lokhner, 1995):

$$|\tau| = \sigma_n^{0.94} \quad [12]$$

Deep drilling has provided direct evidence in support of Byerlee's law for the first few km of the crust (1–14 km) (e.g., Zoback et al., 1993). However, this law is probably not applicable at depths exceeding 30–50 km (e.g., Kirby et al., 1991). At high depth/pressure or temperature, brittle failure may change to semibrittle (e.g., Bos and Spiers, 2002; Chester, 1995) or to some form of ductile-superplastic regime (e.g., Goetze and Evans, 1979). One of the discussed possibilities refers to Peierls plasticity (Goetze and Evans, 1979, see also next section) or to grain boundary sliding (GBS) that is specific to upper mantle rocks (e.g., Drury, 2005). Peierls plasticity takes place at high differential stresses (>100–200 MPa), when mixed dislocation glide and climb occur (Karato, 1998; Karato et al., 1986).

Parameters of the Peierls mechanism are not well known since they have been obtained only in a few experiments (Evans and Goetze, 1979; Goetze and Evans, 1979) at room pressure. Synthetic parameters (e.g., Karato, 1998; Karato et al., 1986) can be used only as rough estimates (Table 3). GBS creep may occur at large strains in relatively cold (<700–800 °C) upper mantle lithosphere (e.g., Precigout et al., 2007; Precigout and Gueydan, 2009; Terry and Heidelbach, 2004). This flow law may eventually explain the absence of distributed seismicity in the mantle, as well as the difference between crustal and mantle seismicity (no GBS creep in the crust). Despite the lack of experimental data for near-Moho and mantle conditions, there is a general agreement that brittle strength reaches maximum values at 30–50 km depth, below which Byerlee's law is apparently replaced by some other behavior such as Peierls flow and the rock strength no longer increases (Kirby, 1991; Kirby et al., 1996). However, some phenomena, such as discovery of apparently brittle ultrahigh-pressure pseudotachylites in exhumed deep fault zones (Austrheim and Bondy, 1994), suggest that brittle-like failure may have been occasionally produced at great depth in large shear zones.

6.03.2.3 Ductile (Viscous) Properties

Viscous behavior applies when the deformational stress is a function of strain rate and does not depend on the strain itself. The term 'ductile,' often associated with strain rate-dependent properties of the rocks, is not related to a particular constitutive relationship but to the ability of materials to change form irreversibly without fracturing. Actually, if the strain rate–stress dependence is not negligible, the material is considered as ductile-plastic if it deforms irreversibly without fracture. When the ductile deformation is characterized by linear strain rate–stress dependence, one speaks of Newtonian viscous deformation. When this dependence is nonlinear, the term 'non-Newtonian viscosity' is applied. At temperatures >300 °C, strain rate-dependent nonlinear dislocation creep is dominant. At very high temperatures (>1330 °C), the deformation appears to be dominated by linear diffusion creep (note, however, that a number of studies have suggested that the upper mantle is partly driven by the dislocation creep (Van Hunen et al., 2005)).

6.03.2.3.1 Diffusion and dislocation creep

The dominant ductile flow mechanisms in the lithosphere–asthenosphere system are associated with the diffusion and dislocation creep. In contrast to brittle deformation, the ductile deformation is extremely dependent on rock type (e.g., Kirby and Kronenberg, 1987). Even small variations in mineral composition may have a strong impact on ductile properties (Brace and Kohlstedt, 1980; Bürgmann and Dresen, 2008; Hier-Majumder et al., 2005; Kirby and Kronenberg, 1987; Kohlstedt, 2007; Mackwell et al., 1998; Tables 1–2). The mechanisms of ductile deformation are variable and abundant: diffusion creep, numerous variants of dislocation creep (dislocation climb, glide, screw, edge, etc.), pressure solution, GBS, and so on. Grain size-sensitive (GSS) diffusion creep (Nabarro-Herring (volume diffusion)) or Coble creep (surface diffusion) (Ashby and Verrall, 1978) is associated with temperature-dependent directional diffusivity of rocks and minerals under applied stress (Table 1):

$$\dot{\varepsilon}^d = Aa^{-m}f_w\Delta\sigma^n \exp(-H(RT)^{-1}) \quad [13]$$

where $\dot{\varepsilon}^d$ is shear strain rate; A is a material constant; a is a grain size; m is a diffusion constant; f_w is the water fugacity factor; n is a power law constant; $\Delta\sigma = \sigma_1 - \sigma_3$ is differential stress; R is Boltzmann's gas constant; H is creep activation enthalpy, $H=Q+PV$, where Q is activation energy, P is pressure, and V is activation volume; and T is temperature in K. For olivine-rich rocks at high-temperature–low-stress conditions, $m=3$ and $n=1$ so that the constitutive law is linear Newtonian.

At high stresses and moderate temperatures <1330 °C, $m=0$ and $n=3$, the creep rate is dominated by grain size-insensitive (GSI) dislocation creep (power law and Dorn's law). The power flow law is strongly non-Newtonian (Table 2) for $\Delta\sigma < 200$ MPa:

$$\dot{\varepsilon}^d = Af_w\Delta\sigma^n \exp(-H(RT)^{-1}) \text{ for } \Delta\sigma < 200 \text{ MPa} \text{ (Power law)} \quad [14]$$

$$\dot{\varepsilon}^d = Af_w \exp\left(-H(1 - \Delta\sigma/\sigma_p)^2/RT\right) \text{ for } \Delta\sigma > 200 \text{ MPa} \text{ (Dorn law)} \quad [15]$$

where $\dot{\varepsilon}_0$ and σ_p are, respectively, maximum strain rate and Peierls stress (lattice resistance to dislocation glide, on the order of several GPa). For tectonically relevant $\Delta\sigma/\sigma_p$ ratios (<0.1), Dorn's behavior is close to plastic behavior (Peierls plasticity) and tends to limit ductile strength in a high-stress regime (Figure 3). This law is not sufficiently well studied and its application may be subject to large uncertainties (Goetze and Evans, 1979).

The effective viscosity μ_{eff} for power flow law can be defined from

$$\tau_{ij} \equiv \mu_{\text{eff}} \dot{\varepsilon}_{ij}^d \quad [16]$$

which yields

$$\mu_{\text{eff}} = \dot{\varepsilon}_{ij}^{d(1-n)/n} A^{-1/n} \exp(H(nRT)^{-1}) \quad [17]$$

The laws [14] to [15] are derived for uniaxial deformation. They should be converted, with all possible reservations, to a form valid for triaxial deformation, via the second invariant (J_2) of strain rate $\dot{\varepsilon}_{ij}^d$ and geometric proportionality factors:

$$\mu_{\text{eff}} = \dot{\varepsilon}_{II}^{d(1-n)/n} (A^*)^{-1/n} \exp(H(nRT)^{-1}) \quad [18]$$

$$\dot{\varepsilon}_{II}^d = (J_2(\dot{\varepsilon}_{ij}^d))^{1/2} \text{ and } A^* = \frac{1}{2}A \cdot 3^{(n+1)/2}$$

where $\dot{\varepsilon}_{II}^d$ is the effective shear strain rate. The diffusion creep takes over for small grain size that is specific for highly sheared material (ductile shear zones) or for very high temperatures. Grain size reduction is believed to be an important mechanism of rock softening and localization in mantle shear zones or in the upper mantle (Karato et al., 1986). Creep mechanisms are strongly dependent on water, water fugacities, and mineralogical and melt content (Karato, 1986).

6.03.2.3.2 Pressure solution, cataclastic flow, Peierls plasticity, GBS flow, and other mechanisms

While dislocation and diffusion creep are the dominant flow mechanisms in the lithosphere and the underlying asthenosphere, a number of secondary but contextually important ductile creep mechanisms are also present at specific pressure–temperature conditions.

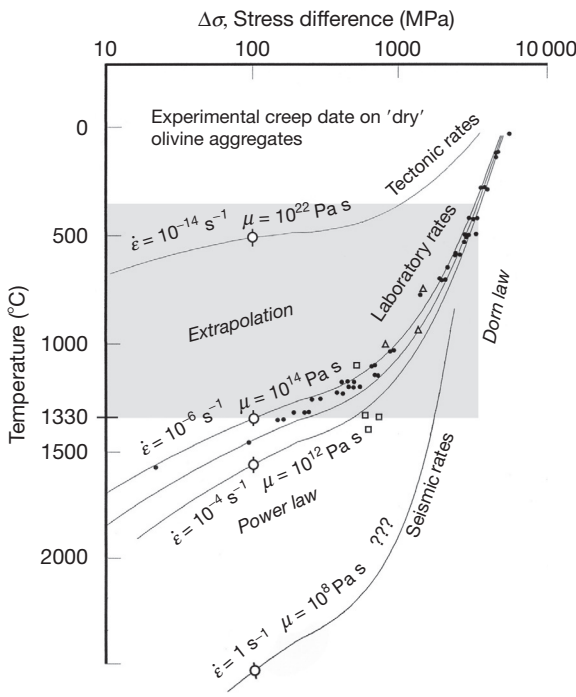


Figure 3 Typical example of experimental data on ductile flow in rocks (olivine aggregates and power and Dorn's flow laws for different temperature–stress domains). Shown also are predicted viscosity values, μ , for 100 MPa stress level (open circles). Note sensitivity to strain rate $\dot{\varepsilon}$ and rock composition (triangles, squares, and black dots correspond to different variants of principally the same olivine aggregates). The typical strain rates used in experiments (10^{-6} – 10^{-4} s $^{-1}$) are ten orders of magnitude higher than those in nature (10^{-14} – 10^{-17} s $^{-1}$), which poses a serious question on the possibility of extrapolation of these data onto geologic timescales (modified from Goetze C and Evans B (1979) Stress and temperature in bending lithosphere as constrained by experimental rock mechanics. *Geophysical Journal of the Royal Astronomical Society* 59: 463–478; Watts AB (2001) *Isostasy and Flexure of the Lithosphere*, p. 458. Cambridge: Cambridge University Press). Hypothetical extrapolation of experimental data to seismic timescales (1 s) predicts very low-viscosity values, yet at these timescales, creep takes place at temperatures that are higher than maximum lithospheric temperature (1330 °C). Consequently, it is unlikely that seismic movements can activate ductile creep in lithospheric mantle.

Pressure solution is one of ‘cold’ ductile flow mechanisms that may occur at shallow depths and at temperatures below 200 °C and thus can compete with brittle deformation. This mechanism refers to the enhanced solubility of minerals under stress/pressure. Application of mechanical stress provokes directional solution of minerals in pore water, which leads to reduction of volume of solid phase equivalent to deformation:

$$\dot{\varepsilon}^d = 12\delta\rho_w D_s \sigma (h^3 \rho \sigma_0)^{-1} \quad [19a]$$

where δ is width of the grain boundary, ρ_w is density of solvent (water), D_s is the diffusion coefficient, σ is stress, h is the initial dimension of the crystal and ρ is the density of the soluble mineral (e.g., silica), and σ_0 is maximum stress. Silica, for example, is perfectly soluble in water at $\sigma_0 \sim 500$ MPa and $T = 500$ °C. Some experimental studies (e.g., Gratier et al., 2006)

have found that eqn [19a] should be corrected to include an exponential term depending on temperature and σ . The resulting flow law is weakly nonlinear power law with $n = 1.7$.

Cataclastic flow or semibrittle flow in porous rocks or at fault surfaces is another well-known example of ‘cold’ ductile behavior that occurs in high-strain regime. Cataclastic flow is associated with strain rate-dependent reduction of friction. It involves distributed microfractures at grain level, such that at a mesoscopic level or hand specimen scale, the rock appears to flow. This flow is often associated with semibrittle flow and treated in conjunction with crystal-plastic flow (Chester, 1988):

$$\tau = \tanh(\alpha\sigma_n) \left(\beta^{-1} \ln \left(\dot{\varepsilon} B^{-1} e^{(Q/RT)} \right) \right) + (1 - \tanh(\alpha\sigma_n)) \tau_f \quad [19b]$$

where α , β , B are material constants and τ_f is frictional stress that corresponds to the Mohr–Coulomb stress (eqn [5]) at low deformation rates and becomes rate-dependent at higher rates (Rice and Tse, 1986):

$$\tau_f = \sigma_n \left(\mu_r - C \ln \left(\frac{\dot{\delta}}{\dot{\delta}_r} + 1 \right) \right) \quad [19c]$$

where $\dot{\delta}$ and $\dot{\delta}_r$ is shear displacement and reference shear displacement rate, respectively, C is an experimental constant, and μ_r is a high-rate friction coefficient.

Peierls plasticity (see also eqn [15]) applies when the stress in the rock reaches a specific limit called Peierls stress. The latter is associated with Peierls energy, which changes with a transition of a dislocation line between the adjacent valleys of the potential relief, by a distance smaller than Burger's vector. At this moment, the dominant creep mechanism becomes dislocation glide and climb. The extended constitutive equation for Peierls plasticity relates to a form of Dorn's law (Evans and Goetze, 1979; Goetze and Evans, 1979):

$$\dot{\varepsilon}_{ij}^d = \dot{\varepsilon}_0 \exp \left(-\frac{Q + p(V - \beta\Delta V_w)}{RT} \left(1 - \frac{\tau_{ij}}{\tau_p} \right) \right) \quad [20a]$$

where $\dot{\varepsilon}_0 = A\alpha$, A, Q, V, P, R , and T are defined in the same way as for the ductile creep laws (see eqn [15]), α is an experimentally defined weakening parameter controlled by water content, β is an adjustable experimental parameter, ΔV_w is molar volume change due to incorporation of hydroxyl ions in the main rock, and τ_p is the shear stress limit (~Peierls stress) that characterizes transition to plastic failure. Regenauer-Lieb et al. (2001) suggested that Peierls plasticity and water-induced weakening may play a major role in localization of deformation at important depth or in subduction/collision zones. However, as mentioned, Peierls rheology is poorly constrained, while Peierls stress is significantly higher than typical tectonic stress, which limits the applicability of this law to high-strain zones.

During dynamic recrystallization, the accommodation of grain size reduction occurs by three competing deformation mechanisms, that is, GSI dislocation creep, GSS diffusion creep, and dry-GBS (GBS) GSS creep (Durham et al., 2009; Precigout et al., 2007). It involves grain size reduction controlled by diffusion creep at high temperatures (>800 °C), whereas dislocation creep and dry-GBS creep are the accommodating

mechanisms at lower temperatures (500–800 °C). GBS creep has been only recently considered in terms of its potential importance for tectonic-scale deformation (e.g., [Precigout et al., 2007](#)). Now, a growing number of studies suggest that like Peierls flow, it can replace Byerlee's law and dislocation creep in lithosphere mantle in a quite important depth range (e.g., [Drury, 2005](#)) corresponding, in continents, to a 20–30 km layer of sub-Moho mantle and, in the oceans, to the bottom of the mechanical lithosphere. It is suggested that this mechanism may be responsible for softening and aseismic localization of shear deformation in the uppermost strong lithosphere mantle (e.g., [Precigout et al., 2007](#)), allowing, for example, for formation of narrow rifts without a necessity for large far-field forces. Dry-GBS creep has been shown to accommodate grain size reduction during dynamic recrystallization and to induce significant weakening at low temperatures. The phenomenological equation for the GBS creep has the same form as for the diffusion creep, yet with highly different parameters, in particular with n in the order of 3:

$$\dot{\varepsilon}^d = A_{\text{GBS}} a^{-m} \tau^n \exp(-H(RT)^{-1}) \quad [20b]$$

where A_{GBS} is the preexponential constant, a is grain size, m is the GBS grain size exponent (typically $m=2$), n is the GBS power law constant (typically $n=3.5$), τ is shear stress, H is creep activation enthalpy, and T is temperature in °K. GBS creep thus combines features of both the diffusion and dislocation power law creep. Analogously to dislocation creep, it operates at high stresses and is highly nonlinear, with n close to that for dislocation power law creep in dry olivine. Yet, similarly to the diffusion creep, GBS creep is highly GSS, which makes of it an efficient mechanism of strain localization in strong mantle. By itself, diffusion creep cannot play a strain localization role in the mantle lithosphere since it operates at high temperatures and small stresses (<10 MPa) and thus cannot result in important strength/stress drops. Diffusion creep also corresponds to Newtonian linear flow ($n=1$); hence, its localizing properties are more limited. Ductile shear band strain localization resulting from the GBS creep may occur in the depth range corresponding to 500–800 °C (40–60 km depth in continents, e.g., [Terry and Heidelbach, 2004](#)) and therefore provide some explanation for the scarcity of earthquakes below this depth. Nevertheless, the hypothesis of the potential role of GBS creep mechanism in the mantle lithosphere needs further investigation.

6.03.2.4 Yield Stress Envelopes

By combining three major rheology laws (elastic, brittle, and ductile), [Goetze and Evans \(1979\)](#) had introduced the YSE for the lithosphere ([Figure 4](#)) defined as a differential stress contour $\sigma^f(z)$, or $\Delta\sigma_{\max}(z)$, such that

$$\begin{aligned} \sigma^f(z) &= \Delta\sigma_{\max}(z) \\ &= \text{sign}(\varepsilon) \min(|\sigma^b(x, z, t, \dot{\varepsilon}, \text{sign}(\varepsilon))|, |\sigma^d(x, z, t, \dot{\varepsilon})|) \end{aligned} \quad [21a]$$

where $\sigma^b(x, z, t, \dot{\varepsilon}, \text{sign}(\varepsilon))$, $\sigma^d(x, z, t, \dot{\varepsilon})$ are the maximum brittle and ductile yielding stresses; $\text{sign}(\varepsilon)$ is a sign function equal to 1 for extension and –1 for compression; t is time; and x refers to the possibility of not only depth (z) but also spatial strength

variations. The differential stress $\Delta\sigma(\varepsilon)$ for the strain $\varepsilon = \varepsilon(x, y, t, \dot{\varepsilon})$ is

$$\Delta\sigma(\varepsilon) = \text{sign}(\varepsilon) \min(|\sigma^f|, |\sigma^e(\varepsilon)|) \quad [21b]$$

where $\sigma^e(\varepsilon)$ is the value of elastic stress for the given strain ε . The lithosphere deforms elastically if $\sigma^e(z, \varepsilon) < \sigma^f(z)$. This implies the existence of a pertinent elastic 'core,' where inelastic strains are negligible. This core, associated with the equivalent elastic thickness, T_e , provides the main contribution to the integrated plate strength, B :

$$B = \int_0^\infty \sigma^f(x, y, t, \dot{\varepsilon}) dz \leq \int_0^\infty \sigma^e(\varepsilon) dz \quad [22]$$

Depth dependence of $\Delta\sigma_{\max}(z)$ stems from many factors among which are temperature, pressure, and composition. The YSEs are computed for a fixed background strain rate (typically, 10^{-15} s^{-1}). As suggested by [McAdoo et al. \(1985\)](#) for oceanic lithosphere and by [Burov and Diament \(1992\)](#) for continental lithosphere, the YSEs can be linearized, which allows for simple parameterization of rheology laws from direct observations of flexure. Linearized YSEs have been used in inelastic flexural models ([Burov and Diament, 1992, 1995; McAdoo et al., 1985; Appendix A](#)). This has allowed for the prediction of T_e for regional studies, as a function of YSE, surface and subsurface loading, thermal distribution, plate structure, and other parameters. By fitting nonlinear flexural models to the observed deformation, it has become possible to test and validate rheological profiles derived from experimental rock mechanics. These models have confirmed the validity of rheological envelopes for a number of regions (e.g., Central Asia ([Burov and Diament, 1992; Watts and Burov, 2003](#)) and European lithosphere ([Cloetingh and Burov, 1996; Tesauro et al., 2009a,b,c](#))).

The formulation of the YSE and its interpretation in terms of the observed equivalent elastic thickness (T_e) of the lithosphere constitutes a major breakthrough in our understanding of the long-term behavior of the lithospheric plates. Computed oceanic YSEs show a remarkable correlation with the measured values of T_e . The predicted depth of the BDT also correlates with deepest microseismicity in the oceanic domain (e.g., [Watts and Burov, 2003](#)).

While the composition and thermal structure of oceanic plates are well established, it is not the case for the continental domains. Continents have a thick crust of diverse structure and properties that vary from region to region. In addition, it is argued ([Jackson, 2002](#)) that in continents, the resistance of mantle olivine is strongly reduced due to the presence of fluids ([Figure 4\(b\); Table 2](#)). Yet, more recent studies have detected high water content only in deep upper mantle below the lithosphere but not in the lithosphere itself ([Katayama et al., 2005](#)). Inspection of the CB ('crème brûlée') YSE published by [Jackson \(2002\)](#) shows that it is not the assumption of wet olivine rheology that makes this YSE exceptionally weak but that of a very thin hot continental lithosphere (800 °C at 60 km depth, estimated equilibrium plate thickness $a=z(1330 \text{ °C}) \sim 100 \text{ km}$). Such conditions may exist in a few places on the Earth but not in the thick old Indian Craton targeted by [Jackson \(2002\)](#). Wet olivine rheology preserves important strength ([Figure 4\(b\)](#), right) in the case of a geotherm computed for a more appropriate equilibrium plate

thickness ($a=z(1330 \text{ }^{\circ}\text{C}) \sim 200 \text{ km}$) and taking into account radiogenic heat sources.

6.03.3 Constitutive Models

Elastic and brittle (plastic) rheologies are strain rate-independent, whereas viscous rheology is strain-independent. However, in the lithosphere, the behavior of elastic and brittle domains becomes strain rate-dependent via interaction with the viscous domain, which, in turn, becomes strain-dependent. Thus, even if the rheological parameters (elastic, ductile, or

brittle) were well constrained, the next question would be how to combine these rheological terms in a constitutive model. There are various possible constitutive models based on either the Maxwell, Voigt, or Kelvin model or their various possible combinations (Figure 4(c)).

6.03.3.1 Maxwell Model

In a Maxwell solid, total strain ε^M equals a sum of the elastic strain ε^e and viscous strain ε^v while viscous and elastic stresses are equal:

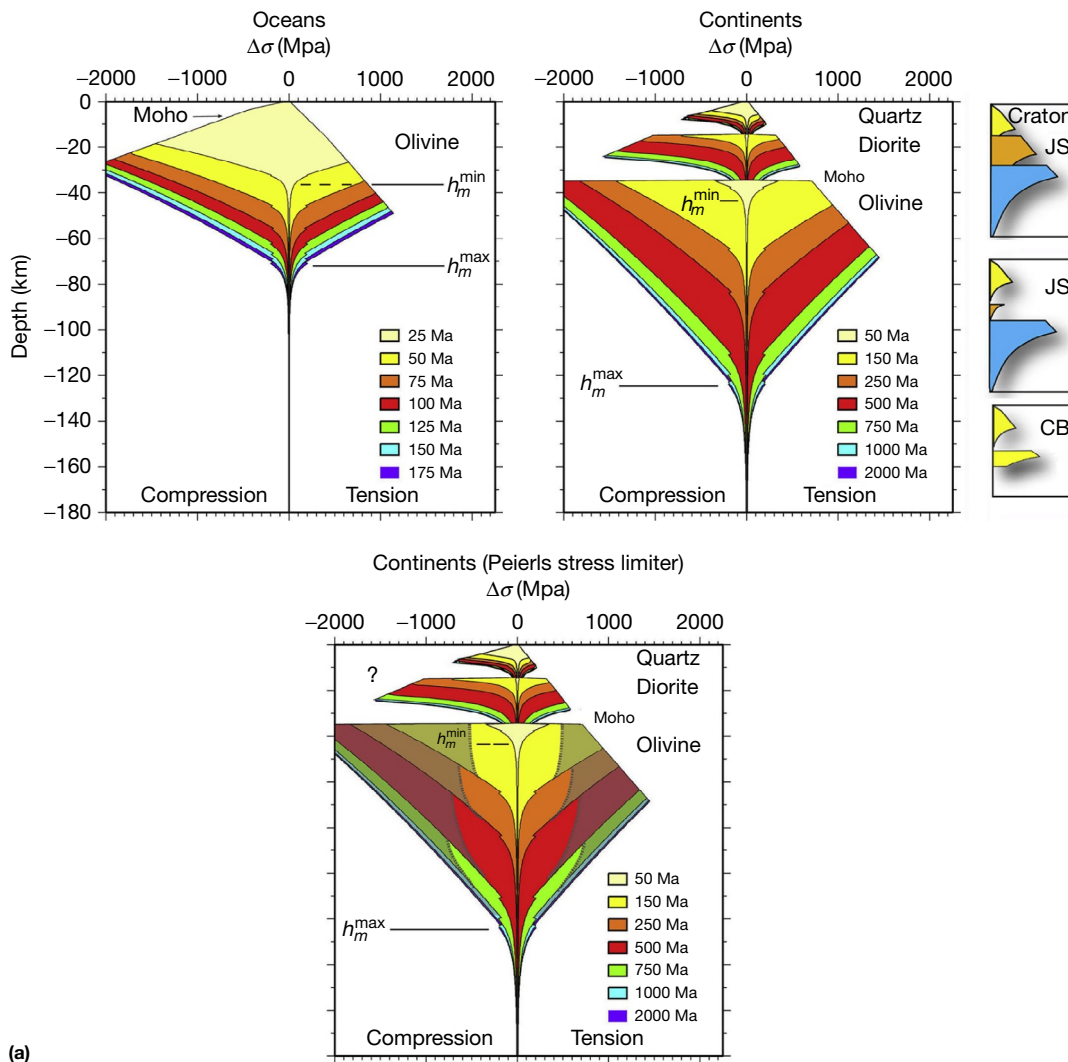


Figure 4 (a) Examples of rheological yield stress envelopes for oceans (as introduced by Goetze and Evans (1979)) and continents (modified from Burov EB and Diamant M (1995) The effective elastic thickness (T_e) of continental lithosphere: What does it really mean? *Journal of Geophysical Research* 100: 3895–3904). The YSE is shown as a function of the thermotectonic age. The main difference between the oceanic and continental lithosphere refers to the thick crust and multilayered structure of the latter, which may lead to mechanical decoupling between the rheological layers and horizontal ductile flow in the intermediate or lower crust. The right panel illustrates different variants of continental YSE: cratonic jelly sandwich (JS, strong lower crust is coupled with strong mantle), classic JS (strong crust is decoupled from strong mantle), crème brûlée (CB, very weak mantle). The bottom panel shows YSE for continental lithosphere under hypothetic assumption that Peierls flow takes place in mantle olivine at high-stress conditions. Although Peierls flow may also occur in other rocks/minerals, the laboratory data are not robust enough for lithosphere-scale interpolation (actually this is also partly the case of olivine/peridotite). The ductile strength of crustal rocks is highly uncertain; in particular, the rheology of quartz-rich upper crustal rocks is subject to large variations.

$$\begin{aligned}\varepsilon_{ij}^M &= \varepsilon_{ij}^e + \varepsilon_{ij}^v \\ \sigma_{ij}^e &= \sigma_{ij}^v\end{aligned}\quad [23]$$

The strain relation is often written in the incremental form

$$\varepsilon_{ij}^M = \varepsilon_{ij}^e + \varepsilon_{ij}^v = S_{ij}/(2G^M) + \sigma_{ij}/(2\mu^M) \quad [24]$$

where e is $\partial e/\partial t$ (incremental strain, or strain rate) and S is $\partial\sigma/\partial t$ (incremental stress, or stress rate). The behavior of this solid is dominated by the rheological term developing larger strain or strain rate. Thus, for most materials, in case of instantaneous strain, the first reaction is elastic and is associated with maximum stress, but in later stages, stress decays due to viscous relaxation at a rate controlled by the Maxwell relaxation time τ_m :

$$\tau_m = \mu/E \quad [25]$$

If τ_m is considerably shorter than the life span of the system, then deformation is effectively viscous (small Deborah number). For the asthenosphere, τ_m is known from postglacial rebound data (e.g., Peltier, 1974). This time is about 10–100

years implying effective viscosity of $1\text{--}5 \times 10^{19}$ Pa s. In the lithosphere, τ_m is on the order of several My, as indicated by data on volcanic island loading (Watts, 2001).

In ‘extended’ Maxwell viscous–elastic–plastic models, the total incremental strain $\varepsilon_{ij}^{M_ext}$ equals a sum of the elastic, plastic, and viscous strain increments:

$$\varepsilon_{ij}^{M_ext} = \varepsilon_{ij}^M + \varepsilon_{ij}^P \quad [26a]$$

If several ductile flow law mechanisms can be activated at the same time, the viscous term ε_{ij}^V in the Maxwell term ε_{ij}^M is often written as

$$\varepsilon_{ij}^V = \varepsilon_{ij}^{Vdc} + \varepsilon_{ij}^{Vdf} + \varepsilon_{ij}^{Vgbs} + \varepsilon_{ij}^{Vp} \quad [26b]$$

where ε_{ij}^{Vdc} , ε_{ij}^{Vdf} , ε_{ij}^{Vgbs} , ε_{ij}^{Vp} are contributions from dislocation, diffusion, GBS, and Peierls creep, respectively. It follows from eqn [26b] that for deformation with constant stress, the effective viscosity is

$$\mu^{eff} = \left((\mu^{Vdf})^{-1} + (\mu^{Vdc})^{-1} + (\mu^{Vp})^{-1} + (\mu^{Vgbs})^{-1} \right)^{-1} \quad [26c]$$

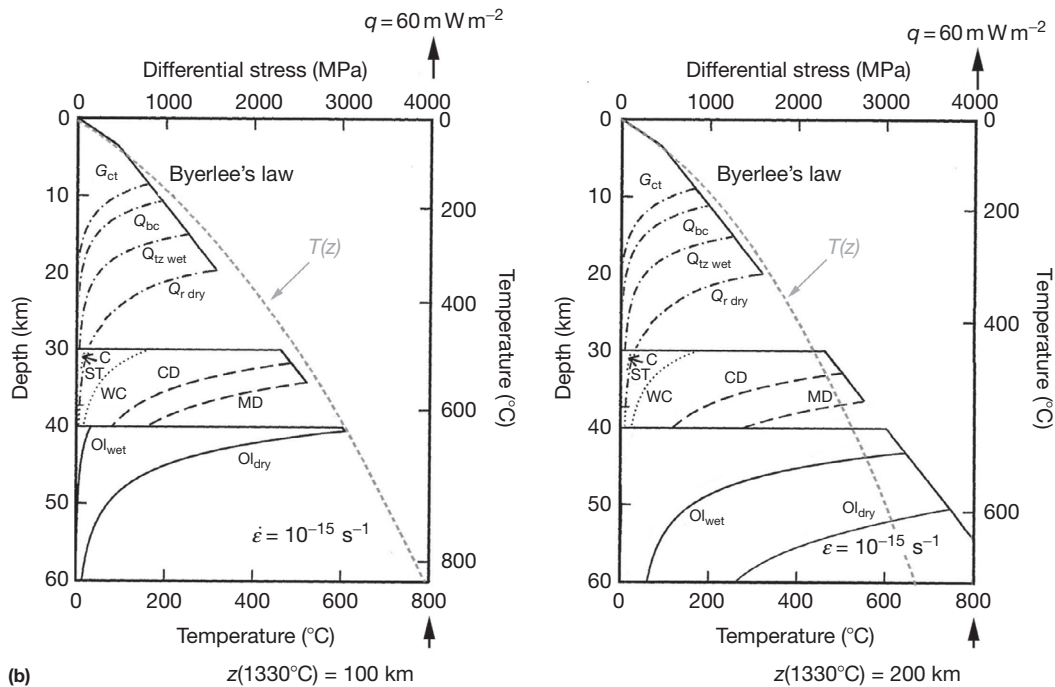


Figure 4 (Continued) (b) Influence of compositional variation, plate thickness $a=z(1330^\circ\text{C})$, and fluid content on continental yield stress envelope (YSE) computed for typical surface heat flow, q , of 60 mW m^{-2} but two different thermal models: equilibrium thermal plate thickness of 100 km (left; Chapman, 1986) and of 200 km (right; plate cooling model, Appendix B (Burov and Diamant, 1995)). CD, dry Columbia diabase; MD, dry Maryland diabase; WC, Pikvitonei granulate; ST and C, diabase from Shelton and Tullis (1981) and Caristan (1982). The upper crust is wet quartzite from Gleason and Tullis (1995); Ol_{dry} and Ol_{wet} are dry and wet dunites from Chopra and Paterson (1984). Q_{bc} refers to dry quartzite from Brace and Kohlstedt (1980). G_{ct} is wet granite from Carter and Tsenn (1987). Q_r is for extra strong dry quartz from Ranalli (1995). Comparison of the YSE computed for two different thermal plate thicknesses demonstrates large ambiguities in estimation of the mantle strength: the continental heat flux used as a common surface boundary condition mainly affects crustal temperature distribution. The mantle part of the geotherm primarily depends on the position of the thermal bottom of the lithosphere. The left ‘weak’ YSE results from erroneous assumption that continents have the same or even smaller thickness than the oceans (Jackson, 2002). The use of the left YSE results in ridiculously small predictions of the mantle strength. Left part of the figure is based on Mackwell et al. (1998). The continental YSEs based on the assumption of weak mantle rheology (left) are dubbed ‘crème brûlée’ models, whereas those that include strong crustal and mantle layers are dubbed ‘jelly sandwich’ rheology. The failure envelopes shown in the left match those from Jackson (2002). The Jackson’s (2002) envelopes are based on Figure 4 from Mackwell et al. (1998). The parameters are given in Tables 2–3.

(Continued)

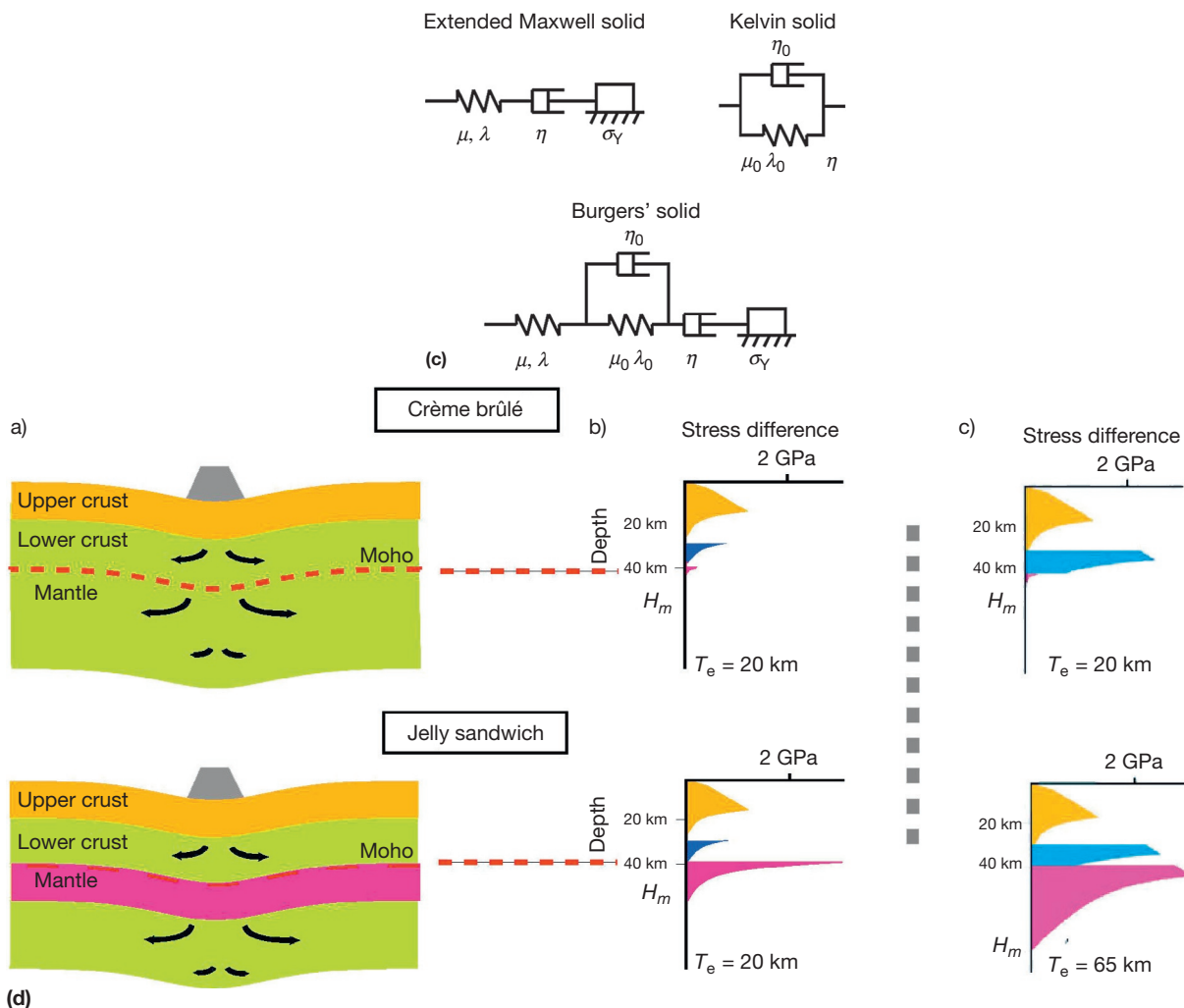


Figure 4 (Continued) (c) Various ways to combine rheological terms in constitutive models of materials: the extended Maxwell serial model, Kelvin parallel model, and Burger's combined model (and so on). The resulting properties of solids largely depend on how the rheological terms are interconnected. Knowledge of the parameters of each rheological term is not sufficient for the prediction of the mechanical behavior of materials. (d) Schematic diagram illustrating contrastingly different models for the long-term strength of continental lithosphere (Burov and Watts, 2006). In the crème brûlée model, the strength is confined to the uppermost brittle layer of the crust, and compensation is achieved mainly by flow in the weak upper mantle. In the jelly sandwich model, the mantle is strong and the compensation for surface loads occurs mainly in the underlying asthenosphere. a – Models of deformation. The arrows schematically show the velocity field of the flow. b – Brace–Goetze failure envelopes for a thermotectonic age of 150 My, a weak undried granulite lower crust, a uniform strain rate of 10^{-15} s^{-1} , and either a dry (jelly sandwich) or wet (crème brûlée) olivine mantle. H_m is the short-term mechanical thickness of the lithosphere and T_e is the long-term elastic thickness. Other parameters are as given in Table 2. The two envelopes match those in Figure 5(b) and 5(d) of Jackson (2002). They yield a T_e of 20 km (e.g., Burov and Diamant, 1995), which is similar to the thickness of the most competent layer. This is because the competent layers are mechanically decoupled by weak ductile layers and so the inclusion of a weak lower crust or strong mantle contributes little to T_e . c – Brace–Goetze failure envelopes for a thermotectonic age of 500 My. Other parameters are as in – b – except that a strong, dry, Maryland diabase has been assumed for the lower crust. The two envelopes show other possible rheological models: one in which the upper and lower crust are strong and the mantle is weak (upper panel) and another in which the upper and lower crust and the mantle are strong (lower panel). The assumption of a strong lower crust in the weak mantle model again contributes little to T_e because of decoupling, although T_e would increase from 20 to 40 km if the upper crust was strong at its interface with the lower crust. In contrast, a strong lower crust contributes significantly to the T_e of the strong mantle model. This is because the lower crust is strong at its interface with the mantle and so the crust and mantle are now mechanically coupled.

It should be noted, however, that there is no direct evidence for the applicability of the rule [26c] in nature. For example, the logarithmic average of the effective viscosities is sometimes used following the hypothesis that the weakest flow

mechanism dominates the overall ductile behavior. The contribution of each ductile flow mechanism can also be estimated from general physical considerations, for example, from total work minimization.

6.03.3.2 Kelvin Model

The alternative Kelvin (Voigt) model implies that the total stress equals the sum of the elastic σ^e and viscous stress σ^v , while ϵ_{ij}^e and ϵ_{ij}^v are equal:

$$\begin{aligned}\sigma_{ij}^K &= \sigma_{ij}^e + \sigma_{ij}^v = 2\mu e_{ij}^k + 2G^k e_{ij}^k \\ \epsilon_{ij}^e &= \epsilon_{ij}^v\end{aligned}\quad [27]$$

Its extended viscous–elastic–plastic version is

$$\begin{aligned}\sigma_{ij}^{K,\text{ext}} &= \sigma_{ij}^K + \sigma_{ij}^P \\ \epsilon_{ij}^e &= \epsilon_{ij}^v = \epsilon_{ij}^P\end{aligned}\quad [28]$$

Although the minerals most probably do not behave as Kelvin solids at microscale, their aggregates and macrostructural assemblages may do.

6.03.3.3 Mixed Models

Observations of long-term loading of the lithosphere such as by seamounts (Watts, 2001) demonstrate a complex behavior, which involves initially Maxwell-type response with an exponential stress drop followed (after several My) by slowdown of stress relaxation so that long-term stress achieves some nearly constant level. This behavior evokes a generalized linear (Maxwell + Kelvin) model, or Burger's model, which represents a serial combination of a Kelvin model with an extended Maxwell model:

$$e_{ij}^B = e_{ij}^M + e_{ij}^K + e_{ij}^P \quad [29]$$

The viscous and elastic parameters of the Kelvin unit are not the same as those of the Maxwell unit. It is possible that relaxation of postseismic deformation may be controlled by the Kelvin term characterized by a viscosity several orders smaller than the Maxwell term (e.g., Pollitz et al., 2001). Present failure to establish any links between the Kelvin and Maxwell viscosities restricts interpretation of postseismic data in terms of the long-term properties of the lithosphere–asthenosphere system.

6.03.4 Uncertainties in the Experimental Rheology Laws

The uncertainties involved in the long-term rheological properties derived from experimental rheology data have produced confusing propositions for the long-term rheological strength of the crustal and mantle parts of the lithosphere (Figure 4(b) and 4(d)). These uncertainties derive from (1) uncertainties in rock mechanics data, (2) uncertainties in the thermal and other data used for construction of YSEs, (3) poor knowledge of the deformation mechanisms that really occur at depth, (4) uncertainties on the constitutive models, (5) additional (unaccounted for) factors influencing rock strength such as frictional heating, pressure variations, fluid content, chemical, or thermodynamic transformations (such as melanitization of shear bands), and (6) micro- and macrostructural effects, for example, layering and anisotropy, from 0.01 to 10^4 m scale.

6.03.4.1 Uncertainties of Rock Mechanics Data

Elastic and Byerlee's brittle parameters are relatively well constrained, with an uncertainty of 10–30% for the relevant depth intervals. Although the validity of Byerlee's law is questionable for fault zones (e.g., Chester, 1995) or at depths/pressures below 30–50 km (Kirby et al., 1991, 1996), this would primarily affect fault and seismic distribution but not regional deformation.

Ductile flow properties are the most uncertain, although modern techniques of experimental rock mechanics allow for sufficiently robust and cross compatible measurements of creep parameters (e.g., Kohlstedt, 2007; Kohlstedt et al., 1995), specifically after the advent of new techniques such as Paterson-type deformation testing machines (e.g., Bürgmann and Dresen, 2008). Yet, it is not the precision of experiments but extrapolation of their results to natural conditions that create major difficulties:

- With rare exceptions, experiments refer to simplified conditions such as uniaxial deformation or torque, whereas real rocks are deformed in several planes. In general, to accelerate deformation yet avoiding brittle failure, experiments are conducted at much higher temperatures than in nature. Extrapolation to lower-temperature conditions is not straightforward, since it is possible that other creep mechanisms may dominate at lower temperature (e.g., in olivine, power law dislocation creep may be replaced by GBS creep at temperatures below 800 °C). Creep mechanisms that take place in each particular experiment are not always well identified. It is not guaranteed that the same mechanisms are activated in natural conditions (e.g., at slower strain rates or lower temperatures). Recent studies based on new techniques (e.g., Patterson triaxial press) suggest that rock strength (e.g., for quartzite) may be twice as high as estimates obtained before the turn of the twentieth century (e.g., Bürgmann and Dresen, 2008). Yet, other studies show that accounting for some additional factors such as oxygen fugacity (Keefner et al., 2011) results in a factor of 5 smaller effective viscosity for dislocation creep (in dunite) than suggested by previous data. This indicates that further, probably significant revisions of rock properties are possible in the near future.
- Experimental strain rates are on the order of 10^{-9} – 10^{-4} s $^{-1}$, which is on average 10^{10} times faster than geologic strain rates (10^{-18} – 10^{-14} s $^{-1}$). Extrapolation of these data to geologic timescales is mathematically 'illegal' because the errors of such extrapolation may be of the same order as or larger than the predicted rock strength.
- The experiments refer to simple monophase minerals or synthetic or selected 'representative' rocks. Extension of their results to real aggregate compositions has to be justified (e.g., Kohlstedt et al., 1995). It is often assumed that the weakest of the most abundant mineral species defines the mechanical behavior of the entire rock. For granites, this is quartz, often replaced by quartzite in laboratory experiments. It was shown, however, that lower amounts of weak phases such as micas or albites may result in significantly smaller strength than that of quartz or quartzite (see discussion in Burov, 2002). It was also noted that polyphase aggregates are weaker than their constituents and that

- different mineral species may take a lead in the experiments and nature (e.g., [Kenis et al., 2005](#); [Kohlstedt et al., 1995](#)).
4. Experimental strain rates may vary in a different way from nature.
 5. Experiments are conducted on small rock samples of homogeneous structure. At larger scales ($>0.1\text{--}1\text{ m}$), rocks, specifically crustal, may be highly structured. Their mechanical resistance may depend on their macrostructure more than on the rheological properties of the microconstituents ([Evans, 2005](#); [Ji et al., 2000](#); [Kohlstedt et al., 1995](#)). For example, in strong mantle peridotites, strain may localize on weak mylonitic shear zones leading to overall weaker behavior (e.g., [Jin et al., 1998](#)).
 6. Water content influences rock strength. In general, rocks contain 0.05–0.1 wt% H_2O . The experiments usually consider ‘wet,’ ‘undried,’ or ‘dry’ rock samples ([Chen et al., 2006](#); [Mackwell et al., 1998](#)). However, for each particular region, it is difficult to know whether the rock is dry, wet, or partially wet (e.g., [Karato, 1986](#)). It is also argued that ‘dry’ experiments never reach the ‘dryness’ of some natural conditions (D. McKenzie, personal communication).
 7. Volatile fugacities and chemical and thermodynamic reactions modify the mechanical behavior of rocks. These factors are basically unknown or poorly controlled in nature.
 8. Temperature–pressure (P – T) conditions of experiments do not represent natural P – T conditions or loading paths (e.g., [Goetze and Evans, 1979](#)). Basically, it is only the ‘ P ’ or ‘ T ’ condition that is respected at any time. For example, in many cases, temperatures used in experiments are significantly higher than in nature.

Due to these uncertainties, [Brace and Kohlstedt \(1980\)](#) and [Kohlstedt et al. \(1995\)](#) had suggested that real crustal rocks may be significantly ‘softer’ than the experimental estimates. As a highly encouraging point, it should be noted, however, that the oceanic YSEs based on the dry olivine flow law demonstrate a very good correlation with the observed T_e values, age, and thermal state of the lithosphere (e.g., [Watts, 2001](#)). For continents, one can attempt to validate or reparameterize rock mechanics data by using observations of long-term deformation, T_e data, and thermomechanical models ([Burov and Watts, 2006](#); [Watts and Burov, 2003](#)).

6.03.4.2 Uncertainties in the Synthetic Yield Stress Envelopes

In addition to the uncertainties involved in the rheology laws, there are many specific YSE uncertainties arising from various assumptions on thermal distribution, background strain rate, plate structure, and rheological composition of the lithosphere.

One of the most misleading, if not disastrous, assumptions is that of the homogeneous background strain rate. Analytic and numerical models (e.g., [Burov and Poliakov, 2001](#); [Kusznir, 1991](#)) predict strong (orders of magnitude) vertical and horizontal variations in strain rate in deforming lithosphere, for example, in the ductile lower crust of continents. As a result, the effective strength may deviate by up to 30–80% from that predicted from constant-rate YSEs.

Ductile behavior is extremely sensitive to temperature and the presence of fluids (e.g., [Chen et al., 2006](#)). A slight variation in the background geotherm, thermal conductivity, or fluid content may ‘transform,’ for example, hard dry quartzite ([Kirby and Kronenberg, 1987](#)) to some equivalent of soft calcite ([Kohlstedt et al., 1995](#)). In power law materials, shear stress weakly depends on the strain rate but strongly depends on temperature, T , and activation energy Q . A simple increase in Q by a factor of 2 ‘converts’ weak quartzite into the hardest olivine or clinopyroxene ([Table 2](#)). In the continental crust, behaviors predicted by the strongest dry flow laws can be turned into those predicted by the weakest wet flow laws by a small adjustment of the poorly constrained concentration of radiogenic heat sources. Internal heat production, not accounted for in laboratory experiments, may also influence long-term creep mechanisms (softening).

The geotherm, $T(z)$, controls not only the ductile strength of the lithosphere but also, indirectly, its brittle strength through the influence of temperature on the depth of the BDT. Different assumptions on $T(z)$ produce important differences in the predicted strength ([Figure 4\(b\)](#)). In continents, age has no unique relation with thermal structure, and the surface heat flow is ‘polluted’ by up to a 50% contribution from crustal radiogenic heat production ([Turcotte and Schubert, 2002](#)). The equilibrium thermal (or geochemical, seismic, or gravimetric) thickness of continental plates, a (defined as the depth to 1330 °C), is an important parameter needed for consistent introduction of bottom boundary conditions in thermal models. For continents, a may vary from 150 to 350 km. a controls the mantle part of the geotherm much more than the surface heat flux, q . This explains why for the same value of heat flux, q , and identical rheological parameters, some authors predict very ‘hot’ geotherms and, consequently, weak mantle behavior ([Jackson, 2002](#); [Mackwell et al., 1998](#)), whereas others (e.g., [Jaupart and Mareschal, 1999](#); [Jaupart and Mareschal, 2007](#) and this study) predict colder geotherms, hence stronger behavior. Seismic and seismic tomography data and geothermal data (e.g., [Jaupart and Mareschal, 1999, 2007](#)) suggest that continental lithosphere should be on average thicker than oceanic lithosphere (150–350 km compared to 100–125 km). However, it is not uncommon that, for simplicity, the same small thickness is imposed for both continents and oceans ([Jackson, 2002](#); [Figure 4\(b\)](#), right). This assumption potentially results in largely underestimated (50–100%) mantle strength.

6.03.4.3 Uncertainties in Deformation Mechanisms in Nature

There is a growing understanding that ductile, elastic, or brittle deformation cannot be treated separately from each other. In general, mixed behaviors should prevail. Semibrittle/semiductile behaviors can be developed near zones of BDT or large shear bands. A number of studies argue that under upper crustal conditions, ‘non-Byerlee’s’ strain rate-dependent frictional mechanisms may be activated simultaneously with ductile creep. This leads to a weak, ductile-like constitutive law for the brittle regime. According to these studies (e.g., [Chester, 1995](#)), upper crustal strength may be limited to maximum 50 MPa at 6–15 km depth. Observations of crustal rebound ([Bills et al., 1994](#)) indicate that the strength of the upper crust

may be strongly reduced below 3 km depth, with an estimated maximum viscosity below 10^{23} Pa s, which suggests stress levels <50 MPa. Many known natural examples show that ductile creep can start (even in pure quartz) at 5–6 km depth (S. Patterson, 2002, personal communication). ‘Conventional’ quartzite rheology (Ranalli, 1995) used for the upper crust is about 4 times stronger than ‘weakest’ estimates found in literature. Yet, it is twice weaker than last estimates obtained using modern Patterson testing equipment (e.g., Bürgmann and Dresen, 2008).

6.03.4.4 Role of Secondary Factors: Frictional Heating, Pressure, Fluid Content, Partial Melting, and Metamorphic Phase Changes

Fluid pressure reduces brittle strength (Figure 1(b)), and a small (<0.1 wt% H₂O) amount of fluids can (e.g., Figure 4(b); Table 2) decrease ductile rock strength by a factor of 2–3 (e.g., Mackwell et al., 1998). Yet, it is practically impossible to estimate fluid content *in situ*. The experimental data generally include only two sets for each type of rock: ‘wet,’ ‘undried,’ and ‘dry.’ ‘Dry’ rock may still have traces of fluid and ‘wet’ rock may be ‘wet’ to different degrees. When fluid content is unknown, the prediction for rock strength remains rather indefinite, between ‘wet’ and ‘dry’ states. Metamorphic phase changes and free fluids are the major factors that affect the lithosphere density and strength of subduction channels (Angiboust et al., 2012). First, activated by fluids, these changes lead to

formation of a very weak serpentinite layer that reduces friction in the subduction channel (e.g., Yamato et al., 2007). Second, dehydration of eclogitized crust leads to creation of a weak mantle wedge with the back-arc zone additionally weakened by associated partial melting. Third, lithosphere bending near subduction zones is greatly enhanced by flexural brittle–plastic yielding (Figure 5(c) and 5(f); Burov and Diamant, 1995) resulting in the formation of a series of water-saturated (lithostatic pressure drop = lower brittle strength) serpentinized (weak) normal faults that provide considerable additional weakening of the plate (Faccenda et al., 2009; Regenauer-Lieb et al., 2001). Combined, these three factors create the necessary conditions for one-sided oceanic subduction. Metamorphic phase changes and fluids also play a similar role at passive margins and in many other contexts. For example, melanitization of shear bands is sought to play a major role in strain localization in a variety of tectonic settings. In this case, the rheology of the host rock is of minor importance, while the deformation is conditioned by very particular properties of ultraweakened shear zones. In general, prograde metamorphic phases are denser and mechanically weaker than the parent rock. Thus, eclogitization of the crust may play an important role in the force balance acting on the subducting slab. Metastable reactions at the 410 km phase transition boundary have a double effect: depleted downwellings and fertile upwellings push–pull the slab in opposite directions.

Frictional heating $\partial T_{\text{shear}}/\partial t$ at fault zones (Regenauer-Lieb et al., 2001) may decrease ductile (including Peierls and GBS)

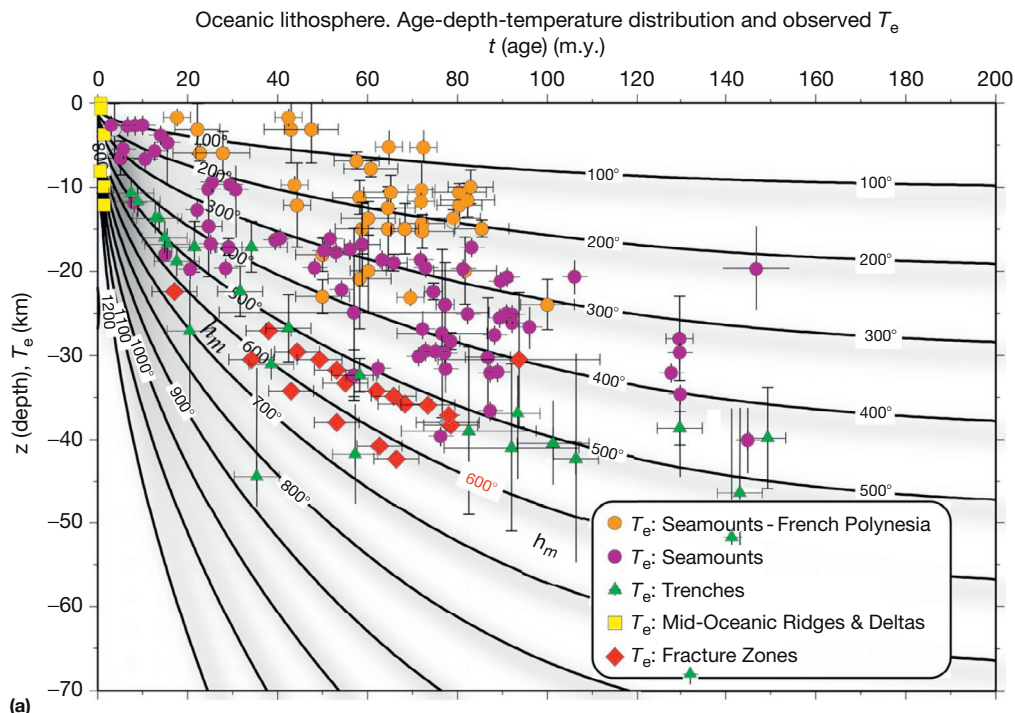


Figure 5 (a) Revealed correlation between the observed flexural strength T_e and age–temperature of the oceanic lithosphere. Thermal distribution is computed according to the plate cooling model (Burov and Diamant, 1995; Parsons and Sclater, 1977). The T_e data are superimposed with computed geotherms. The relevant estimates refer to zones with normal thermal gradient such as fracture zones and trenches. Naturally, the cases of seamount loading cannot be fitted with the standard cooling model due to both viscoelastic relaxation (younger mountains) and local thermal rejuvenation of the underlying lithosphere by hot-spot activity (Watts, 2001). However, locally adjusted thermal models confirm T_e correlation with the depth of the geotherm 400–500 °C, specifically for seamounts older than 10 My (Watts, 2001).

(Continued)

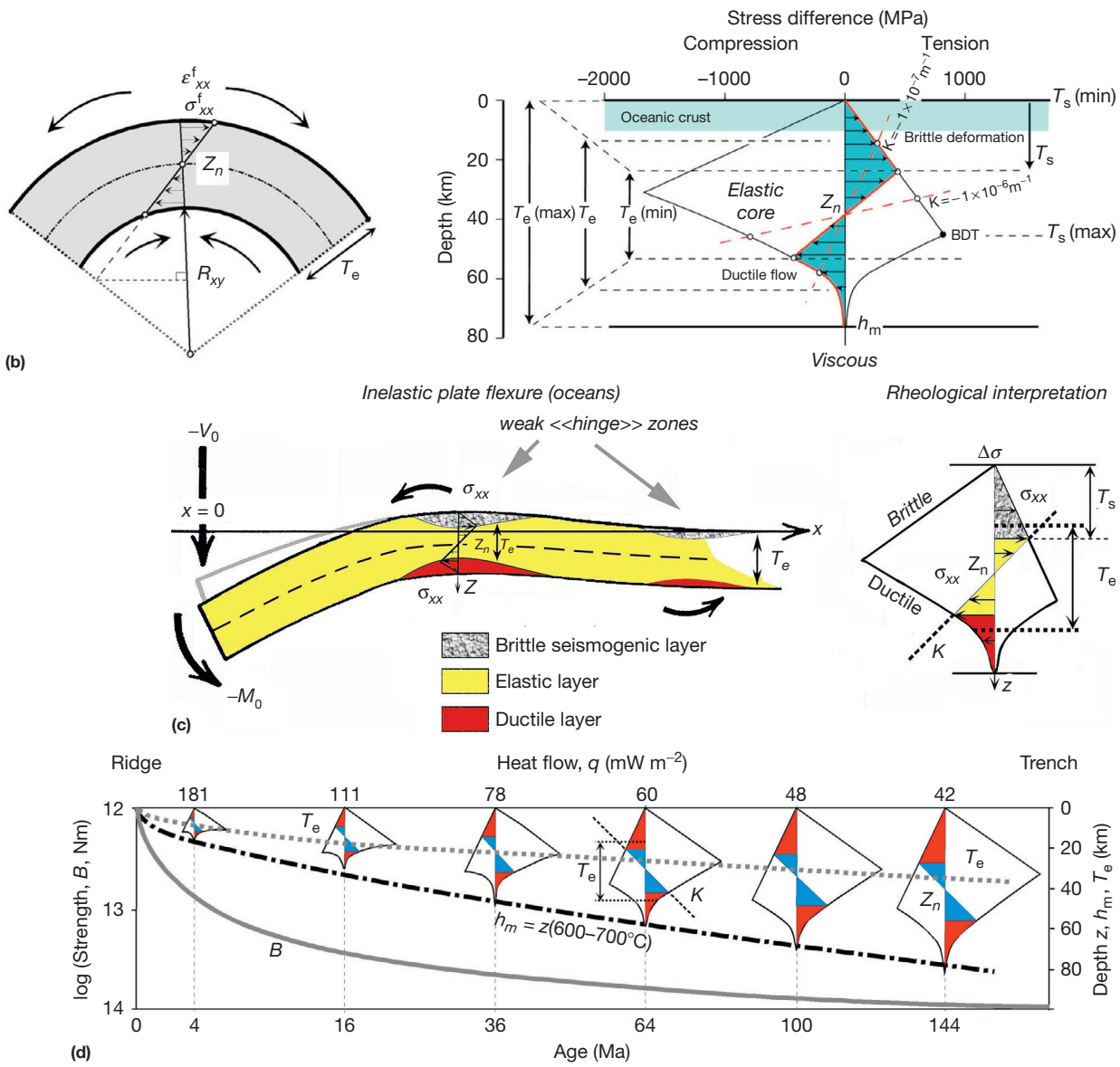


Figure 5 (Continued) (b) (left) Sketch of stress distribution due to bending of an ideal elastic plate. (right) Sketch of stress distribution in a bending viscous–elastic–plastic oceanic plate and interpretation of the seismogenic layer, T_s , and equivalent elastic thickness, T_e , of the oceanic lithosphere in terms of rheology (YSE) and its dependence on flexural stress gradient (reproduced from Watts AB and Burov E (2003)). Lithospheric strength and its relationship to the elastic and seismogenic layer thickness. *Earth and Planet Science Letters* 213: 113–131. ε_{xx}^f , σ_{xx}^f , and R_{xy} are flexural strain, stress, and local radius of flexure ($R_{xy} = -K^{-1}$), respectively. Thin solid line shows the YSE for 80 Ma oceanic lithosphere. The brittle behavior is controlled by Byerlee’s law, the ductile behavior by olivine power flow law ($n=3, A=7 \times 10^{-14} \text{ Pa}^{-3} \text{ s}^{-1}, Q=512 \text{ kJ mol}^{-1}$ (Kirby and Kronenberg, 1987)), and the thermal structure by the cooling plate model (Parsons and Sclater, 1977). The solid red line shows the stress difference for a load that generates a moment, M , of $2.2 \times 10^{17} \text{ N m}^{-1}$ and curvature, K , of $5 \times 10^{-6} \text{ m}^{-1}$. The figure shows that the load is supported partly by an elastic ‘core’ and partly by the brittle and ductile strength of the lithosphere. The red-dashed lines show the cases for K of $1 \times 10^{-7} \text{ m}^{-1}$ and $1 \times 10^{-6} \text{ m}^{-1}$, which bracket the range of observed values at trench–outer rise systems (Goetze and Evans, 1979; Judge and McNutt, 1991; McNutt and Menard, 1982). The figure shows that T_s corresponds to the depth of the intersection of the moment–curvature curve with the brittle deformation field but could extend from the surface, T_s (min), to the brittle–ductile transition (BDT), T_s (max). T_e , in contrast, could extend from the thickness of the elastic core, T_e (min), to the thickness of the entire elastic plate, T_e (max). Both T_s and T_e depend on the moment generated by the load and, hence, the plate curvature. Yet, T_s increases with curvature, while T_e decreases. This figure represents an ideal case of pure bending stress in which T_e and T_s can be interrelated. Generally, lithospheric regions where strain is sufficient to define T_s are in state of failure that may be largely produced by in-plane tectonic stress rather than by bending stress. In this case, T_s and T_e anticorrelate or have no direct relation. (c) Reinterpretation of flexure of an oceanic plate (Figure 2(a)) under assumption of realistic rheology (see also (b)). Inelastic flexure results in ‘plastic hinging,’ for example, formation of weak hinge zones at the inflection points. The observed T_e is thus horizontally variable and differs from that of an elastic plate. Flexural weakening is supposed to help initialization of subduction of cold old lithosphere. (d) Variation of the mechanical strength, of integrated strength B and equivalent elastic thickness, T_e , of the oceanic lithosphere as function of age and thermal structure. T_e of the lithosphere actually depends on the gradient of bending stress related to local plate curvature, K . T_e approximately equals the size of the ‘elastic core’ plus half size of the underlying brittle zone and half size of the ductile zone beneath. Note that B correlates with T_e . Note also that T_e cannot be interpreted as a depth to some specific level in the lithosphere. Yet, it correlates well with h_m or geotherm to 400–500 °C (reproduced from Watts AB (2001) *Isostasy and Flexure of the Lithosphere*, p. 458. Cambridge: Cambridge University Press).

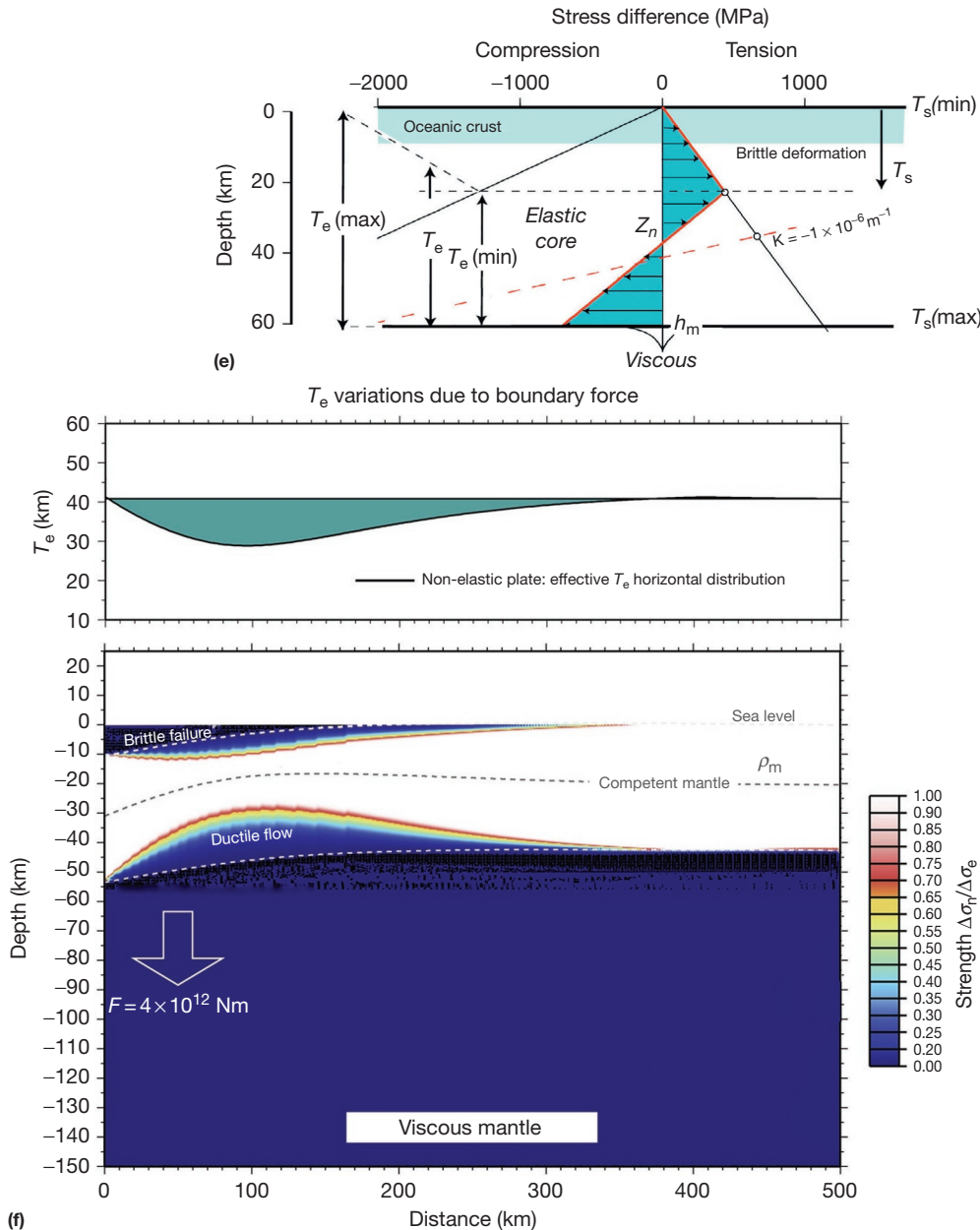


Figure 5 (Continued) (e) YSE based on the ‘crème brûlée’ rheology model: interpretation of the seismogenic layer, T_s and equivalent elastic thickness, T_e , under assumption of Jackson (2002) that the mechanical strength of the lithosphere is concentrated in the brittle layer. This case considers brittle–elastic lithosphere with zero strength ductile part, for the same typical amount of flexure ($K = 5 \times 10^{-6} \text{ m}^{-1}$) and T_s value (20 km) as in the case shown in (b). The figure demonstrates inconsistency of two simultaneous assumptions: of weak ductile mantle and $T_e = T_s$, due to geometric incompatibility between seismogenic layer (T_s) and elastic thickness (T_e). If $T_s = 20 \text{ km}$, then $T_e > 40 \text{ km}$. (f) Computed variations of oceanic lithosphere strength and elastic thickness in a bending viscous–elastic–plastic plate of 70 Ma (see also (c)). Plate flexure is caused by a boundary force of $4 \times 10^{12} \text{ N}$ per unit length. Note the formation of a large weakened zone including normal faulting at top. It is believed that water penetrates in the flexurally induced normal faults resulting in additional drastic weakening of the lithosphere (reduction of brittle strength due to fluid pressure and serpentinization). Together with inelastic yielding, these factors allow for easy bending of oceanic plates at subduction zones, thus making subduction possible (without that strong old oceanic plates even though negatively buoyant will not subduct (i.e., flex down), due their high strength) (reproduced from Burov EB and Diamant M (1995) The effective elastic thickness (T_e) of continental lithosphere: What does it really mean? *Journal of Geophysical Research* 100: 3895–3904).

strength, provoking metamorphic changes resulting in the appearance of softer phases or a change in fluid content (and thus in strength) through hydration/dehydration reactions:

$$\frac{\partial T_{\text{shear}}}{\partial t} = \text{frac} \times (\rho C_p)^{-1} \sigma_{II} \frac{\partial e_{II}^{\text{v,p}}}{\partial t} \quad [30]$$

where $\partial e_{II}^{\text{v,p}}/\partial t$ is an inelastic contribution to the effective shear strain rate. Slow (geologic rates) friction may produce about 100 °C temperature rise in shear zones such as major faults or subduction channels (Turcotte and Schubert, 2002). This would result in a local 30–50% strength reduction in quartz-rich and metamorphic rocks. Rapid seismic slip may generate,

at short timescales, very high temperatures resulting in melting (pseudotachylites) and hence in very low resistance to shear (e.g., John et al., 2009). Accounting for frictional weakening is an ambiguous problem because the strength drop due to ductile shear primarily depends on the absolute value of the temperature anomaly. Yet, while it is easy to estimate the total amount of thermal energy generated by shear, quantitative evaluation of the associated temperature anomaly is difficult due its strong dependence on the thickness of the shear band, stress, slip rate, and secondary factors such as fluids.

Rock behavior is also strongly conditioned by elastic properties. Although the criteria for brittle–plastic failure do not depend on elasticity, viscous–elastic behavior and shear heating do depend on it. Hence, behavior of the whole brittle–ductile–elastic system depends on elastic properties. Elastic modules increase with pressure and density, changing the effective behavior of the system. These parameters control stress relaxation in the lithosphere and may be responsible for transient states lasting for several My. Elasticity is responsible for the accumulation of mechanical energy; the elastic contribution to the shear strain rate is thus less than the total strain rate in the computation of shear heating.

Partial melting may play an important role in the evolution of spreading centers, passive margins, and rift and subduction systems. It can result in significant weakening and localization of deformation. Partial melting is usually addressed using the approach developed by McKenzie and Bickle (1988) and Katz et al. (2003).

The behavior of lithospheric plates is largely conditioned by deformation at their boundaries (e.g., collision). These boundaries are characterized by specific conditions. In particular, the subduction channel undergoes continuous phase changes and, consequently, rheology changes. Unfortunately, data on the rheology of metamorphic rocks are not abundant. As mentioned, the very few ideas that we can learn from direct observations in outcrops and rare laboratory experiments suggest that metamorphic rocks (e.g., micas; schists, serpentine, and eclogite) are considerably weaker than their parent phases.

6.03.4.5 Possible Ways to Parameterize Rheology Data for Geologic Timescales

There may be several ways to constrain rock rheology for geologic timescales (Figure 2(b)):

1. Observations of deformation in response to tectonic loading.
 - Observations of isostatic compensation: flexure, estimates of the equivalent elastic thickness of the lithosphere, T_e (e.g., Burov and Diamant, 1995, 1996; Forsyth, 1985; Pérez-Gussinyé and Watts, 2005; Watts, 2001).
 - Neotectonic vertical motions related to postglacial rebound and lake and submarine volcanic loading (e.g., Bills et al., 2007; Kaufmann and Amelung, 2000; Larsen et al., 2005; Passey, 1981; Peltier, 1974; Watts, 2001).
 - Physical estimates of minimal integrated strength of the lithosphere required for (1) subduction, (2) transmission of tectonic stresses over large spatial scales, and (3) stability of large geologic structures such as seamounts over their respective life spans (e.g., Bott,

1993; England and Molnar, 1997, 2005; Lachenbruch and Morgan, 1990).

- Observations of lithospheric folding (wavelength as a function of the integrated strength; Cloetingh et al., 1999; Gerbault et al., 1999; Lambeck, 1983; Table 5).
 - Indirect geophysical and geologic data tracing the geometry of deformed lithosphere and anomalous (e.g., low viscosity or high water content) zones: attenuation of S-waves, seismic anisotropy, petrology (P - T - t) paths, magnetotelluric sounding, gravity, observations of ductile and brittle behaviors in the outcrops including exhumed fault, fossil shear zones and crustal roots, and paleostress estimates (e.g., Austrheim and Boundy, 1994; Bürgmann and Dresen, 2008; Chen and Molnar, 1983; Cloetingh and Banda, 1992; Govers et al., 1992; Jolivet et al., 1998; Molnar and Tapponnier, 1981; Wei et al., 2001; Wever, 1989).
 - Estimates of the minimal integrated strength of the lithosphere required for long-term stability of geologic structures, subduction or transmission of tectonic stresses, and forces over large spatial scales, including horizontal pressure gradients caused by lateral variations in lithospheric density structure and topography (gravity potential energy theory, e.g., England and Molnar, 2005). For example, lithosphere must be strong enough to transmit ridge push and slab pull forces in the order of 10^{11} – 10^{13} N per unit length.
 - Lithosphere-scale numerical thermomechanical models of tectonic processes integrating multidisciplinary data, which allows for physical testing of the validity of data and hypotheses on lithosphere rheology; direct mechanical or thermomechanical models testing the stability of geologic structures or tectonic deformation styles as a function of implied rheological properties (e.g., Bassi, 1995; Beuchert and Podladchikov, 2010; Beuchert et al., 2010; Bird, 1991; Brun, 2002; Burov and Watts, 2006; Toussaint et al., 2004).
2. Observations of deformation in response to short-term loading.
 - Tidal deformation (e.g., Bills et al., 1994).
 - Postseismic relaxation (e.g., Avouac, 2007; DallaVia et al., 2005; Sabadini and Vermeersen, 2004).
 - Geodetic (GPS-INSAR) data (e.g., England and Molnar, 2005; Montesi, 2004).

Some authors argue about possible relationships between maximum depths of intraplate seismicity and long-term rheology (e.g., Jackson, 2002; Maggi et al., 2000). However, due to the different timescales of seismic events and long-term deformation, these relationships, if real, are not straightforward (e.g., Bürgmann and Dresen, 2008; Burov and Watts, 2006; Watts and Burov, 2003) and can hardly be exploited in practice.

Data based on observations of long-term deformation allow one to constrain a number of parameters such as T_e , F , σ , u , D_e , τ , h , L , λ , ϕ (Figure 2(b)), where T_e is directly related to the integrated plate strength (B) and F , σ , u are respectively horizontal force, stress, and convergence/extension velocity that are ultimately linked to maximum stress/strain values supported by the lithosphere, as well as to possible deformation styles: for example, continental subduction is virtually impossible for values of u below $2\text{--}3 \text{ cm year}^{-1}$ for a

Table 5 Estimates (Cloetingh et al., 1999 and references therein) for wavelengths of lithospheric folding (λ), effective elastic thickness (T_e), thermal age, t_o , the onset of folding (Ma), duration of folding (Ma)

λ (km)	T_e (km)	λ/T_e	Thermal age (Ma)	t_o , Onset of folding (My BC)	Present state of folding	Type
200–250 (1)	<40	>4–5	60	8	Active deformation	B
500–600(2)	50–70	10	400–600	60	Preserved	N
200 (3)	30	6–7	200	60	Preserved	B
200 (present)–>400–500 (preserved) (4)	25 (after recent reheating at 200 Ma)	8	>700	400–700	Preserved	B
300–360 (5)	>15*	>20	175–400	8–10	Active deformation	B
100–200 (6)	Not available, approx. >30	4–6	>100	60	Preserved	B/N
200? (7)	20–35	10–15	300	6	Active subsidence	N
200–250 (8)	15	13	175	8–10	Active deformation	B/N
350–400 (9)	6–9*	>30	<20	4–6	Active deformation	N
300 (10)	10–30	10	30	6–8	Active deformation	B/N
40 (11)	20–25*	2	<20	6–8	Active deformation	N
50 (12)	20–25*	2	20	6–8	Active subsidence	N
600 (13)	>100	6	>1200	1200	Preserved?	B
60 (14)	<10	6	65	35–8 My	Active deformation	B/N

Numbers in brackets refer to data sources: (1) Indian Ocean, (2) Russian platform, (3) Arctic Canada, (4) Central Australia, (5) Western Gobi, (6) Paris Basin, (7) North Sea Basin, (8) Ferghana and Tajik basins, (9) Pannonian Basin, (10) Iberian Basin, (11) Southern Tyrrhenian Sea, (12) Gulf of Lion, (13) Transcontinental Arch of North America, (14) Norwegian Sea. 'B' means regular folding style, 'N' means 'irregular,' and 'B/N' stands for the cases displaying both types of folding behavior. It is noteworthy that cases of abnormally high (>10) or low (<4) λ/T_e ratios (marked with *) correspond to hot (thermally reset) lithospheres, which implies dominant crustal folding. The high ratios often correspond to very weak lithospheres loaded by large amounts of sediment, which increases the wavelength of folding. Small λ/T_e ratios (<4) may refer to plastic hinging achieved at large amounts of shortening, for which wavelength is a simple function of the amount of shortening and does not depend on h or T_e .

three-layer lithosphere (Burov and Yamato, 2008; Toussaint et al., 2004) or 1 cm year⁻¹ for a four-layer lithosphere (Yamato et al., 2007). D_e and τ are, respectively, the Deborah number and the relaxation/growth time of Rayleigh–Taylor instabilities related to viscosity and density contrasts in the lithosphere. λ is the characteristic wavelength of unstable deformation (folding or boudinage; see later Section 6.03.5.7), which is a function of the thickness of the competent layers within the lithosphere. h and L are, respectively, the characteristic height and horizontal size of process-induced topography, related to plate strength and rheology. ϕ is the subduction or major fault angle that can be indicative of the brittle properties and overall plate strength (subduction) of the plate.

Interpretations of short-term deformation data are not certain, because there is no evidence that mechanisms of short-term deformation are the same as the mechanisms of long-term deformation. As mentioned, this concerns first of all not only intraplate seismicity data but also postseismic relaxation data (e.g., Freed et al., 2007). For example, it is suspected that accelerated postseismic creep may occur due to cavitation in fine-grained mylonitic shear zones in the lower crust. By comparison with rock mechanics experiments, one can expect that the duration of deformation should exceed several years to assure that it is relevant to long-term properties.

6.03.5 Rheology and Structure of the Oceanic Lithosphere

6.03.5.1 Goetze and Evans Yield Stress Envelopes: Age Dependence of the Integrated Strength

Yield stress envelopes (Figure 4(a)) for oceanic lithosphere are based on Byerlee's law for the brittle part and on the dry olivine flow law for the ductile part. A single olivine flow law is generally used as thin basaltic oceanic crust deforms in the brittle regime and does not need a separate flow law. The geotherms $T(z)$ used for computation of the ductile strength are derived from a half-space cooling plate model assuming constant surface and bottom temperature boundary conditions (Parsons and Sclater, 1977; Turcotte and Schubert, 2002):

$$\frac{T - T_{z0}}{T_m - T_{z0}} = \text{erf} \left(\frac{z}{2\sqrt{\chi t}} \right) \quad [31a]$$

$$\frac{z}{2\sqrt{\chi t}} \equiv \eta$$

where t is time (age), χ is thermal diffusivity, and erf is error function,

$$\text{erf}(\eta) = \frac{2}{\sqrt{\pi}} \int_0^\eta e^{-\lambda^2} d\lambda \quad [31b]$$

$$\gamma(T_{z0}) \approx z|_{x=0} + A\sqrt{\chi t} \quad [31c]$$

T_m is both the initial and bottom temperatures (e.g., 1330 °C), T_{z0} is the surface temperature (e.g., 0 °C), and $z|_{x=0}$ is the depth of the spreading center (e.g., 2500 m). $\gamma(T_{z0})$ is model-predicted depth of sea bottom derived under the assumption of simple local isostasy (i.e., $T_e=0$), for which the value of the parameter A varies from 0.0625 to 0.0825 depending on the assumed reference density. As can also be seen from [Figure 4\(a\)](#), the mechanical bottom h_m of the lithosphere roughly follows the isotherm of 500 °C:

$$h_m \approx z(500^\circ\text{C}) \approx (\chi t)^{1/2} \quad [32]$$

Predictions of sea bottom depths based on eqns [31] and the hypothesis of local isostasy fit the observations only for ages smaller than 70–100 Ma. For older ages (yet far from subduction zones), the predicted bottom depths are 20–30% larger than the observed bathymetry, mainly because the lithospheric strength increases with age, resulting in growing contribution from regional isostatic compensation that locally negates a part of thermal subsidence, and because the lithosphere reaches nearly stationary state, for which the half-space cooling model is no more applicable. Some authors also point to the effect of small-scale convection below the lithosphere that may be equivalent to constant basal heat flow boundary condition, instead of constant temperature boundary condition ([Doin and Fleitout, 1996](#)). Assumption of small-scale convection, whose existence is yet to be proved, would shift the geotherms of 500–600 °C up by about 100 °C. It provides a slightly better fit between the predicted and observed bathymetry for old lithosphere (>100 Ma). However, as mentioned previously, a similar effect can be expected from strengthening of the lithosphere with age or due to the fact that the lithosphere approaches a permanent regime.

6.03.5.2 Rheology and Observations of Flexure (T_e Data)

The lithosphere responds to surface and subsurface loads by bending ([Figure 2\(a\)](#)). Bending is characterized by vertical deflection, $w(x)$ with a local radius of curvature, $R_{xy}(x)$ or curvature, $K(x) = -R_{xy}^{-1} = \partial^2 w / \partial x^2$. The amplitude and wavelength, λ , of bending depend on the flexural rigidity D or equivalent elastic thickness T_e . D actually provides a direct measure for the integrated long-term strength of the lithosphere and is linked to the equivalent elastic thickness of the lithosphere, T_e : $D = ET_e^3(12(1-v^2)^{-1})$. The flexural equation, when written in the form that uses bending moment $M_x(x)$, is rheology-independent. The elasticity is then used as the simplest rheological interpretation of bending strength. D and hence T_e are estimated by fitting the observed flexural profiles (Moho depression for continents or bathymetry for oceans) to the solution of thin plate equation:

$$\frac{\partial^2}{\partial x^2} \left(\underbrace{\frac{ET_e^3}{12(1-v^2)} \frac{\partial^2 w(x)}{\partial x^2}}_{D(x)} \right) + \frac{\partial}{\partial x} \left(F_x \frac{\partial w(x)}{\partial x} \right) + \Delta \rho g w(x) = \rho_c g h(x) + p(x) \quad [33]$$

where F_x is the horizontal fiber force, $\Delta \rho$ is the density contrast between surface material (topography/sediment) and

asthenosphere, ρ_c is the density of surface material, $h(x)$ is the initial topographic elevation, and $p(x)$ is any additional surface or subsurface load. For inelastic plates, T_e and D represent the ‘condensed’ plate strength linked to the integrated plate strength B (eqn [22]). T_e is therefore a direct proxy for the long-term integrated strength of the lithosphere, B (see [Watts, 2001](#)). For example, for a single-layer plate of thickness h_m with $T_e = T_{e_ocean}$,

$$B = \int_0^\infty \sigma_{xx}^f(x, y, t, \dot{t}) dz \text{ while } T_{e_ocean} \\ = \left(12 \left(\frac{\partial \sigma_{xx}^f}{\partial y} \right)^{-1} \overbrace{\int_0^{h_m} \sigma_{xx}^f(z - Z_n) dz}^{M_x(x)} \right)^{1/3}; T_{e_ocean} < h_m \quad [34]$$

where σ_{xx}^f is bending stress ([Burov and Diament, 1995](#)). For an inelastic rheology, T_e is smaller than h_m ([Figure 5\(b\)](#)) and has no direct geometric interpretation but is derived from D and M . D and T_e may spatially vary due to their dependence on local bending that leads to localized plate weakening (called *plastic* or *ductile hinging*) in the areas of utmost flexure ([Figures 2\(b\)](#) and [5\(c\)](#)), for example, near *subduction zones* or below mountains and islands. M and D are obtained from depth integration of bending stress σ_{xx}^f which is a function of local plate curvature $K(x) = \partial^2 w / \partial x^2$ (e.g., [Burov and Diament, 1995](#)):

$$\sigma_{xx}^f(z, K) \approx \min \left(\sigma_b(z), \sigma_d(z), K(z - z_n(K)) E (1 - v^2)^{-1} \right) \\ D(x, K) = \left| \frac{M(x, K)}{K} \right| \\ T_e(x, K) = \left(M(x, K) \frac{12(1-v^2)}{EK} \right)^{1/3} \quad [35]$$

Here, $z_n(K)$ is the ‘floating’ depth to the neutral stress free plane: $z_n(K) \rightarrow 0.5h_m$ as $K \rightarrow 0$. By comparing observations of flexure in the regions of long-term surface loading by, for example, ice, sediment, and volcanoes, to the predictions of simple elastic plate models, it has been possible to estimate T_e and thus B , in a wide range of geologic settings. Oceanic flexure studies suggest that T_e is in the range 2–40 km and depends on load and plate age ([Figure 5\(a\)](#)). These results are consistent with the predictions of rock mechanics, so that T_e values follow the age-controlled depth to 400–500 °C ([Figure 5\(d\)](#)). The Brace–Goetze YSEs ([Brace and Kohlstedt, 1980; Goetze and Evans, 1979](#)) predict that strength should increase until the depth of the BDT and then decrease in accordance with the brittle and ductile deformation laws. In oceanic regions, the failure curves are approximately symmetrical about the BDT where the brittle–elastic and elastic–ductile layers contribute equally to the strength. Since both T_e and BDT generally exceed the mean thickness of the crust (~7 km), there is a little doubt that the largest contribution to the strength of oceanic lithosphere comes from the mantle, not the crust.

[McAdoo et al. \(1985\)](#) used eqns [35] to calculate the ratio of $T_e(K)$ to h_m for the middle value of oceanic thermal age of 80 Ma, a dry olivine rheology, and a strain rate of 10^{-14} s^{-1} . They showed that for low curvatures (i.e., $K < 10^{-8} \text{ m}^{-1}$), the ratio is 1, indicating little difference between the elastic thickness values. However, as plate curvature increases, the ratio

decreases as T_e (K) decreases. For $K=10^{-6}\text{ m}^{-1}$, the ratio is ~ 0.5 , indicating a 50% reduction in the elastic thickness.

The tendency of the oceanic lithosphere to yield in the seaward walls of trenches can be understood in terms of simple mechanical considerations. Ideal elastic materials support any stress level. In the case of real materials, stress levels are limited by rock yield strength at corresponding depths. Flexural strain in a bending plate increases with distance from the neutral plane. Consequently, the uppermost and lowermost parts of the plate are subject to higher strains and may experience brittle or ductile deformation as soon as the strain cannot be supported elastically. These deforming regions constitute zones of mechanical weakness since the stress level there is lower than it would be if the material maintained elastic behavior and, importantly, the stress there is not greater or not lower than it would be at the limits of the elastic core that separates brittle and ductile regions. The level of brittle and ductile stress, however, is very far from being negligible. A load emplaced on the oceanic lithosphere will therefore be supported partly by the strength of the elastic core and partly by the brittle and ductile strength of the plate. The significance of T_e values that have been estimated at trenches is that it reflects this combined, integrated, strength of the plate.

As the topography of the Moho is accessible only from indirect observations, flexural models use various techniques to compute the geometry of the Moho or of the basement from gravity anomalies. Departures of these anomalies from those predicted by local isostatic models (e.g., Airy and Pratt) have long played a key role in the debate concerning the strength of the lithosphere. Modern isostatic studies follow either a forward or inverse modeling approach. In forward modeling, the gravity anomaly due, for example, to a surface (i.e., topographic) load and its flexural compensation is calculated for different values of T_e and compared to the observed gravity anomaly. The 'best fit' T_e is then determined as the one that minimizes the difference between observed and calculated gravity anomalies (e.g., Watts, 2001). In inverse (e.g., spectral) models, gravity and topography data are used to estimate T_e directly by computing the transfer function between them as a function of wavelength (e.g., admittance or coherence) and comparing it to model predictions. As for all potential field data, the inversion of gravity data has no unique solution. This makes inverse gravity–flexural methods generally less reliable than direct models in complex continental settings, although recent developments in this domain are marked by very significant improvements (Kirby and Swain, 2009, 2011) so that one has to draw a distinction between most admittance and early coherence analyses, which often used incorrect loading models or bias-prone windowing approaches, and the latest generation of synthetic-tested studies. Nevertheless, since inverse methods do not take into account boundary forces and moments at plate boundaries, they are still prone to biased results in the areas affected by active tectonics.

In oceanic regions, however, forward modeling and inverse modeling yield similar values of T_e . This is no better demonstration of this along the Hawaiian–Emperor seamount chain. Forward modeling reveals a mean T_e of 25 ± 9 km, while inverse (spectral) modeling based on the free-air admittance method yields 20–30 km (Watts, 1978). When the T_e estimates are plotted as a function of load and plate age (Figure 5(a) and

5(d)), they yield the same result: T_e increases with age of the lithosphere at the time of loading, being small (2–6 km) over young lithosphere and large over old lithosphere (>30 km).

6.03.5.3 Flexural Strength and Initiation of Oceanic Subduction

Strengthening of the lithosphere with age creates a number of difficulties for explanation of initialization of oceanic subduction (Cloetingh et al., 1982). Despite the widespread view that lithosphere subducts when it reaches maximum negative buoyancy due to cooling with age, at this moment, it also reaches a maximum flexural strength (Figure 5(d)) that normally should prevent downward bending of the plate and hence subduction. It has been argued (Cloetingh et al., 1982) that conditions for oceanic subduction initiation could be optimal for a narrow time interval around an age of 30 Ma after seafloor spreading, when gravitational instability and relatively low strength occur simultaneously. Later, McAdoo et al. (1985) and then Burov and Diament (1995) had provided a mechanism (Figures 2(a), 5(c), and 5(f)) that explains the possibility of downward bending of strong lithosphere due localized weakening cased by bending strains in the brittle and ductile parts of the plate. This phenomenon, called plastic hinging, results in local 30–50% T_e reduction allowing the plate to 'turn' over the weakened zone. Finally (see also Section 112.4.4), Faccenda et al. (2009) had suggested that flexural weakening of the lithosphere is further enhanced by fluids penetrating in the brittle part of the plastic hinge zone (Figure 5(c) and 5(f)). Fluids result in reduction of lithostatic pressure and hence of brittle strength and also reduce the ductile strength through serpentinization.

6.03.5.4 Intraplate Seismicity (T_s), T_e , and Brittle–Ductile Interactions

Intraplate seismicity is concentrated in a specific depth interval called the seismogenic layer (Figure 6(a)). The thickness, T_s , of this layer averages 15–20 km and rarely exceeds 40–50 km in both oceanic and continental lithosphere. In continents, most earthquakes thus naturally happen in the crust, since its average thickness is on the order of 40 km. Sub-Moho continental mantle earthquakes are rare (e.g., Deverchere et al., 1991; Monsalve et al., 2006; Tesauro et al., 2008; Figure 6(b)) to a point that their very existence is sometimes doubted (Jackson, 2002; Maggi et al., 2000).

According to rock mechanics data, brittle properties of the oceanic and continental lithosphere cannot significantly differ from each other. Hence, the similarity of T_s in oceans and adjacent continents might be suggestive of similar stress levels and thus of transmission of tectonic stress from oceanic to continental domain. However, some authors suggest that T_s is related to long-term lithospheric strength and thus to T_e (Jackson, 2002; Maggi et al., 2000; Figure 6(a)). These authors go further by suggesting that these parameters are equivalent thus inferring that the strength of the lithosphere resides only in its brittle part. For continents, this means that all plate strength is concentrated in the crust and implies that all previous T_e estimates for old continental plates that exceed crustal

thickness are incorrect. These ideas gave birth to the ‘crème brûlée’ rheology model for continents (strong crust–weak mantle), in contrast to the ‘jelly sandwich’ rheology model (strong upper crust–strong mantle).

From the mechanical point of view, it can be demonstrated that T_s and T_e cannot correspond to the same layer in the lithosphere (Burov and Watts, 2006; Watts and Burov, 2003).

Mechanical considerations suggest that T_s has its own significance. Of course, this does not exclude the possibility that T_s and T_e may have similar values. Yet, it was shown (Burov and Watts, 2006) that if $T_s \approx T_e$, then about half of the plate strength has to be supported by its ductile part. In this particular case, the quasielastic resistant core of the plate includes brittle and ductile layers in similar proportions.

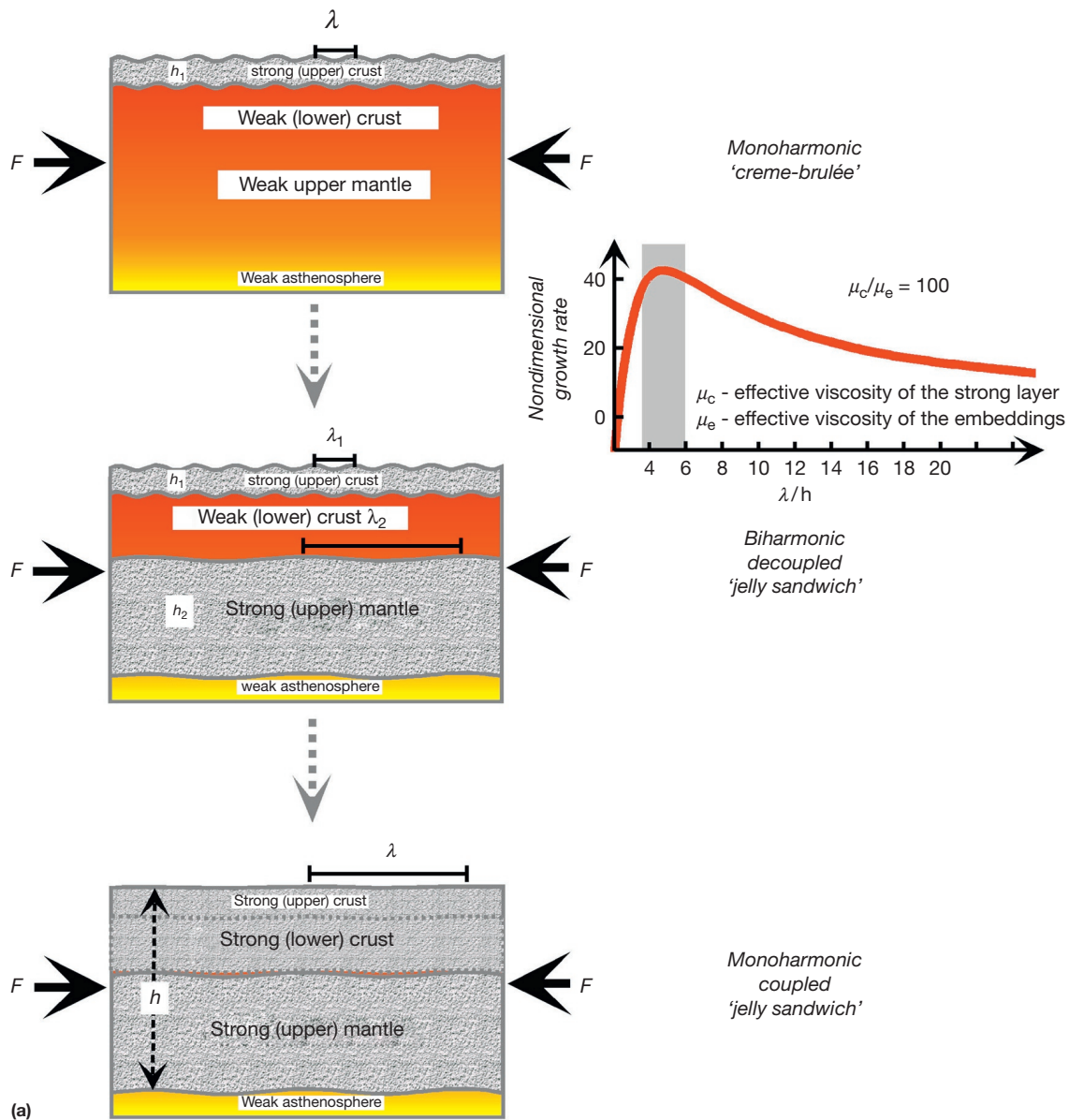


Figure 6 (a) Sketch of typical folding models for continental lithosphere (h_1 and h_2 are thicknesses of the competent crust and mantle, respectively). The system is submitted to compression by horizontal tectonic force F . In the case when the lower crust is weak (‘crème brûlée’ rheology model), the upper crust may fold independently of the mantle part (wavelength λ_2), with a wavelength λ_1 (decoupled, or biharmonic folding), which corresponds to the ‘jelly sandwich’ rheology model *sensu stricto*. Very young (<150 Ma) and very old (>1000 Ma) lithospheres (single competent layer or coupled crust and mantle) develop monoharmonic folding. Note that we call ‘jelly sandwich’ all rheological profiles that include both strong upper crust and mantle; thus, the case of very old coupled lithosphere from the bottom of the figure also corresponds to the ‘jelly sandwich’ concept. Inset shows the analytic estimate for the growth rate of strongly non-Newtonian folding (coupled layers, non-Newtonian rheology) as a function of λ/h for a typical ratio of the effective viscosities of the competent layer and embeddings (100 (reproduced from Burov EB, Lobkovsky LI, Cloetingh S, and Nikishin AM (1993) Continental lithosphere folding in Central Asia (part 2), constraints from gravity and topography. *Tectonophysics* 226: 73–87)). Shaded rectangle shows the range of the dominating λ/h ratios (4–6).

It was found, from force balance considerations (e.g., Bott, 1993; Cloetingh and Wortel, 1986; Molnar and Lyon-Caen, 1988; Zoback, 1992), that representative tectonic stresses and intraplate forces cannot exceed 100–600 MPa and 10^{13} N per unit length (meter), respectively. Byerlee's law predicts that brittle strength linearly increases with pressure and, hence, depth (Figures 1, 4(a), 4(b), and 5(b)). Near the surface, brittle strength is 0–20 MPa, but it is 30–100 times higher in oceanic and continental mantle at 40 km depth: 0.6–2 GPa in oceans (depending on fluid pressure) and around 2 GPa in continents (no fluid pressure). Figure 5(b) demonstrates that bending stress, and thus the probability to reach brittle strength limits, decreases while approaching the neutral surface. For the previously mentioned two reasons, the upper crustal layers fail more easily than mantle layers. At 50 km depth (the maximum depth of distributed seismicity), dry brittle rock strength is 2 GPa. Assuming a 100 km thick lithosphere, one needs a horizontal tectonic force of 10^{14} Nm to reach this strength. This value is improbable since it is one or two orders of magnitude higher than estimates for intraplate forces. A 2 GPa stress level may probably be reached only exceptionally, for example, at location of inflection points, where the sum of tectonic and bending stress is maximum. Yet, as mentioned, the absence of preexisting fractures in temperature-pressure healed mantle rock would prohibit Byerlee's failure even if the differential stress level meets the required limit.

Discussions on continental rheology stem from both the uncertainties in the rheology laws and the conflicting results on T_e from continental studies. In contrast, oceanic T_e estimates are considered to be robust. T_e - T_s relations thus can be best understood using oceanic data. When all oceanic T_s data and T_e

data are plotted on the same depth plot, they appear to correlate (Figure 6(a)). Yet, when one separates the extensional and compressional events, the correlation is not observed: extensional earthquakes are systematically found at two times shallower depth than the corresponding T_e values (Watts and Burov, 2003). This can be understood if one remembers that brittle (Byerlee's law) extensional failure requires nearly two times smaller stress than compressional failure. This leads to the conclusion that earthquake depths are primarily controlled by intraplate stress level. Contrary to T_e , for a fixed intraplate force per unit length F , T_s must decrease with increasing integrated strength of the lithosphere B ($F < B$):

$$T_s \approx Y \left(F/T_e + \sigma_{xx}^f |_{z=T_s} \right) / \rho g \quad [36]$$

$T_e(\text{oceans}) < \approx 0.7 h_m$

The factor $Y = 0.6^{-1} - 0.85^{-1}$ comes from eqn [9], and $\sigma_{xx|_z}^f = T_s$ is flexural stress (eqns [35]) at the depth $z = T_s$. Equation [36] shows that T_s decreases with increasing T_e . Thus, T_s and T_e do not correlate but anticorrelate for all $F < B$ ($F = B$ corresponds to whole-scale plate failure and is incompatible with flexural deformation; $F > B$ is not possible). For an unbent plate, T_s can be equal to T_e only if $T_e = (0.8 F/\rho g)^{1/2}$. If $F = 10^{13}$ N m, $T_s < 15$ –16 km, but $T_e = 30$ km (Figure 5(b)). For smaller F , $T_s < \frac{1}{2} T_e$. If one accepts the CB rheology model where ductile mantle has no contribution to the bending strength (Figure 5(e)), then $T_e \geq 2 T_s$, which means that this hypothesis is mechanically inconsistent with the assumption that T_e and T_s are equivalent. Flexural stress σ_{xx}^f may increase the value of T_s by a factor of 2–3, but at the same time, it would decrease T_e by the same factor (Figure 5(e)). As result, in oceans,

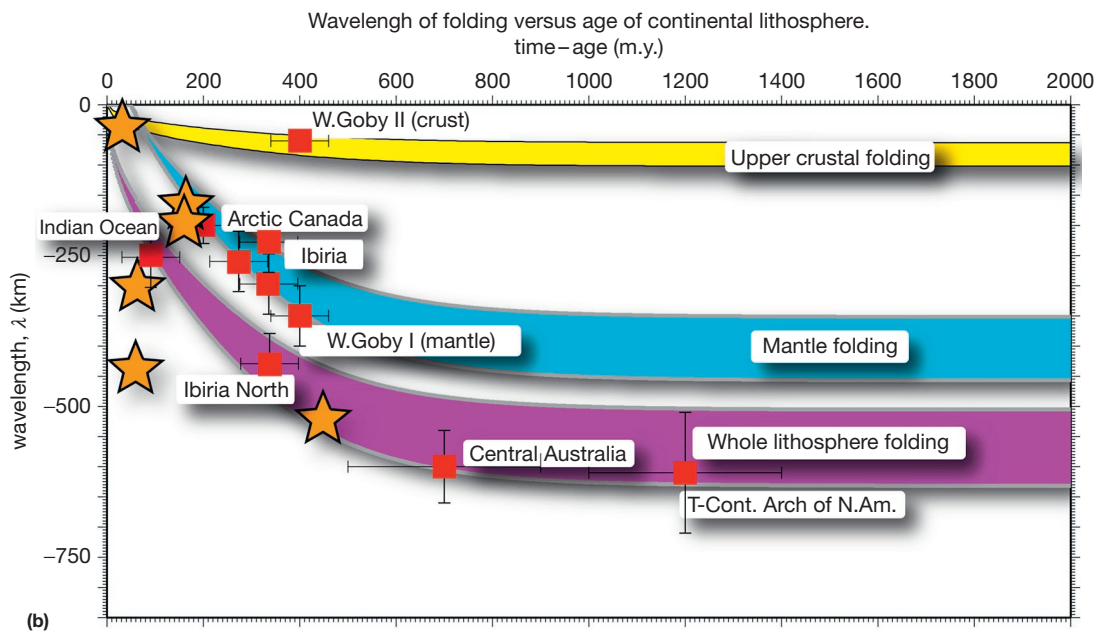


Figure 6 (Continued) (b) The observed wavelength of folding (Table 5) as a function of thermal age (calculated according to the model of Burov et al. (1993)). Numbers correspond to the ones used in the Table 5. Squares show the cases of 'regular' folding, whereas the stars mark 'irregular' cases (variable wavelengths, large amounts of shortening, important sedimentary loads, etc.). Different theoretical curves correspond to the crustal, mantle (supporting the presence of the decoupled rheology), and 'welded' folding (modified from Cloetingh S, Burov E, and Poliakov A (1999) Lithosphere folding: Primary response to compression? (from central Asia to Paris Basin). *Tectonics* 18: 1064–1083).

(Continued)

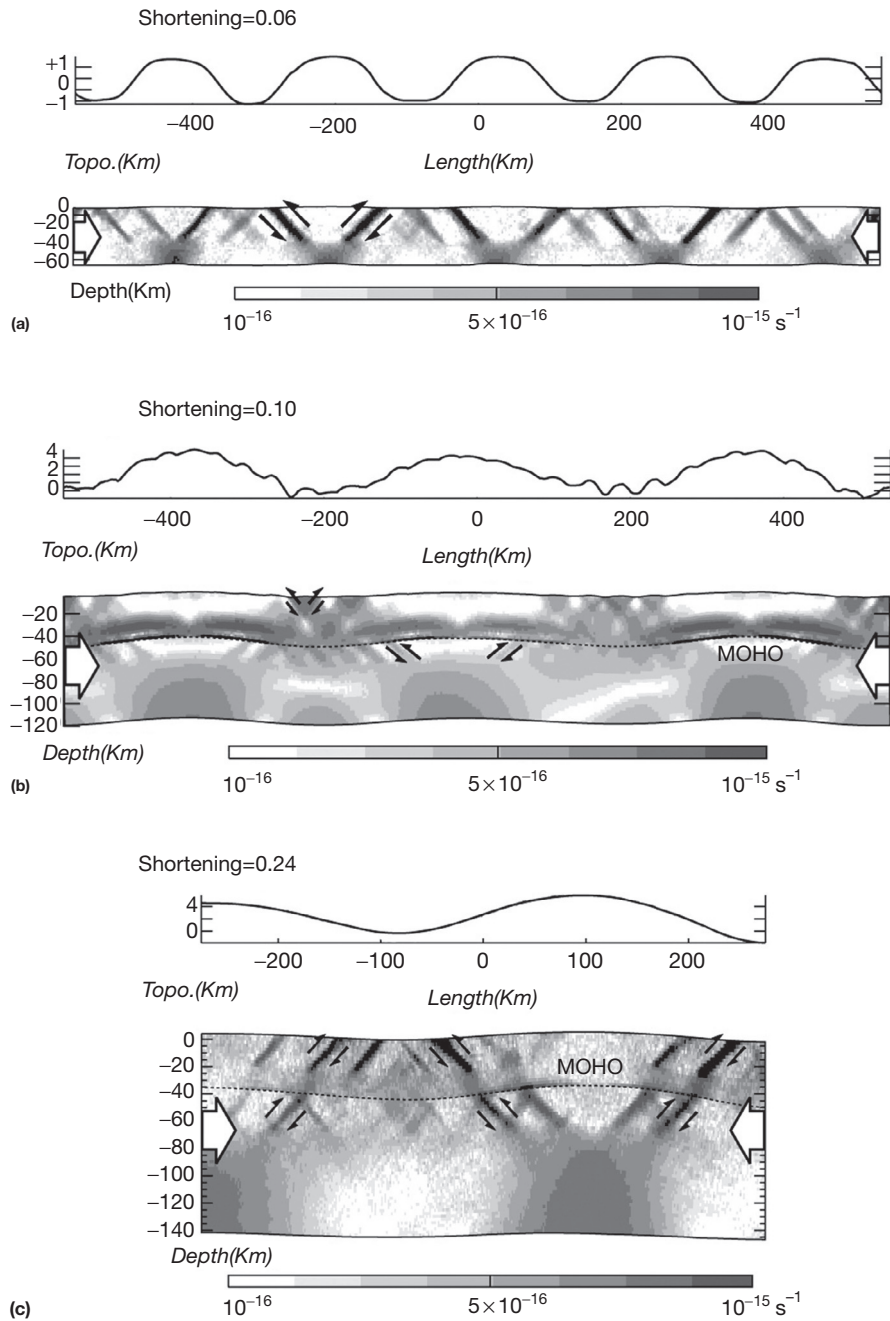


Figure 6 (Continued) (c) Topography and logarithm of strain rate field predicted from the direct numerical thermomechanical experiments on high-amplitude folding in brittle–elastic–ductile for oceanic lithosphere, in case ‘a’ ($T_e \sim 40$ km rheology profile 4 for 50–75 Ma in [Figure 9\(a\)](#)), and continental lithosphere in case ‘b’ ($T_e \sim 60$ km, rheology profile 2 for 250 Ma in [Figure 9\(a\)](#)) and case ‘c’ ($T_e \sim 80$ km, rheology profile 2 for 750–1000 Ma in [Figure 9\(a\)](#)). All snapshots correspond to ~ 7 My since the onset of shortening (modified from Gerbault M, Burov EB, Poliakov A, and Dagnières M (1999) Do faults trigger folding in the lithosphere? *Geophysical Research Letters* 26: 2271–2274). Cases ‘b’ and ‘c’ correspond to the ‘jelly sandwich’ lithorheological structures from [Figure 4\(a\)](#) and [4\(d\)](#). The experiments confirm the ideas presented in (a) (e.g., biharmonic folding in case ‘b’ with two different wavelengths developing together) and demonstrate the possibility of the development of large-scale folding despite of concurrent intense brittle faulting. *De facto*, folding controls localization of brittle faults that tend to localize at the inflection points of folds.

T_s and T_e cannot approach each other until the plate preserves some elastic core ($F < B$). The maximum intraplate stress ($\sigma_{xx}^f + F/T_e$) is limited to 2 GPa in compression and about 1 GPa in extension ([Figure 4\(a\)](#)). This yields $T_s < 40$ –50 km, which is compatible with the observations ([Maggi et al., 2000](#)).

As seen from [Figure 5\(b\)](#) and [5\(c\)](#), the strong mechanical core associated with T_e is centered at the neutral plane of the plate, z_n , whereas the seismogenic layer T_s is shifted toward the surface. This shows why T_s cannot have same geometric interpretation as T_e . Since bending stresses are minimal near z_n , the

earthquakes are favored only at some depth above or below z_n (**Figure 5(b)** and **5(c)**). The brittle strength linearly increases with depth, making deeper earthquakes less probable. It is thus natural that earthquakes are more frequent above z_n . For a pure elastic plate, z_n is located in the middle of the plate. For a brittle–elastic–ductile plate with a typical YSE, z_n is only roughly located in its middle, depending on the proportion between the integrated strengths of the brittle and ductile domains (**Figure 5(b)** and **5(c)**). In most common case, the sizes of these domains are comparable, $z_n \approx \frac{1}{2}T_e(\text{max})$ and $T_s < \frac{1}{2}T_e$. If the ductile part is very weak (e.g., near the ridges, age $< 4\text{--}10$ Ma), the plate strength is concentrated in the brittle–elastic layer T_s . In this case, earthquakes must occur at depths $<\approx(T_e(\text{max}) - T_e)$ (**Figure 5(c)**), while $T_e(\text{max}) - T_e < \frac{1}{2}T_e$ except for extreme amounts of flexure. Hence, in a plate with a very weak ductile part, the equality $T_s = T_e$ is impossible unless the plate undergoes a strong nonflexural deformation. Yet, in the latter case, T_e has no meaning. T_s may be equal to T_e only if the plate has a quasisymmetrical strength distribution, that is, comprises *equally* strong brittle and ductile part (**Figure 5(b)**). Needless to say, this configuration is incompatible with the crème brûlée rheology model.

It is noteworthy that the previous considerations are valid only under the hypothesis that T_s and T_e are both related to flexural deformation of the lithosphere, the only context a link between these two quantities may have some sense. If the lithosphere undergoes important nonflexural deformation or just transmits important tectonic stress, T_s would not be expected to have any relation to T_e .

6.03.5.5 Intraplate Seismicity and Ductile Creep

Rock mechanics data suggest that in addition to Byerlee's friction law, a semibrittle/semiductile strain rate-dependent plastic flow may increasingly occur beginning at 10–15 km depth, with a frictional component that is not observed at depths $>40\text{--}50$ km ([Bos and Spiers, 2002](#); [Chester, 1995](#); [Ranalli, 1995](#)). Starting from this depth, Peierls and GBS creep is more likely than brittle failure. This probably explains why intraplate earthquakes are rare below 40–50 km depth in both the oceanic and continental lithosphere.

The most puzzling point refers to the observation that in the oceans, for given plate age, the maximum earthquake depth appears to correlate with the depth to the isotherm $\sim 400\text{--}500$ °C. This depth is about 40–50 km for plate ages between 70 and 180 Ma but is much shallower near spreading centers. Thermal models of lithosphere are quite uncertain, so quite a few earthquakes may also occur below the 500 °C isotherm depth (e.g., [Watts, 2001](#)). At any rate, correlation of the maximum earthquake depth with temperature cannot be directly linked to the long-term ductile strength because at seismic strain rates, the entire upper mantle behaves as an elastic material (**Figure 4**). One possible explanation may be related to the fact that brittle failure can be activated only on preexisting microfractures. Microfractures are likely to be healed under pressure in hot ductile mantle below the depth to 500 °C. Ductile healing occurs in all kinds of rocks, particularly in the presence of fluids. However, there is an essential

difference between the dislocation creep characteristic of both hot lower crustal and mantle rocks and the GSS GBS (grain boundary sliding) creep that is more specific for olivine and can be activated in relatively narrow temperature–pressure interval between 500 and 800 °C, thus at 40–70 km depth just below the continental Moho ([Drury, 2005](#)). GBS creep is strongly favored by a reduction in grain size under large strains and may result in localized strength drop and formation of ductile shear bands in the sub-Moho mantle. Meanwhile, rock retains considerable strength ($\sim 200\text{--}400$ MPa), which, however, is smaller than for dislocation creep and is much smaller than the hypothetical brittle strength at 40 km depth (several GPa). The rock recovers its initial strength and deforms by dislocation creep as the grains regrow.

Hence, weak ductile shear bands will likely form in the sub-Moho mantle instead of high-stress brittle shear bands. Then, sub-Moho rocks will not be able to accumulate significant elastic stresses and seismogenic stress release becomes improbable. Since the GBS creep is specific for mantle and not for crustal rocks, this might explain the scarcity of earthquakes below the continental Moho and sharp seismic transition between the crust and mantle.

That said, continental subcrustal earthquakes are rare but not unknown (e.g., [Monsalve et al., 2006](#); [Tesauro et al., 2011](#); **Figure 6(b)**). There are also cases where earthquakes extend to really great depths (more than 300 km) while producing conventionally looking focal-depth solution mechanisms corresponding to simple shear sliding. The physical mechanisms of deep earthquakes are still not understood, but it is agreed that deep seismicity is not related to Byerlee's brittle sliding, for obvious reasons such as ultimate growth of brittle strength with increasing pressure and healing of the preexisting fractures under combined increase of temperature and pressure with depth ([John et al., 2009](#); [Kirby et al., 1991](#); [Scholz, 1990, 2002](#)). As pointed out ([Green, 2007](#)), the only high-pressure shearing instabilities identified by experiment require generation *in situ* of a small fraction of very weak material differing significantly in density from the 'parent material.' Growing evidence ([Green, 2007](#)) suggests that earthquakes shallower than 400 km are most probably initiated by breakdown of hydrous phases and those below 400 km depth, as a shearing instability associated with breakdown of metastable olivine to its higher-pressure polymorphs. For example, intermediate depth earthquakes (below 300–400 km) may be caused by sliding on ductile shear bands that get weakened due to fluid-induced metamorphic reactions and due to shear heating that under these conditions may lead to thermal runaway ([John et al., 2009](#)). These mechanisms are only weakly related to the initial rock strength, and it has been known for some time that, unlike shallow (i.e., depths $<50\text{--}70$ km) earthquakes, deep earthquakes produce very few aftershocks. This aftershock behavior is an important argument that the earthquake generating mechanism differs between shallow and deep earthquakes. Indeed, in contrast to brittle shear bands, ductile shear bands are expected to self-weaken allowing for continuous sliding until all elastic energy accumulated in surrounding rock is realized, which reduces the possibility of further aftershocks. The observation of double seismic zones in subductioning slabs, one of which is the slab/mantle wedge interface but

the second one is located near the neutral plane of the plate, also adds to the arguments in favor of the nonbrittle mechanisms of deep seismicity.

6.03.5.6 Constraints on the Long-Term Viscosity from Subsidence Data

Volcanic islands such as Hawaii present an ideal example of point loading that can be used to evaluate long-term lithospheric strength (Watts, 2001). Acting as an almost instantaneous surface load, islands produce local depression, whose geometry and amplitude are reflected in seismic stratigraphic data. It was shown that the primary response of the lithosphere involves the integrated strength that is different from the long-established strength. In general, the lithosphere exhibits high flexural strength within the first 10 My after loading (e.g., for Hawaii, $T_e(t=0)=90$ km; Watts, 2001), which progressively decays toward some asymptotic value (for Hawaii, $T_e(t\rightarrow\infty)=30$ km; Walcott, 1970). It is remarkable that the strength decay is exponential, as for a Maxwell solid, only within interval of a few My; after that, strength remains unchanged or slowly increases with time following the common thermal age dependence. The subsidence data suggest that the characteristic relaxation times in the lithosphere are on the order of several My. Compared to the Maxwell relaxation times in the asthenosphere (10–100 years), it suggests that the average lithosphere viscosity is 10^4 – 10^5 higher than the asthenospheric viscosity (10^{19} – 5×10^{19} Pa s). This yields a rough estimate of 10^{23} – 10^{24} Pa s for the depth-averaged viscosity of oceanic lithosphere and suggests that elastic strain plays an important role in long-term deformation.

6.03.5.7 Large-Scale Lithospheric Folding

A number of observations (e.g., Weissel et al., 1980) reveal periodic undulations of the seafloor in zones of intraplate compression such as the Indian Ocean (see also discussion on continental folding in the following sections). These undulations may reflect compressional instabilities that develop in stiff layers overlying weaker layers or embedded in a weaker matrix (Figure 7). The minimal stiffness (viscosity) ratio needed for development of folding is ~ 100 (Biot, 1961). The wavelength, λ , of folding is roughly proportional to 5–10 thicknesses of the competent layer, h_m :

$$\begin{aligned}\lambda &= 2\pi h_m (\mu_1/\mu_2)^{\frac{1}{\lambda}} \text{ (viscous rheology, no gravity)} \\ \lambda &= 2\pi (F/\Delta\rho g)^{\frac{1}{\lambda}}, F \approx B \approx 2\mu_1 \dot{\epsilon} h_m \text{ (viscous gravity folding)} \\ \lambda &= 2\pi (Gh_m/F)^{\frac{1}{\lambda}} \text{ (elastic buckling, no gravity)} \\ \lambda &= 2\pi (2D/F)^{\frac{1}{\lambda}}, F \approx (4D\Delta\rho g h_m)^{\frac{1}{\lambda}} \text{ (elastic gravity buckling)}\end{aligned}\quad [37]$$

where μ_1 is the average viscosity of the lithosphere and μ_2 is the viscosity of the asthenosphere. In the case of the Indian Ocean, the observed λ is on the order of 250 km (Weissel et al., 1980), implying a 50 km thick stiff layer. This value agrees with eqn [36] and is close to T_e estimates for Indian Ocean (40–50 km; Watts, 2001; Figure 5(a)). The wavelength of lithosphere folding thus can be used as a proxy for long-term strength of the lithosphere, in the same way as T_e (compare Figure 7(b) with Figures 5(a) and 8). According to both theory and experiments,

noticeable folding develops in layered systems with competence contrasts higher than 100. The viscosity of the underlying asthenosphere is known to be on the order of $1\text{--}5 \times 10^{19}$ Pa s. Hence, one can conclude that the average viscosity of the oceanic lithosphere is $> 10^{21}$ – 10^{22} Pa s. This estimate provides only a lower bound on the mean viscosity of the lithosphere since λ is weakly dependent on μ_1/μ_2 in the range $10^2 < \mu_1/\mu_2 < 10^4$. Consequently, μ_2 can vary from 10^{21} to 10^{24} Pa s.

6.03.6 Rheology and Structure of the Continental Lithosphere and Continental Margins

6.03.6.1 Common Goetze and Evans Yield Stress Envelopes

Similar to the oceanic lithosphere, the continental YSEs are derived from common assumptions such as the rheological structure, crustal thickness, lithosphere thickness $a=z(1330^\circ\text{C})$, thermal structure, and strain rate field. Since the continental crust is much more variable in its structure and composition than the oceanic crust, there is much larger variety of possible continental YSEs (Figure 9). In contrast to the oceanic lithosphere, the thermal structure of continental plates is not well constrained because (1) they may have undergone several major thermal events in their history, (2) the thermal thickness, a , of continents is not well defined, and (3) about 50% of the continental surface heat flux is due to relatively variable radiogenic heat production in the upper crust and it is also influenced by surface processes and spatial variation in thermal properties. The common thermal model refers to cooling of a multilayer plate heated from below (Afonso and Ranalli, 2004; Burov and Diament, 1992, 1995; Appendix B). This model is characterized by a time of cooling t , also called thermotectonic age, has a vertically heterogeneous structure, and accounts for radiogenic heat production in the crust. According to this model, the thermal structure of the continental lithosphere becomes stationary after 400–700 Ma since the last major thermal event (e.g., Burov and Diament, 1995; Jaupart and Mareschal, 2007).

The assumed difference in the mechanical properties of the upper crust, lower crust, and mantle may lead to the appearance of weak ductile zone(s) in the lower crust that allows for mechanical decoupling of the upper crust from the mantle (e.g., Bird, 1991; Chen and Molnar, 1983; Kuznir and Park, 1986; Lobkovsky and Kerchman, 1992). Crust–mantle decoupling occurs if the lower crust is mechanically weaker than mantle olivine at the Moho boundary. This decoupling implies the possibility of lateral flow in the lower crust, enhanced by dissipative heating, grain size reduction, and possible metamorphic changes (Burov et al., 1993; Lobkovsky and Kerchman, 1992). For ‘common’ quartz-dominated crust, decoupling should always occur, except for thin (e.g., rifted) crust (<20 km). For other crustal compositions (diabase, feldspar, quartz-diorite, etc; Figures 4(a) and 9), decoupling might take place in most cases, except in very old cold lithospheres (age > 750 Ma). The presence of fluids (wet/dry rheology) also promotes crust–mantle decoupling.

A number of independent data sources provide additional constraints on the choice of crustal rheology. These include T_e and other deformation data, seismicity distributions (Chen and Molnar, 1983; Cloetingh and Banda, 1992; Deverchere et al., 1993; Govers et al., 1992; Molnar and Tappognon, 1981), seismic reflectivity and velocity anomalies (P and S),

attenuation of S velocities associated with ductile zones or fluids (e.g., Kusznir and Matthews, 1988; Wever, 1989), petrology data (Cloetingh and Banda, 1992), and data from magnetotelluric soundings, which serve as indicators of the presence of melts and fluids (Wei et al., 2001).

6.03.6.2 Age Dependence and Other Dependences of the Integrated Strength of the Lithosphere

As for the oceans, T_e data are the main proxy for the long-term strength of continental lithosphere (Figure 8). In continents, T_e ranges from 0 to 110 km and shows only partial relationship with age. Although the continental lithosphere should

strengthen while getting colder with time (Figure 8), there is no such a clear T_e age dependency in continents as in oceans (Figure 5(a) and 5(d)). Many plates have experienced thermal events that have changed their thermal state so that it does not correlate anymore with their geologic age (e.g., Kazakh shield (Burov et al., 1990) and Adriatic lithosphere (Kruse and Royden, 1994)). On the other hand, after 400–750 Ma (Figure 8), the temperature distribution in the lithosphere approaches equilibrium state and does not evolve with age. As mentioned, the interpretation of the surface heat flux in the continental domain is ambiguous because of uncertain crustal heat generation and thermal effects associated with erosion, sedimentation, and climatic changes (Jaupart and Mareschal,

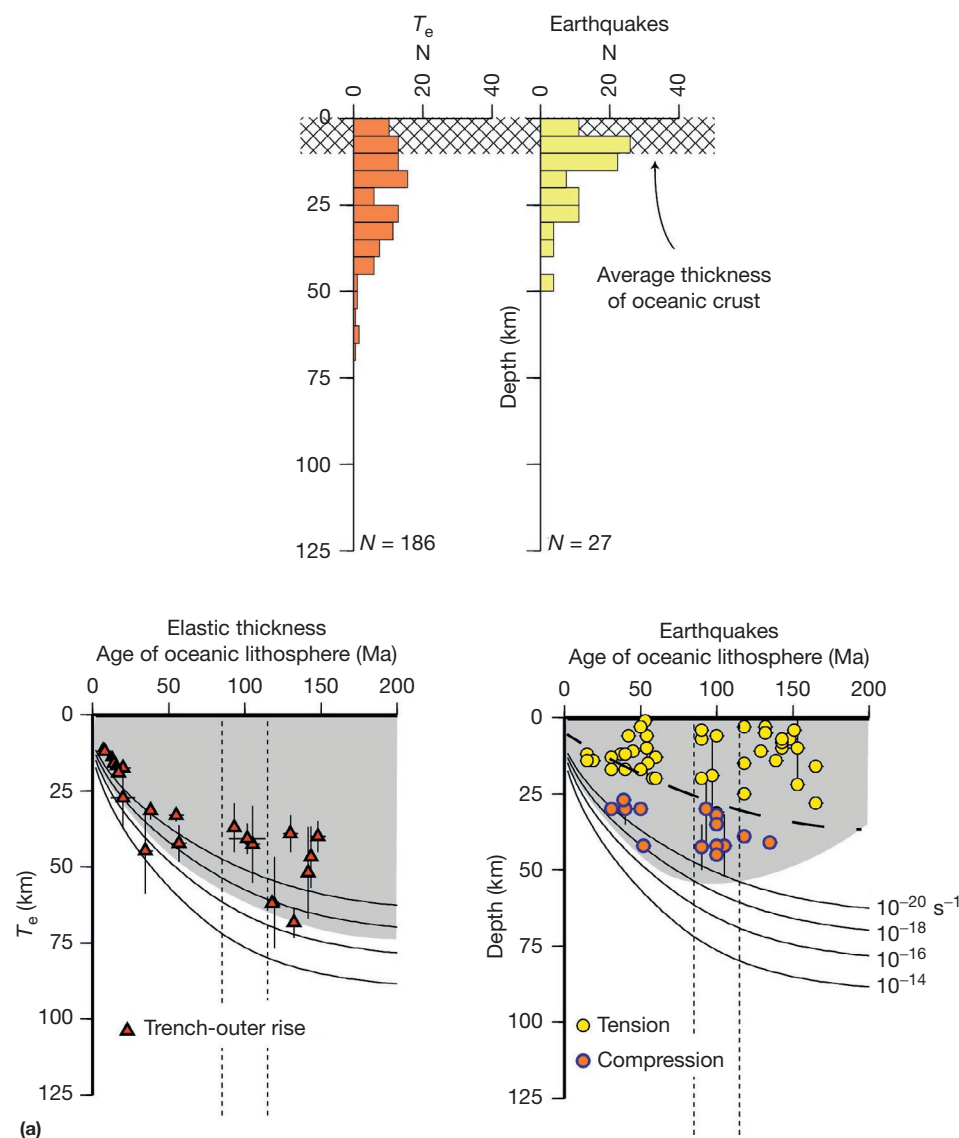


Figure 7 (a) Summary of T_e and T_s estimates for deep-sea trench–outer rise systems (reproduced from Watts AB and Burov E (2003). Lithospheric strength and its relationship to the elastic and seismogenic layer thickness. *Earth and Planet Science Letters* 213: 113–131). Data based on Table 6.1 of Watts (2001) and Table 1 of Seno and Yamanaka (1996). The T_e estimates have been corrected for curvature. Solid lines show the YSE based on the same rheological structure as assumed in Figure 4(a), a stress difference of 10 MPa, and thermal ages of oceanic lithosphere of 0–200 Ma.

(Continued)

2007). Surface heat flow mainly reflects crustal processes and should not be used to infer the subcrustal geotherm (England and Richardson, 1980).

The base of the mechanical lithosphere in continents, h_m , is referred to the isotherm of 700–750 °C, below which the yielding stress is <10–20 MPa (higher than in oceans; temperature at the base of the mechanical lithosphere results from pressure effect on ductile strength, since in continents, the depth to 500–750 °C is greater than in the oceans). The mean background strain rates are typically known within one order of accuracy. As can be seen from Figure 9(b), such uncertainty is acceptable, since it affects the yield stress limits by no more than 10%.

As mentioned, the rheological meaning of T_e in the continents is not as clear as it is in the oceans (Figures 5 and 8). The T_e data show a somewhat bimodal distribution, with low values clustering at 30–40 km and high values clustering at 80 km (Burov and Diamant, 1995; Watts, 2001). The reason for this clustering probably refers to the influence of plate structure. That is, depending on the ductile strength of the lower crust, the continental crust can be mechanically coupled or decoupled with the mantle resulting in highly differing T_e . Burov and Diamant (1992) had shown for ‘typical’ continental lithosphere that the weak ductile zones in the lower crust do not allow flexural stresses to be transferred between the strong (brittle, elastic, or ductile) layers of the jelly ‘sandwich.’ As result, there are several ‘elastic’ cores inside the bending plate. In such a multilayer plate, flexural stress and strain levels are significantly smaller than in an equivalently bent monolith plate of same thickness. Consequently, its T_e , which is a measure of integrated bending stress, is also reduced. T_e of a multilayer plate reflects the combined strength of all the brittle,

elastic, and ductile layers. Yet, it is not a simple sum of thicknesses of these layers ($h_1, h_2 \dots, h_n$) (Figure 10(a); Appendices A and B):

$$T_e(\text{YSE}) \sim (h_1^3 + h_2^3 + h_3^3 \dots)^{1/3} = \left(\sum_{l=1}^n h_l^3 \right)^{1/3} \quad [38]$$

Thus, in the case of two equally strong but decoupled layers ($n=2$) of total thickness h (e.g., crust and mantle), $T_e \approx 0.6 h$ instead of h , that is, the integrated strength is reduced roughly by a factor of 2 compared to a monolayer plate (e.g., old craton with strong coupled lower crust). The meaning of T_e (YSE) in the continents thus becomes clearer. It reflects the integrated effect of *all* competent layers that are involved in the support of a load, including the weak ones.

If the multilayered continental lithosphere is subject to large loads, it flexes, and the curvature of the deformed plate, K , increases. T_e (YSE) is again a function of K and is given (Burov and Diamant, 1995, 1996) by (Figure 10(b))

$$T_e(\text{YSE}) = T_e(\text{elastic}) C(K, t, h_{c1}, h_{c2}, \dots) \quad [39]$$

where C is a function of the curvature, K , the thermal age, t , and the rheological structure. A precise analytic expression for C is bulky (Burov and Diamant, 1992), although Burov and Diamant (1996) provided a first-order approximation for a ‘typical’ case of continental lithosphere with a mean crustal thickness of 35 km, a quartz-dominated crust, and an olivine-dominated mantle, which, they indicate, is valid for $10^{-9} < K < 10^{-6} \text{ m}^{-1}$. T_e (YSE) then simplifies to

$$T_e(\text{YSE}) \approx T_e(\text{elastic}) \left(1 - (1 - K/K_{\max})^{1/2} \right)^{(1/2 + 1/4(T_e(\text{elastic})/T_e(\max)))} \quad [40]$$

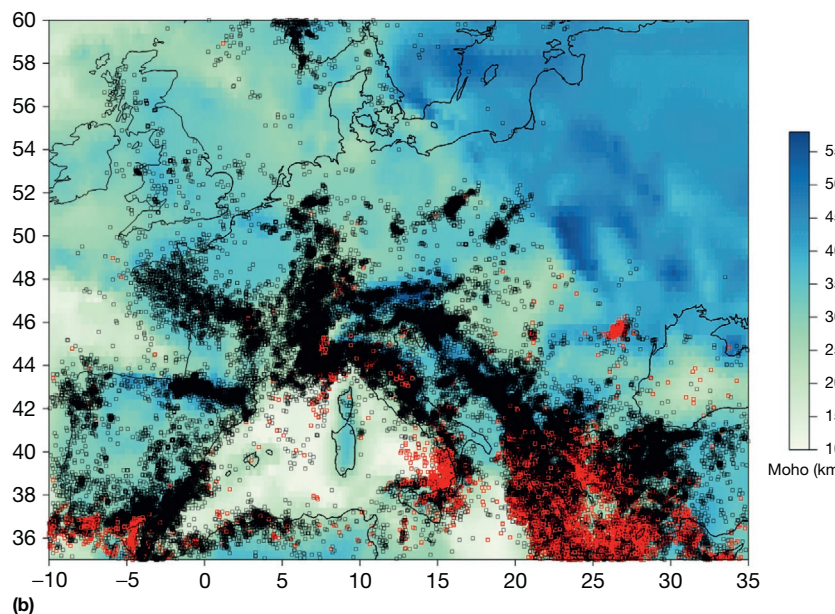


Figure 7 (Continued) (b) Seismicity distribution in Europe (Tesauro et al., 2008). The database contains more than 100 000 seismic events with magnitude between 1 and 9 for the time period 1973–2010. Black and red circles correspond to the earthquakes located in the crust and mantle lithosphere, respectively. The data on crustal thickness come from EuCRUST-07 (Tesauro et al., 2009a,b,c). Intraplate sub-Moho earthquakes in continental domain are rare but not exclusive, specifically in the areas with crustal thickness <20–30 km.

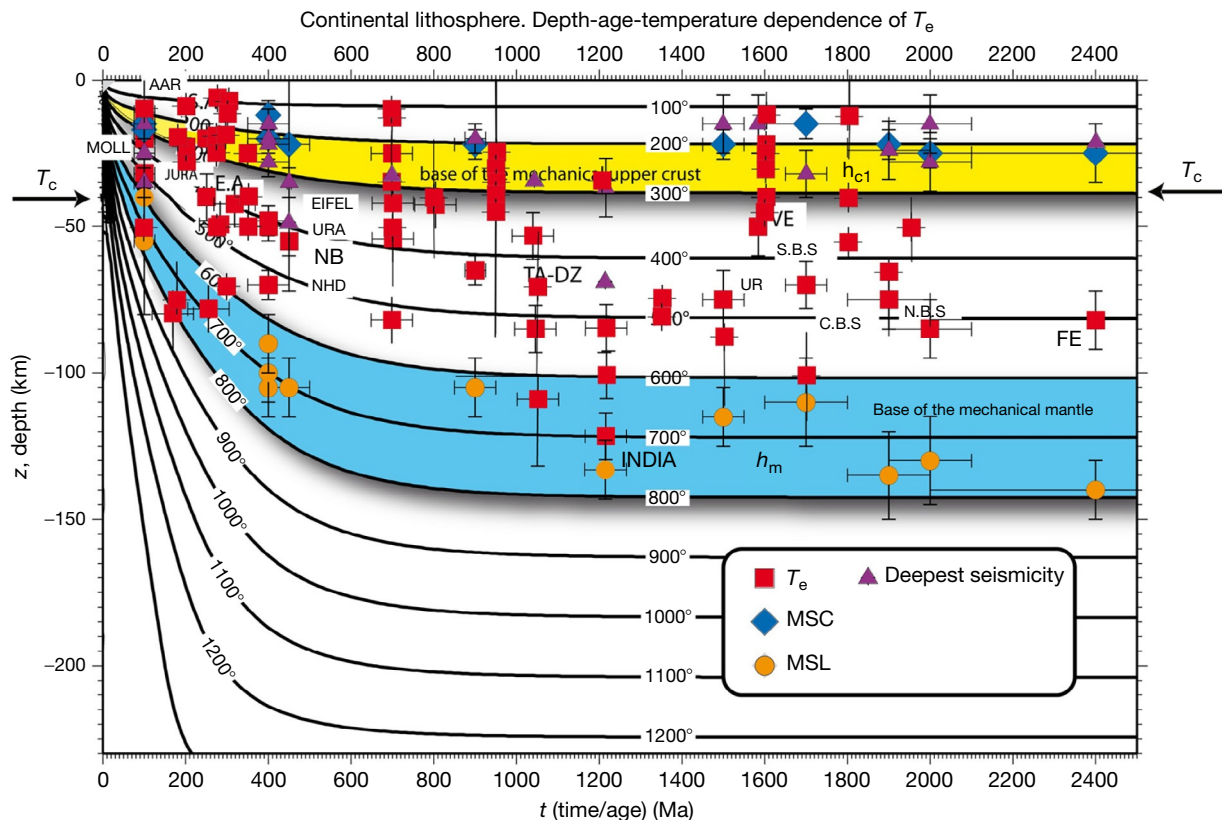


Figure 8 Compilation of observed elastic thickness (T_e) against age of the continental lithosphere at the time of loading and the thermal model of the continental lithosphere (equilibrium thermal thickness, $a = z(1330\text{ }^\circ\text{C})$, of 250 km (Appendix B). Also shown is the depth to the mechanical base of the lithosphere and maximum depths of seismicity (where available). The data refer to the studies that have taken into account – at minimum – surface topography loads. Where available, we preferred estimates based on robust forward models rather than on debated spectral models. In particular, common variants of FAA admittance technique (e.g., Jackson, 2002; McKenzie and Fairhead, 1997) are not applicable in areas of elevated topography (e.g., mountain ranges and plateaus), as well as near plate boundaries (since it cannot account for boundary forces associated with collision and slab pull) (Burov and Watts, 2006; Jordan and Watts, 2005; Lowry and Smith, 1994; Watts, 2001; Watts and Burov, 2003)). The lines are isotherms with account for radiogenic heat production in the crust. Filled squares are estimates of T_e in collision zones (foreland basins and thrust belts); filled circles correspond to postglacial rebound data. Isotherms 250–300 °C mark the base of the mechanically strong upper crust (quartz). The isotherms 700–750 °C mark h_m , the base of the competent mantle (olivine). Note that there are no significant changes in the thermal structure of the lithosphere after ~750 Ma, though there are significant reductions in T_e even for these ages. These reductions are obviously caused by differences in crustal structure and rheology. The notations are foreland basins/mountain thrust belts data: E.A., Eastern Alps; W.A., Western Alps; AD, Andes (sub-Andean); AN, Apennines; AP, Appalachians; CR, Carpathians; CS, Caucuses; DZ, Dzungarian basin; HM, Himalayas; GA, Ganges; KA, Kazakh shield (north Tien Shan); KU, Kunlun (south Tarim); NB, north Baikal (chosen since this part of the Baikal rift zone is believed to represent a ‘broken’ rift currently dominated by flexural deformations); TA, central and north Tarim; PA, Pamir; TR, Transverse Ranges; UR, Urals; VE, Verkhoyansk; ZA, Zagros. Postglacial rebound zones: L.A., Lake Algonquin; FE, Fennoscandia; L.AZ, Lake Agassiz; L.BO, Lake Bonneville; L.HL, Lake Hamilton. Data sources: S.A., AN., CR., HM, NB, KA, TA, PA, KU, GA, AD, TA, W.A. E.A., DZ, AP, GA, TR, VE, FE: (Burov and Diament, 1995 and references therein; Watts, 2001). Other data sources (ZA, L.A., L.AZ, L.BO, L.HL): (Watts, 1992, 2001).

where K_{\max} (in m^{-1}) = $(180 \times 10^3) / (1 + 1.3T_e(\text{min})/T_e(\text{elastic}))^6$, $T_e(\text{max}) = 120 \text{ km}$, $T_e(\text{min}) = 15 \text{ km}$, and $T_e(\text{elastic})$ is the initial elastic thickness prior to flexure, which can be evaluated from eqn [38].

We show in Figure 10(d) and 10(e), therefore, how T_e and T_s would be expected to change using the more precise analytic formulations of Burov and Diament (1992, 1995, Appendix A). The Figure illustrates how the thickness of the brittle and ductile layers evolve with different loads and, hence, curvatures. On bending, brittle failure and, hence, the potential for seismicity preferentially develop in the uppermost part of the crust. The onset of brittle failure in the mantle is delayed, however, and does not occur until the amount of flexure and, hence,

curvature is very large. Observations of curvature in regions of large continental loads provide constraints on the brittle strength of continental lithosphere. Curvatures range from 10^{-8} m^{-1} for the sub-Andean to $5 \times 10^{-7} \text{ m}^{-1}$ for the West Taiwan foreland basins (Watts and Burov, 2003 and references therein). The highest curvatures are those reported by Kruse and Royden (1994) of $4-5 \times 10^{-6} \text{ m}^{-1}$ for the Apennine and Dinarides forelands. Figure 10(d) and 10(e) shows, however, that plate curvatures of 10^{-6} m^{-1} may not be sufficiently large to cause brittle failure in the subcrustal mantle, unless the flexed plate is subject to an externally applied tectonic stress. In the case illustrated in Figure 10(d), the stress required to cause failure in the subcrustal mantle for this plate curvature is 350 MPa

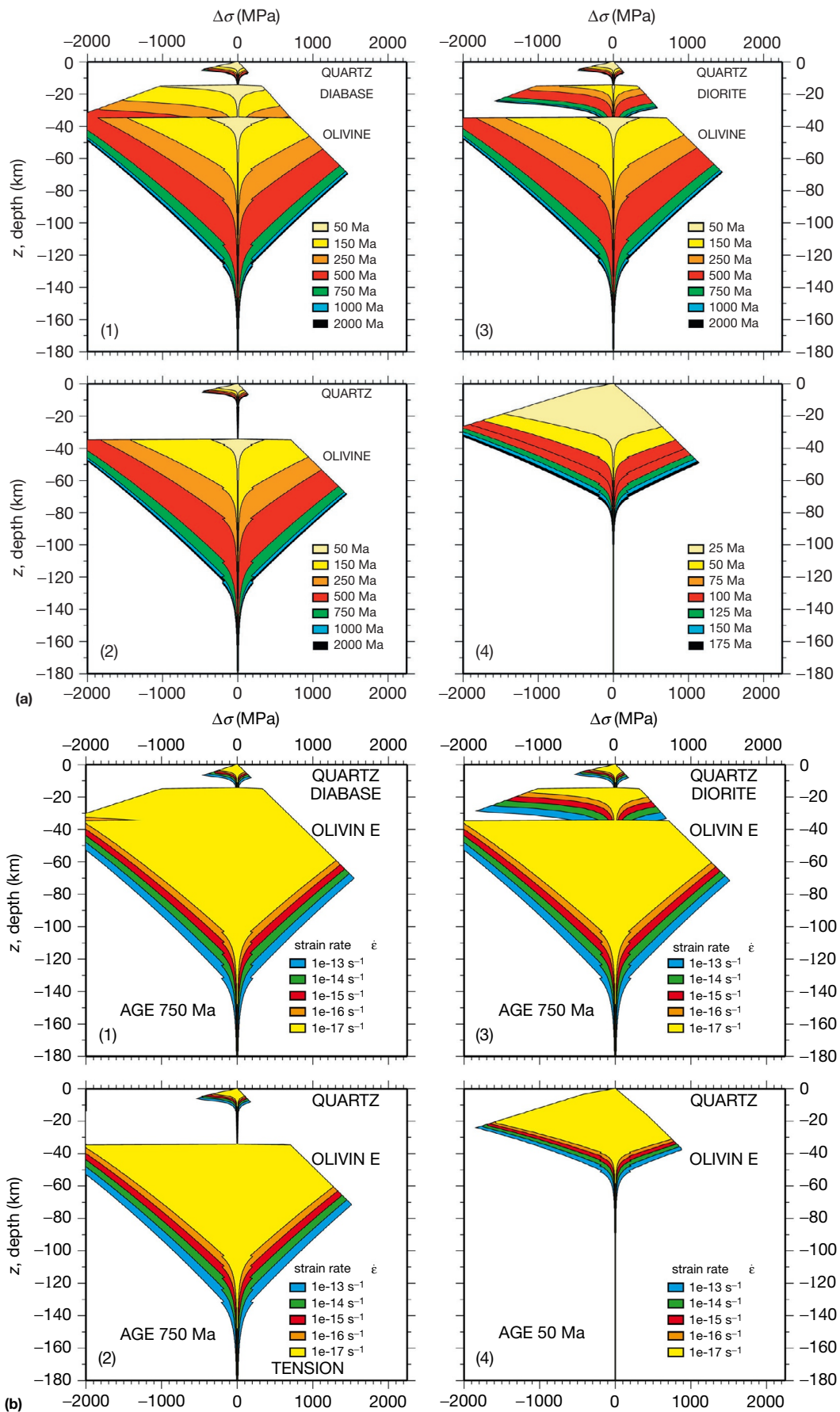


Figure 9 (a) Continental YSE as a function of thermotectonic age and crustal composition (reproduced from Buoy EB and Diamant M (1995) The effective elastic thickness (T_e) of continental lithosphere: What does it really mean? *Journal of Geophysical Research* 100: 3895–3904). Equilibrium thermal thickness 250 km. Upper crust is controlled by quartz rheology, and mantle lithosphere is controlled by dry olivine rheology. Cases 1, 2, and 3 – rheological envelopes for different lower crustal compositions: diabase, quart-diorite, and quartz, respectively. For comparison, oceanic YSE case (4) is shown in right bottom corner (thermal thickness 150 km). (b) Continental YSEs as function of the background strain rate and crustal composition (see also (a)).

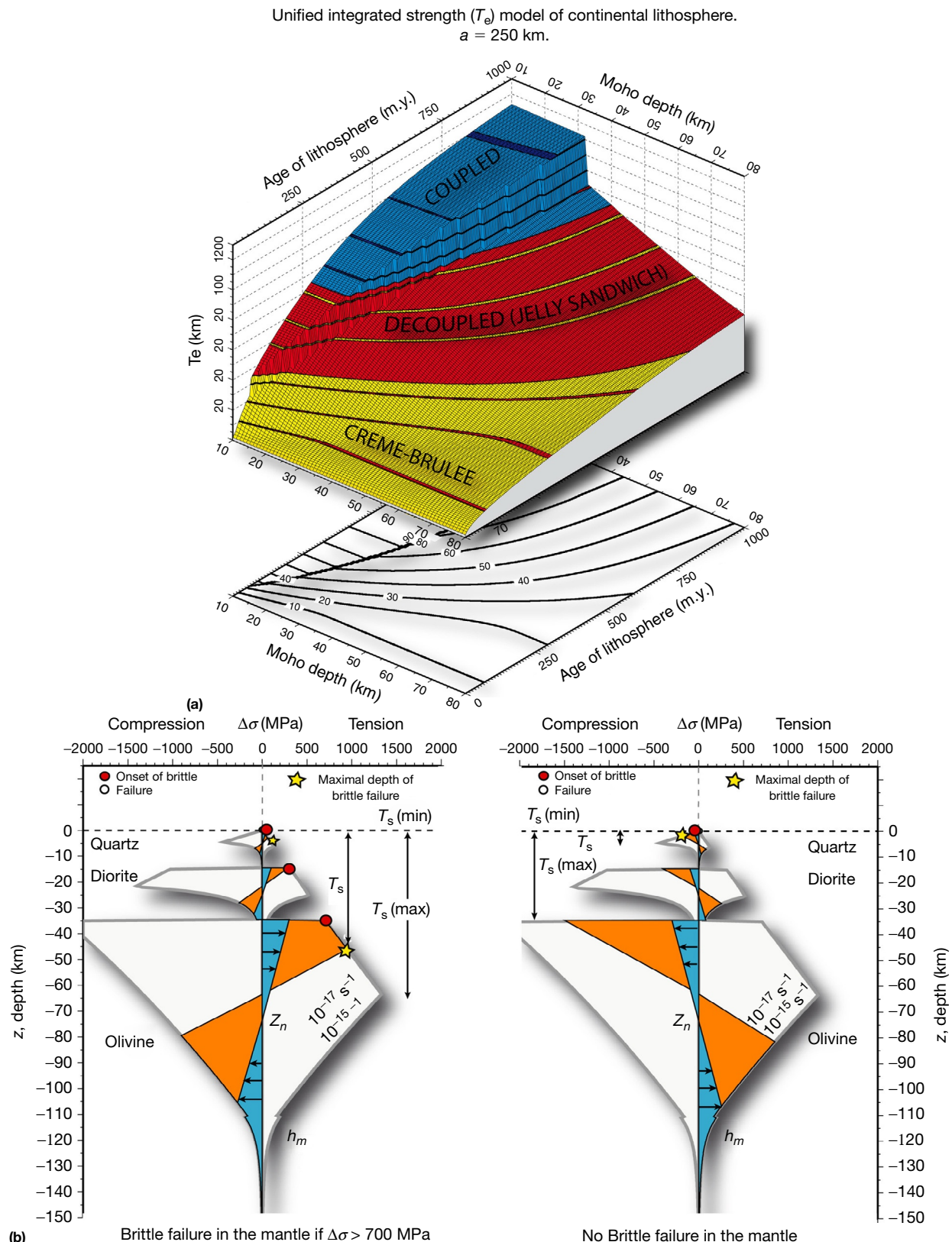


Figure 10 (a) Unified model of flexural strength of lithosphere, computed using equations of [Appendices A](#) and [B](#), for dry quartz upper crust, quartz-diorite lower crust, and dry olivine mantle ([Tables 3–4](#)). Equilibrium thermal thickness, $a=250$ km ([Appendix B](#)). (b) Stress distribution within continental YSE for concave upward and concave downward flexure (see text).

(Continued)

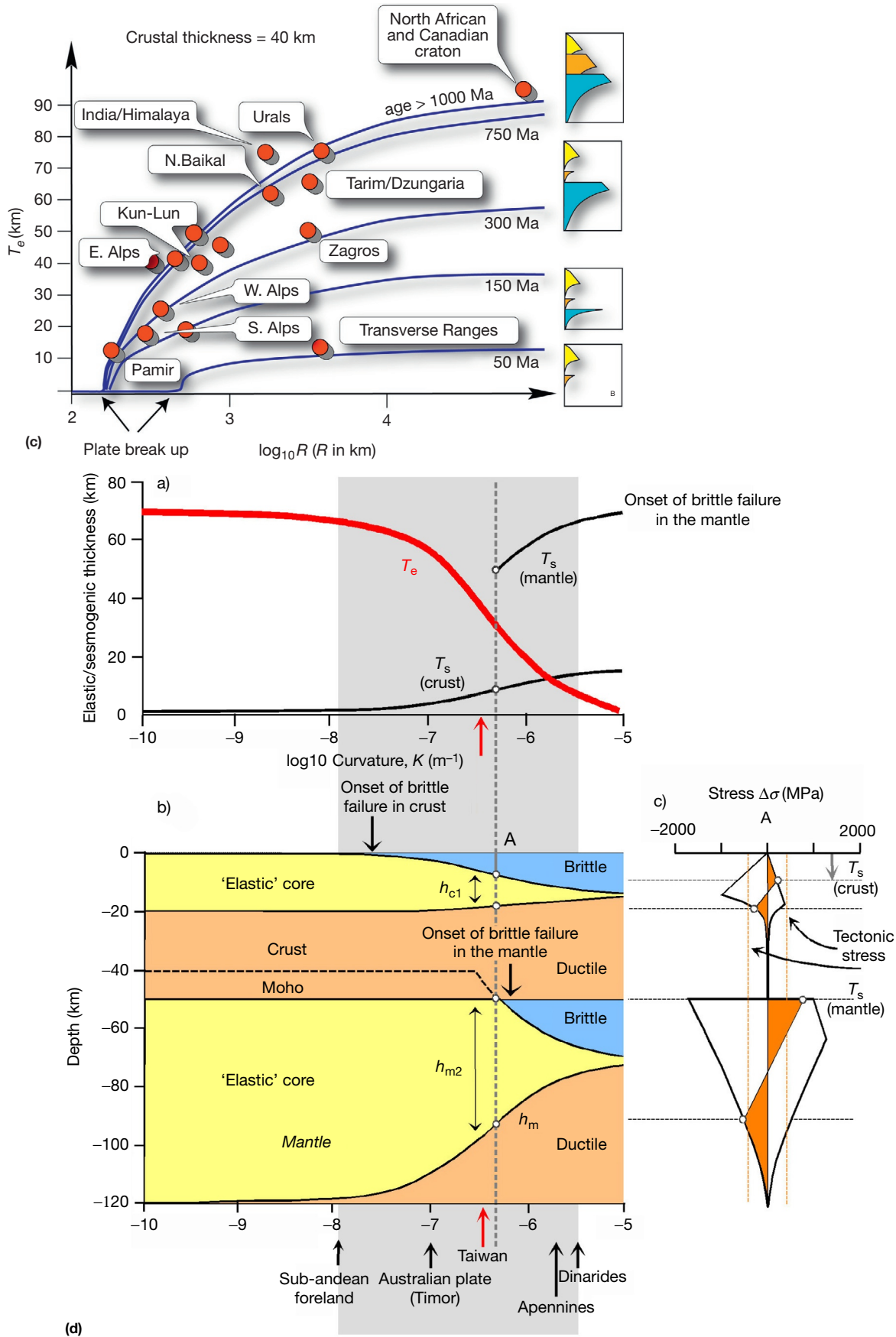


Figure 10 (Continued) (c) Predicted dependence of continental T_e on age and curvature of the lithosphere, computed for normal crustal thickness, T_c , of 40 km and compared with the data for continental plates with normal crustal thickness. Right: geometry of corresponding YSEs (same rheological parameters as in (a)). (d) Predicted relationships between the rheology structure, age, plate curvature K , T_e , and T_s for continental lithosphere with two-layer rheological structure. T_e and T_s as a function of curvature in a two-layer classical 'jelly sandwich' plate (strong upper crust, weak lower and intermediate crust, and strong mantle).

assuming 'dry' Byerlee's law. This is already close to the maximum likely value for tectonic boundary loads (e.g., Bott, 1993), suggesting that brittle failure and, hence, earthquakes in the mantle will be rare. Instead, seismicity will be limited to the uppermost part of the crust where rocks fail by brittle deformation, irrespective of the stress level. This limit does not apply, of course, to T_e . For curvatures up to 10^{-6} m^{-1} , Figure 10(d) and 10(e) shows that for the observed plate curvature range, T_e is always larger than T_s . Only for the highest curvatures (i.e., $K > 10^{-6} \text{ m}^{-1}$) will $T_e < T_s$. Of course, stress estimates shown in Figure 10(d) and 10(e) depend on the assumed rheology. In particular, frictional strength at depth may be several times smaller than the prediction of Byerlee's law in case of pore fluid pressure (reduction by a factor of 5; Figure 1). Yet the presence of fluids will also reduce the ductile rock strength by the same or higher amount. As a result, the rock may choose to flow rather than to break; T_e will be reduced and plate curvature

would be higher for the same load. It thus appears difficult to favor mantle 'seismicity' by simple brittle strength reduction due to the presence of fluids.

Finally, it should be noted that the dependence of T_e and T_s on the state of stress and plate curvature may result in strong lateral variations of T_e and T_s at both local and regional scales (Figure 10(d)-10(g)). The computations (Burov and Diamant, 1995) demonstrate that surface loads (elevated topography or sedimentary loading and plate boundary forces) may result in strong lateral variations of both T_e and T_s . Surface or subsurface loading may decrease T_e (and increase T_s) by 30–50% (or more in case of initially weak plates). In particular, the lithosphere beneath mountain ranges or large sedimentary basins (rifts and forelands) may be significantly weakened resulting in more 'local' compensation of the surface loads. In subduction/collision zones, localized weakening due to plate bending under boundary forces may result in steeper slab dip

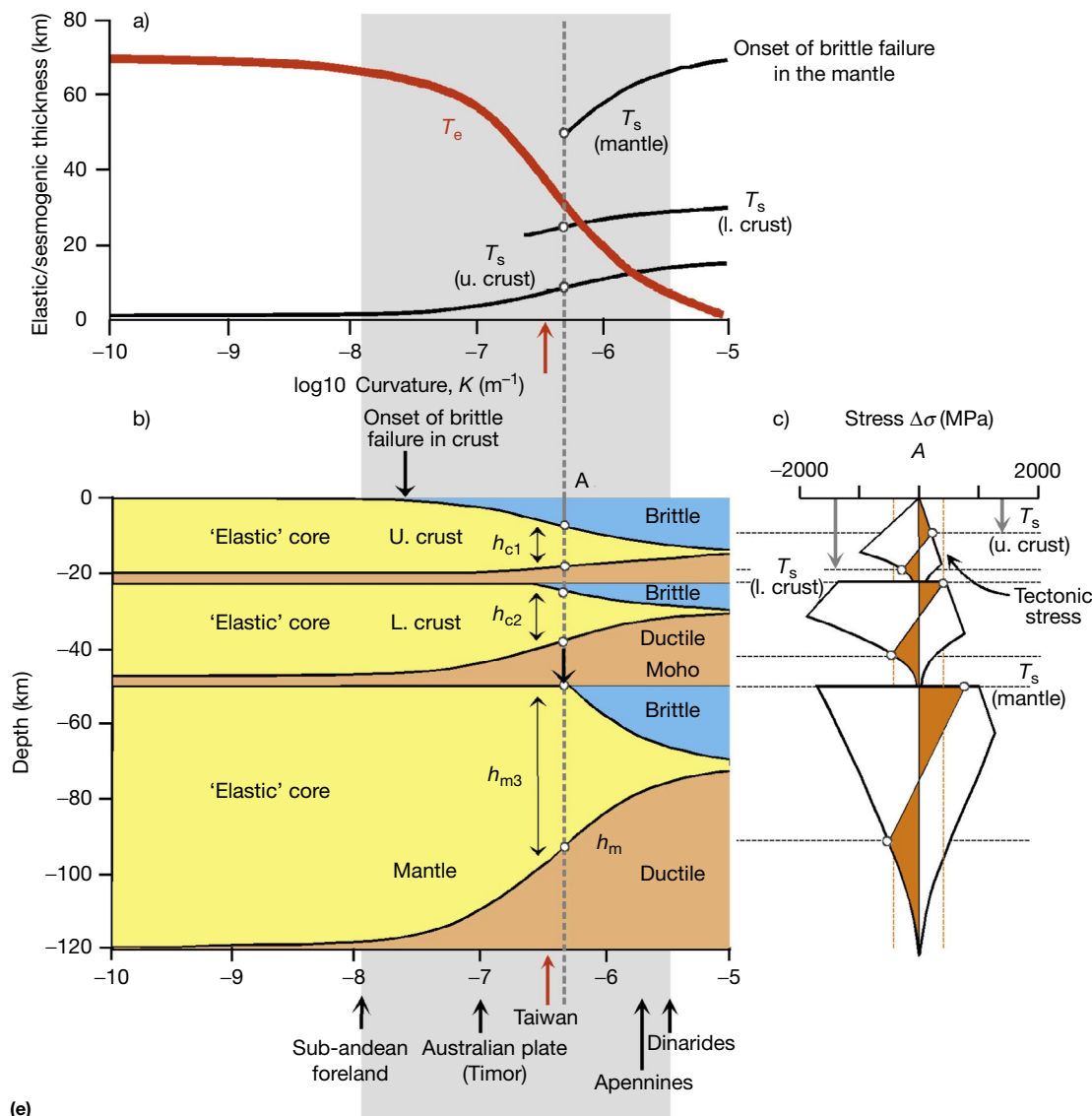


Figure 10 (Continued) (e) Predicted relationships between the rheology structure, age, plate curvature K , T_e , and T_s for continental lithosphere in a three-layer continental plate (strong upper crust, strong lower or intermediate crust, and strong mantle).

(Continued)

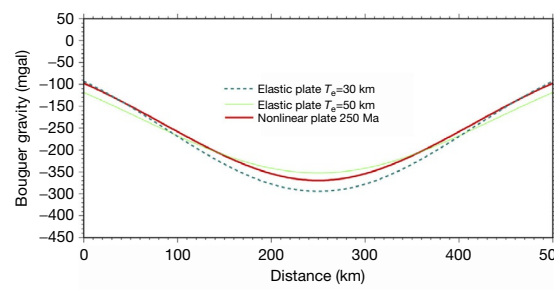
and accelerated slab breakoff. In case of weakened lithosphere (e.g., abnormal heat flux and metamorphic reactions leading to strength drop), loading may result in total failure of the plate (local isostasy). Similar results are expected in active rift zones and metamorphic core complexes (e.g., Buck, 2007; Burov and Cloetingh, 2007).

6.03.6.3 Seismicity, T_s , BDT, and Long-Term Strength

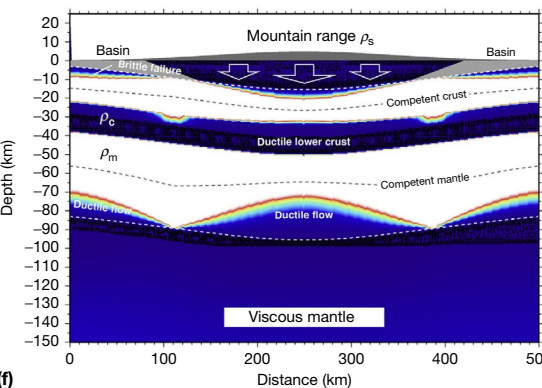
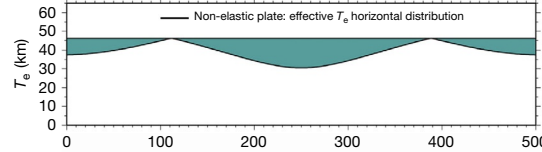
The considerations of the previous section (see also Figure 10) suggest a dual role for the continental subcrustal mantle. In regions of low curvature, the mantle may be devoid of earthquakes but largely involved in the support of long-term flexural-type loads. In regions of high curvature, however, the mantle may be seismic, but the support of long-term loads is confined mainly to the crust rather than the mantle. Despite differences in their timescales, we may therefore be able to use the presence or absence of mantle earthquakes, at least in the plate interiors, as a proxy for whether it is the crust or mantle that is mainly involved in the support of long-term loads. This

discussion should be considered in strict relation to the common, but probably incorrect (at least for great depths), assumption that prefractured ‘Byerlee’s’ rock provides a more favorable background for activation of unstable catastrophic sliding than geologically ductile rock. At seismic timescales, all rock down to lower mantle behaves as an elastic or elasto-plastic media. Any zones of mechanical weakness (fractures or ductile shear zones) may thus serve for nucleation of short-term brittle failure.

Figure 11 summarizes the data and the expected relationship between T_s and curvature for thermal ages of the continental lithosphere of 50, 500, and 1000 Ma. The circles show the maximum observed curvatures and, hence, the maximum likely value of T_s . In the decoupled case, T_s does not exceed 15 km, which corresponds well with observations. Moreover, as for the oceans, T_e and T_s are more likely to anticorrelate than correlate. T_e always exceeds T_s , irrespective of thermal age and curvature. High T_e values limit the amount of curvature due to flexure, and hence, the ratio of T_e to T_s increases with thermal age (and strength). The coupled case has the potential to yield higher values of T_s , but as T_e

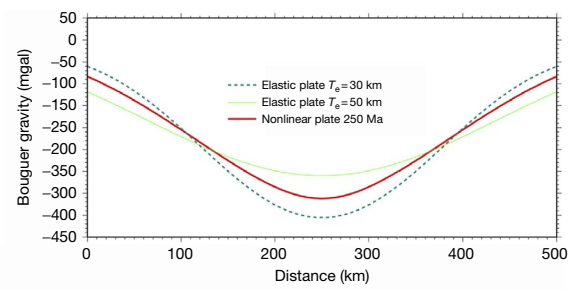


T_e and Gravity variations due to topography load

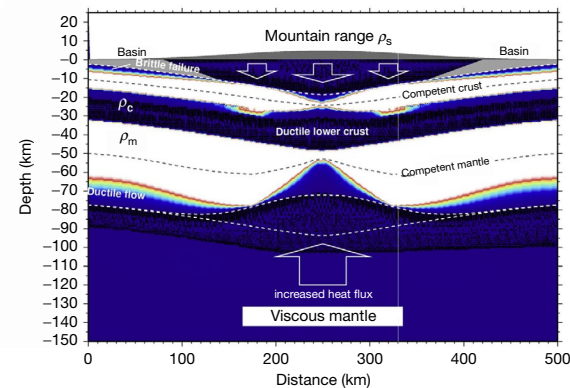
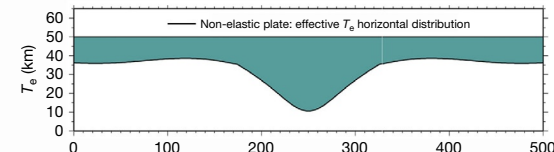


(f)

Figure 10 (Continued) (f) Computed lateral strength (T_e) variations in continental lithosphere (strength envelope from (d)) caused by surface loading (i.e., Gaussian mountain range 3 km height, Gaussian width 200 km) (reproduced from Burov EB and Diament M (1995) The effective elastic thickness (T_e) of continental lithosphere: What does it really mean? *Journal of Geophysical Research* 100: 3895–3904). The color code corresponds to the ratio of the elastic stress for given amount of strain (elastic prediction) to the real stress value (inelastic correction). The zones characterized by stress ratio 1 are effectively elastic. The zones with smaller ratio correspond to inelastic deformation (weakening), brittle or ductile.



T_e and gravity variations due to topography load. Heating from below



(i)

increases, then curvature decreases. The ratio of T_e to T_s is therefore maintained. Interestingly, it is the oceanic lithosphere (Figure 11) that is associated with the highest values of T_s . The reason for this is that the oceanic crust is much thinner than its continental counterpart, and Byerlee's friction law extends, uninterrupted, without the assistance of weak zones such as ductile lower crust in continents, from the uppermost part of the crust to the underlying mantle.

As discussed in Section 112.5.5, intraplate seismicity in continental areas is mainly located in the upper crust, while it is often suggested that the lower crust or intermediate crust is too weak to deform in the brittle regime (e.g., Chen and Molnar, 1983). As also mentioned in Section 112.5.5, a number of studies have also indicated the presence of seismic events in the lower crust as well as in the upper mantle (Cloetingh and Banda, 1992; Deverchere et al., 1991, 1993; Doser and Yarwood, 1994; Monsalve et al., 2006; Shudofsky, 1985; Shudofsky et al., 1987). Even if sub-Moho seismicity exists, it is clear that mantle microearthquakes are rare and do not form a distinct population (e.g., Aldersons et al., 2003). There is evidence from seismic reflection profiles that the continental Moho is sometimes offset by faults (Burov and Molnar, 1998;

Cloetingh and Banda, 1992; Klemperer and Hobbs, 1991), although the significance of this observation is not entirely clear.

Even though experiments suggest that brittle shear instabilities are unlikely at pressures corresponding to continental Moho depths (40 km) while mantle peridotites are prone to aseismic ductile shear banding due to specific localizing mechanisms such as GBS creep (Section 112.5.5), there is also an alternative explanation for little or absent mantle seismicity (Jackson, 2002). This author suggests that the mantle has a very low short-term ductile strength and thus deforms in ductile regime at seismic timescale. This, we believe, is a confusion. Even if one admits that the mantle is fluid at geologic timescale, it does not mean that it may flow at seismic timescale. Extrapolation of rock mechanics data (Figure 3) suggests that at seismic timescale, ductile creep cannot be activated within the lithospheric temperature–stress range: one needs temperatures higher than 1500–2000°C or stresses >1 GPa (Burov and Watts, 2006; Watts and Burov, 2003). On the other hand, there is little doubt that mantle is stronger than the asthenosphere, which has a viscosity of $\sim 5 \times 10^{19}$ Pa s at a strain rate of 10^{-15} s^{-1} . Recomputing flow stress for seismic timescale (eqn

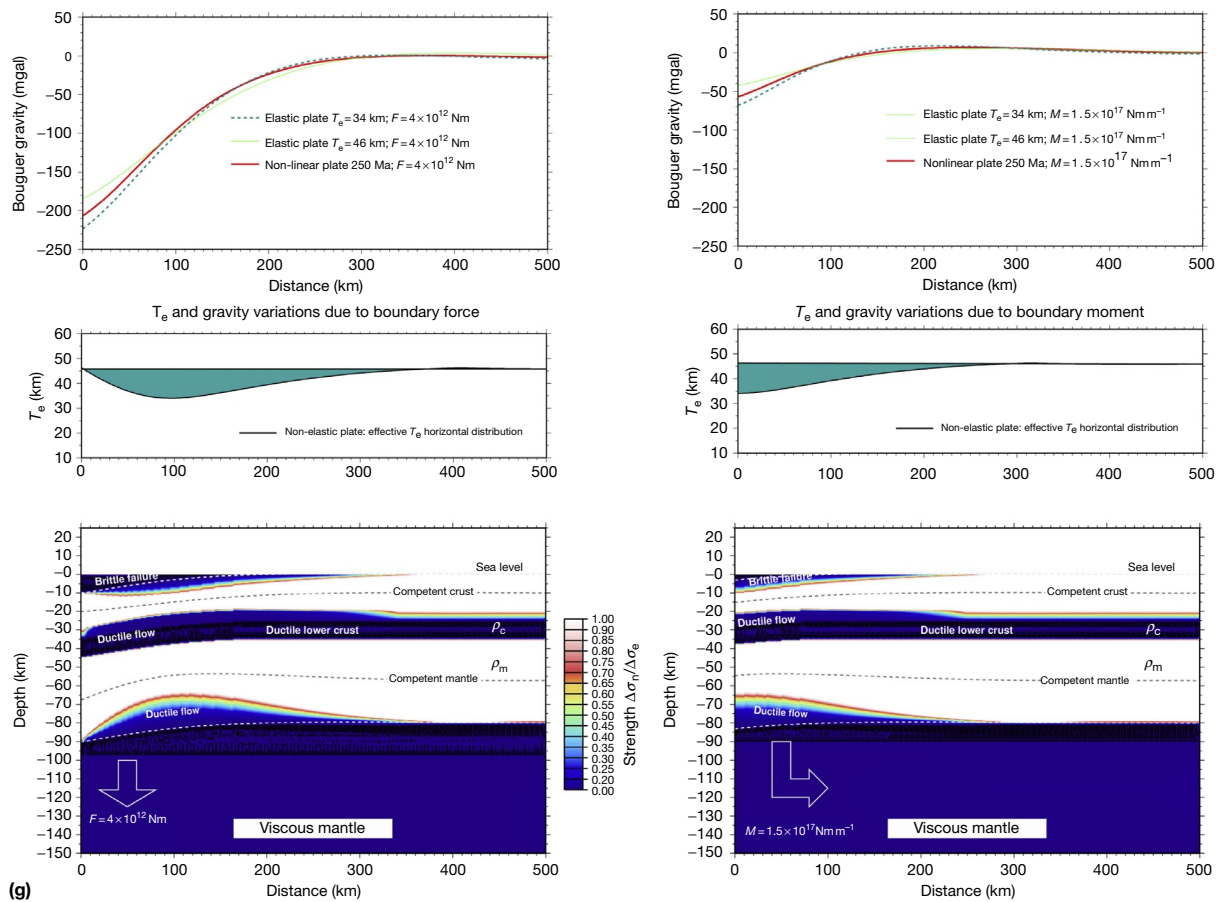


Figure 10 (Continued) (g) Computed lateral strength (T_e) variations in continental lithosphere, loaded on the end (cutting force F , right, or flexural moment M , left (Burov and Diamant, 1995)). The color code corresponds to the ratio of the elastic stress for given amount of strain (elastic prediction) to the real stress value (inelastic correction). The zones characterized by stress ratio 1 are effectively elastic. The zones with smaller ratio correspond to inelastic deformation (weakening), brittle or ductile. Note the absence of brittle failure in the uppermost mantle (compare with Figure 5(f) for the oceanic lithosphere).

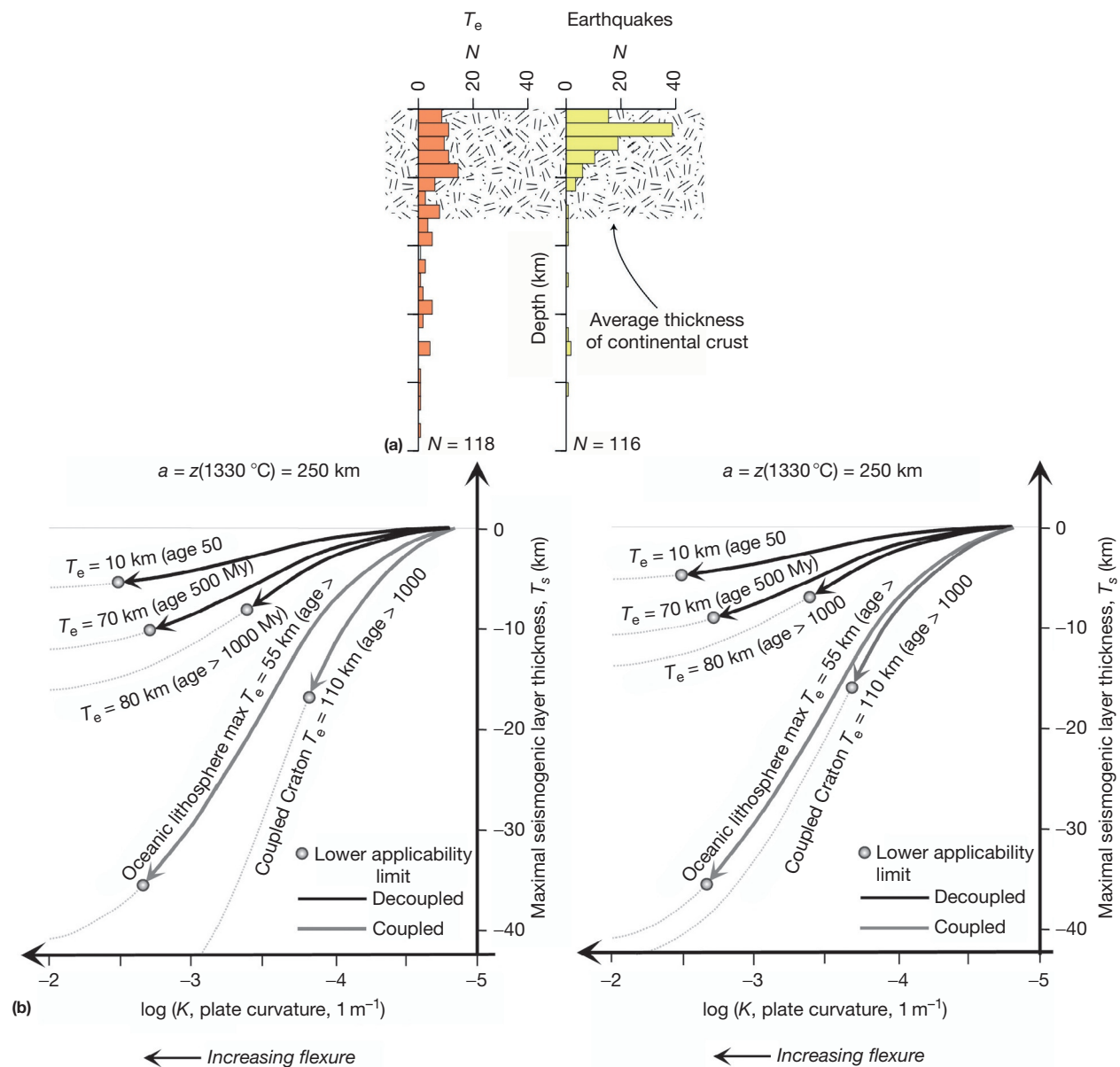


Figure 11 (a) Compilation of data on continental T_s compared with the data on T_e (reproduced from Watts AB and Burov E (2003) Lithospheric strength and its relationship to the elastic and seismogenic layer thickness. *Earth and Planet Science Letters* 213: 113–131). (b) Relationships between the plate curvature, T_e , and T_s for different ages of the lithosphere. (left) Assumption of equilibrium thermal thickness of the lithosphere, $a=250 \text{ km}$. (right) $a=125 \text{ km}$. Black curves are for decoupled rheology, while gray curves are for coupled rheology.

[13], strain rates of $10^1\text{--}10^4 \text{ s}^{-1}$) shows that even for such a ‘weak’ rheology, the yield stress must be on the order of 10–100 GPa, that is, 10 to 1000 times higher than any imaginable tectonic stress. This proves that in no case, the absence of seismicity cannot be regarded as a sign of rheological weakness. Finally, it should be kept in mind that seismicity is related to frictional release of elastic strain accumulated during the interseismic period (Scholz, 1990). Hence, if one assumes that mantle is so weak that it prevents deep brittle seismicity, then it should be characterized by Maxwell relaxation times on the timescale of postseismic rebound (from several seconds to 1 month). This would lead to an inconsistent conclusion that the lithosphere mantle is 3 orders of magnitude weaker

($\mu=10^{16} \text{ Pa s}$) than the asthenosphere, where relaxation times are 100–1000 years.

The assumption of weak mantle rheology clearly does not hold in regions where T_e is greater than crustal thickness ($T_e \sim 40\text{--}110 \text{ km}$), ductile, instead of brittle, shear strain localization in the mantle (Section 112.5.5), and/or insufficient level of intraplate stress compared to high brittle strength resulting from strong confining pressure at Moho depth (Scholz, 1990). According to Byerlee’s law, the brittle rock strength, σ_b , scales as lithostatic pressure or $\sigma_b \approx 0.6\rho g z - 0.85\rho g z$. The level of intraplate stress is limited to several hundreds of MPa. For a stress level of 500 MPa, maximum seismic depth is 15 km. For exceptionally high stress levels of

1 GPa, this depth extends to 30 km, which is still above normal Moho. In the case of weak lower crust, transition of deviatoric stresses between crust and mantle is attenuated. Then, the mantle stress level is reduced, specifically in case of bending. **Figure 10** shows, for example, that bending stresses may exceed ductile limits in the lower crust inducing flow and decoupling even in initially coupled system. The horizontal far-field stresses that are detected, for example, in Europe (see Müller et al., 1992), may also result in crust–mantle decoupling. The vertical gradient of bending stress can be calculated from the observed radius of plate flexure. Therefore, it is possible to predict the conditions for brittle crustal or mantle seismicity from direct observations of flexure (Burov and Diamant, 1992; Cloetingh and Burov, 1996).

The rare cases of lower crustal or sub-Moho mantle intraplate seismicity can be roughly classified as follows:

1. Zones of more or less homogeneous lower crustal seismicity (e.g., Albert rift, East Africa (Doser and Yarwood, 1994; Morley, 1989; Seno and Seito, 1994; Shudofsky, 1985; Shudofsky et al., 1987; Seno and Seito, 1994)).
2. Zones of localized seismicity, generally along deep faults (Baikal rift (Deverchere et al., 1991), Rhine graben (Brun and Gutscher, 1992; Brun et al., 1991; Fuchs et al., 1987)).

Cases of deep seismicity are more frequent in extensional settings and more rare in compressional settings. This confirms once again the idea that depth of seismicity is related to intraplate stress level. Indeed, the level of tectonic stresses is limited by available plate driving forces and by rock strength. One needs two to three times higher stress for brittle failure in compression than in tension (**Figure 1**), with or without fluid pressure. Under homogeneous compression, brittle rock strength, and thus stress needed to break the rock, may increase by a factor of 2, whereas under extension, it may be reduced by a factor 2 (Petri and Podladchikov, 2000; **Figure 1**), with or without fluid pressure. Under homogeneous compression, brittle rock strength, and thus stress needed to break the rock, may increase by a factor of 2, whereas under extension, it may be reduced by a factor 2 (Petri and Podladchikov, 2000; **Figure 1**). Consequently, for the same intraplate stress level, maximum seismic depth is two to five times deeper for tension than for compression.

The differentiation between zones of distributed and localized seismicity can be related to various conditions associated with seismogenic stress release:

- a. A more ‘basic’ composition (Cloetingh and Banda, 1992; Stephenson and Cloetingh, 1991). In the areas where the lower crust has low temperature of creep activation (diabase, granulites, diorite, etc.), it may favor distributed cracking at depths corresponding to 300–400 °C (20–35 km). There may be also instabilities caused by compositional differences in the lower crust (e.g., Sibson, 1980).
- b. Variation of unstable-to-stable frictional slip on deeply penetrating faults (Tse and Rice, 1986). The BDT refers to a bulk rheological property, while earthquakes are associated with frictional instabilities. Localized strain rate acceleration along the faults may keep material brittle even at Moho depths (40–50 km). Deep mantle-penetrating faults are suspected, for example, in the northern Baikal rift or in Fergana basin (Burov and Molnar, 1998; Deverchere et al., 1993)

c. Nonbrittle metastable mechanisms of seismogenic stress release. This may be related, for example, to ductile shear banding potentially associated with unstable phase changes and thermal runaway, reorientation of crystalline grids, and a few other mechanisms, which are subject of intensive discussions (e.g., Govers et al., 1992; Green, 2007; John et al., 2009; Kirby et al., 1991). The inapplicability of Byerlee’s law at depths exceeding 40–50 km was outlined in a number studies (e.g., Goetze and Evans, 1979; Kirby et al., 1991).

6.03.6.4 Physical Considerations Beyond the Observations of Flexure, Gravity Potential Theory, Intraplate Stresses

Simple physical considerations can be used to estimate minimal strength of the lithospheric plates needed to support surface topography and tectonic loads or to deform in accordance with the observed deformation styles. The tectonic forces are limited by the energy of plate driving motions and by lithospheric strength. The ratio of surface topography loads to horizontal tectonic forces (Argand number (Ar)) indicates whether a mountain range is mechanically stable or it collapses under its own weight. The maximum short-term height, and thus weight of mountains, is limited by gravity forces and by brittle strength of surface rocks. The long-term height, and the amplitude of crustal roots, also depends on the long-term strength of the supporting crust and mantle. Based on these considerations, a number of authors (e.g., Artyushkov, 1973; Dahlen, 1981; England and Houseman, 1989; Fleitout and Froidevaux, 1983) have developed conceptually elegant models allowing estimates of the minimal average stress levels in the lithosphere. This approach is based on computation of intraplate gravity-driven stresses caused by horizontal variations in plate thickness and by density contrasts $\Delta\rho$. Isostatically compensated topography creates lateral pressure and potential energy differences that have to be balanced by horizontal tectonic stresses (σ_{xx}) to keep the topography at surface:

$$\int_0^{h_m} \Delta\rho g y dy = \int_0^{h_m} \sigma_{xx} dy = B_{\min} \quad [41]$$

This allows us to put lower bounds on the integrated plate strength B_{\min} . It was found that gravity-driven forces, and thus counterbalancing tectonic forces F and B_{\min} , should vary from 10^{12} to 10^{13} N per meter (i.e., per unit length in out-of-plane direction). Depending on plate thickness, this yields average intraplate stresses σ_{xx} of 10–100 MPa, on the order of values (yet smaller) obtained by Cloetingh and Wortel (1986) from dynamic plate modeling.

6.03.6.5 Gravitational Stability Analysis: Rayleigh–Taylor Instabilities or Survival of Cratons, Continental Margins, and Mountain Roots

The crème brûlée and the alternative jelly sandwich rheology models imply fundamental differences in the mechanical properties of mantle lithosphere. One can explore the stability of mantle lithosphere by posing the question, ‘What do the different rheological models imply about the persistence of topography for long periods of geologic time?’ (Burov and Watts, 2006).

The most stable continental lithosphere units are cratons. Their stability is favored by the presumed positive buoyancy of the depleted cratonic mantle and, as can be suggested, by its high integrated strength resulting from a cold thermal structure and mantle dehydration (resulting in dry olivine rheology). The mean heat flow in Archean cratons is $\sim 40 \text{ mW m}^{-2}$, which increases to $\sim 60 \text{ mW m}^{-2}$ in flanking Phanerozoic orogenic belts (Jaupart and Mareschal, 1999). As Pinet et al. (1991) had shown, a significant part of this heat flow is derived from radiogenic sources in the crust. Therefore, temperatures at the Moho are relatively low ($\sim 400\text{--}600^\circ\text{C}$). The mantle must therefore maintain a fixed, relatively high viscosity that prevents convective heat advection to the Moho. Otherwise, surface heat flow would increase to $> 150 \text{ mW m}^{-2}$, which would be the case in an actively extending rift (e.g., Slater et al., 1980). Since heat flow this high is not observed in cratons and orogens, then a thick, cool, stable mantle layer should remain that prevents direct contact between the crustal part of the lithosphere and the convective upper mantle.

The positive or neutral buoyancy of Mg-rich depleted cratonic mantle is largely accepted, but not well quantified, because most data come from mantle xenoliths, whose representativeness for the bulk mantle lithosphere is discussible (e.g., Artemieva, 2009a,b), and also because these data are not unambiguous (i.e., there are cases when xenoliths predict negative buoyancy for composite depleted mantle (Watremez et al., 2013)). The second factor of craton stability, the presumably high integrated strength of their mantle, is confirmed from flexural studies (e.g., Watts, 2001). Yet, most commonly used stagnant lid stability models based on viscous rheology fail to explain long-term thermal survival of cratons. Recently, Beuchert et al. (2010) had shown that accounting for realistically high temperature-dependent viscosity ratio in the cratonic mantle can provide conditions for thermal craton stability for billions of years. Yet, it should be noted that the problem of survival of cratons also refers to their capability to support tectonic forces and significant buried loads such as inherited crustal heterogeneities over long time spans (e.g., Burov et al., 1998). Thermomechanical models accounting for crustal heterogeneities indicate high integrated strength of the cratonic mantle (Burov et al., 1998; Francois et al., 2013) and confirm previously obtained T_e data (e.g., Watts, 2001).

Young fertile oceanic mantle lithosphere is expected to have a negative buoyancy starting from an age of 30 to 50 My. The negative buoyancy of the mantle lithosphere at subduction zones is widely considered as a major driving force in plate tectonics. The evidence that, in contrast to depleted cratonic mantle, normal, undepleted continental mantle is in average 20 kg m^{-3} denser than the underlying asthenosphere and is gravitationally unstable has been reviewed by Stacey (1992), among others. This instability is commonly accepted for Phanerozoic and younger lithosphere. Irrespective, volumetric seismic velocities, which are generally considered a proxy for density, are systematically higher in the lithospheric mantle than in the asthenosphere. Depending on its viscosity, the undepleted mantle lithosphere therefore has the potential to sink as the result of Rayleigh–Taylor (RT) instability (e.g., Buck and Toksöz, 1983; Houseman et al., 1981).

One can estimate the instability growth time (i.e., the time it takes for a mantle root to be amplified by e times its initial

value) using Chandrasekhar's (1961) formulation. In this formulation, a mantle Newtonian fluid layer of viscosity, μ , density, ρ_m , and thickness, d , is placed on top of a less dense fluid asthenospheric layer of density ρ_a and the same thickness. (This formulation differs from that of Conrad and Molnar (1997) who used a fluid layer that is placed on top of a viscous half-space. However, both formulations are valid for instability amplitudes $< d$.) The most rapidly growing instability wavelength, λ , is Ad where $2.5 < A < 3.0$ and the corresponding growth time, t_{\min} , is $B\mu[(\rho_m - \rho_a)gd]^{-1}$ where $6.2 < B < 13.0$ and g is average gravity. One can evaluate t_{\min} for a particular μ by assuming $(\rho_m - \rho_a) = 20 \text{ kg m}^{-3}$ and $80 < d < 100 \text{ km}$. If the continental mantle can support large stresses ($> 2 \text{ GPa}$) and has a high viscosity ($10^{22}\text{--}10^{24} \text{ Pa s}$), as the jelly sandwich model implies, then t_{\min} will be long ($> 0.05\text{--}2 \text{ Ga}$), that is, comparable with age of cratons. If, on the other hand, the stresses are small ($0\text{--}10 \text{ MPa}$) and the viscosity is low ($10^{19}\text{--}10^{20} \text{ Pa s}$), as the crème brûlée model suggests, then it will be short (0.2–2.0 My).

The consequences of these growth times for the persistence of surface topographic features and their compensating roots or antiroots are profound. The long growth times implied by the jelly sandwich model imply that orogenic belts, for example, could persist for up to several tens of My and longer, while the crème brûlée model suggests collapse within a few My.

We have discussed earlier a constant viscosity and a large viscosity contrast between the lithosphere and asthenosphere. A temperature-dependent viscosity and power law rheology result in even shorter growth times than the ones derived here for constant viscosity (Conrad and Molnar, 1997; Molnar and Houseman, 2004). If either the viscosity contrast is small or a mantle root starts to detach, then eqn [1] in Weinberg and Podladchikov (1995) suggests that the entire system will begin to collapse at a vertical Stokes flow velocity of $\sim 1 \text{ mm year}^{-1}$ for the jelly sandwich model and $\sim 100\text{--}1000 \text{ mm year}^{-1}$ for the crème brûlée model (note that these flow velocities depend strongly on the characteristic wavelength of the instability, that is, width of the mantle root, which is assumed here to be λ). Therefore, our assumptions imply that a surface topographic feature such as an orogenic belt would disappear in less than 0.02–2 My for the crème brûlée model, whereas it could be supported for as long as 100 My–2 Gy for a jelly sandwich model.

A most straightforward way to discriminate between different thermorheological concepts for cratons is to test their implications for craton stability using forward thermo-mechanical models. Unlike conventional studies, which impose a rigid top as upper boundary condition, thus forcing zero topography, Francois et al. (2013) implemented free-surface boundary condition, which allows for analysis of stability of surface and Moho topography, in addition to that of the LAB. The possibility to track subtle variations in surface ($> 10 \text{ m}$) and Moho topography presents a prime feature of this approach. The second novelty for lithosphere stability analysis refers to account for inherited crustal heterogeneities that represent very substantial subsurface loads and hence play an essential role in the mechanical equilibrium of cratonized lithosphere. These models also implemented explicit viscous(ductile)–elastic–plastic(brittle) rheology laws in large-strain numerical formulation, instead of common viscous or

viscous–pseudoplastic rheologies (Lenardic et al., 2003) or viscoelastic rheologies (Beuchert et al., 2010) used for lithosphere stability analysis. Finally, a petrologically consistent density structure (computed using the reference thermodynamic code Perple_X) (see Appendix Supplementary Item D) has been used for full consistency with mineralogical data.

In all experiments, the initial ‘model box’ is 3000 km long and 600 km deep. The mechanical boundary conditions are as follows: (1) the upper surface is free (free stress and free slip condition in all directions), (2–3) constant horizontal velocity, v_x , at the lateral sides ($v_x = 0$ in most experiments), and (4) pliable hydrostatic Winkler basement (Burov et al., 1998). The experiments exploring the impact of a laterally heterogeneous crust in the absence of far-field tectonic forcing show large differences between the three thermorheological models (Figure 12). Surface topography is highly unstable for both the IM and CB rheologies (Figure 12) with differences in topographic heights on the order of 5000–8000 m (at 200 My, Figure 12), which are inconsistent with stratigraphic data for the Canadian and Australian cratons (see Francois

et al., 2013 and references therein). In contrast, for the JS rheology, the differences in topographic height do not exceed 200 m (Figure 12) and remain within the observed range of topographic roughness. The Moho geometry also shows marked differences between all three models after 200 My. For the JS model, the initially prescribed 10 km Moho steps are well preserved. For the IM model, the Moho geometry is partly preserved but locally diverges strongly from the initial geometry. For the CB model, the initial steps are flattened to only 1–2 km after 200 My. The LAB boundary shows a similar trend and is increasingly unstable from the JS to IM and CB rheology. The CB model exhibits 40–80 km LAB undulations that progressively lead to small-scale convective instabilities and the removal of a large portion of the mantle lithosphere. For the IM and CB models, the mantle lithosphere is thinned in a number of places by a factor of 1.5–2 after 200 My. Given that the growth rate of viscous instabilities is an exponential function of time (Houseman et al., 1981), this indicates that 200 My constitutes the maximum half-life time span of a compositionally positively buoyant CB mantle (Figure 12). It is

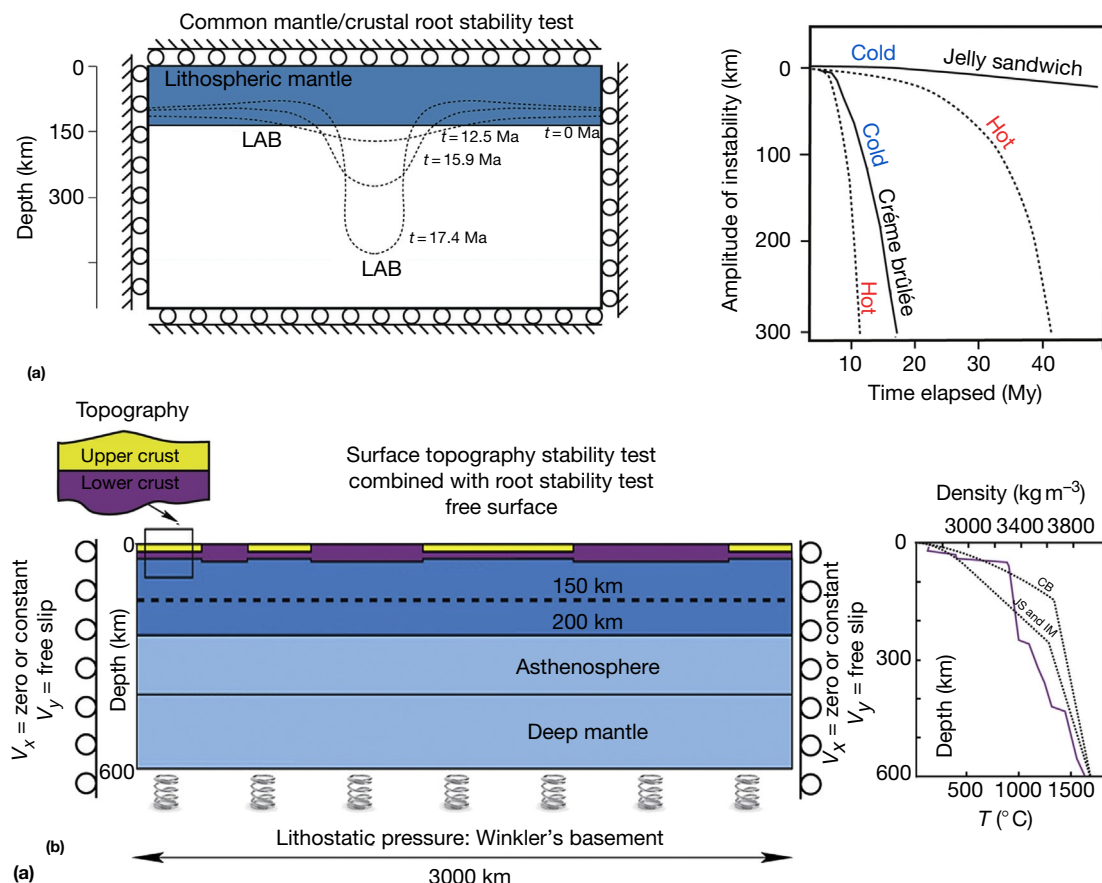


Figure 12 (a – left) The conventional model for stability analysis of lithosphere (Rayleigh–Taylor instability) with negatively buoyant depleted mantle. LAB: lithosphere–asthenosphere boundary. (a – right) Typical model geometry. Predicted amplitudes of mantle root as a function of time for end-member rheological concepts (JS, ‘jelly sandwich,’ and CB, ‘crème brûlée’). Amplitudes are computed for two end-member geotherms, ‘cold’ and ‘hot’ (see Burov and Watts, 2006). (b – left) The alternative surface topography stability model for a cratonic lithosphere with positively buoyant undepleted mantle (Francois et al., 2013). Compared with the conventional models, this model tests surface topography sensitivity to large lateral heterogeneities in crustal structure that are widespread in cratons. (b – right) Density and tested thermal structures (‘hot’ and ‘cold’ corresponding to contrasting thermal models of the lithosphere behind the ‘CB’ and ‘JS’ rheology (Watts and Burov, 2003). The density is computed in accordance with petrologic thermodynamic data on lithosphere and mantle composition.

(Continued)

noteworthy that the half-life time of negatively buoyant mantle is five to ten times shorter (Burov and Watts, 2006; Houseman et al., 1981), confirming the idea that compositional buoyancy is a crucial – yet not sufficient – controlling factor in the preservation of cratons (e.g., Burov and Watts, 2006).

The comparison between the models involving CB or JS rheology with a homogenous or heterogeneous crust shows that the strength of the mantle lithosphere is a major stabilizing factor for both surface topography and subsurface interfaces (i.e., Moho and LAB), while a strong crust alone is insufficient to keep topography stable over significant time spans. The experiments without far-field tectonic forces indicate that the buoyancy and strength of the strong mantle lithosphere are both necessary to allow for the long-term preservation of cratons. While the previous studies have already shown that lithospheric strength matters for cratonic stability, these experiments show that it is the subcrustal mantle lithosphere and not the thick cratonic crust

that plays a major role in cratonic stability. It has been concluded (Francois et al., 2013) that dry olivine dislocation creep rheology is most appropriate for cratonized mantle lithosphere.

In addition to the analysis of craton stability, a number of authors (e.g., Burov and Molnar, 2008; Burov and Watts, 2006; Burov et al., 1998; Okaya et al., 1996; Willingshofer and Cloetingh, 2003) have made estimates of strength of normal (undepleted) lithosphere needed for support of long-term normal loads such as orogenic topography, crustal roots, or inherited heterogeneities and/or tectonic forces (Figure 13(a)). These estimates show that strong lithosphere mantle with at least 20–30 km thick mechanical core is needed for stability of crustal and topographic structures during characteristic life spans of geodynamic processes.

Figure 13(b) summarizes resultants of numerical experiments with normal orogenic loading exerted on lithosphere with undepleted mantle part. The surface load is represented

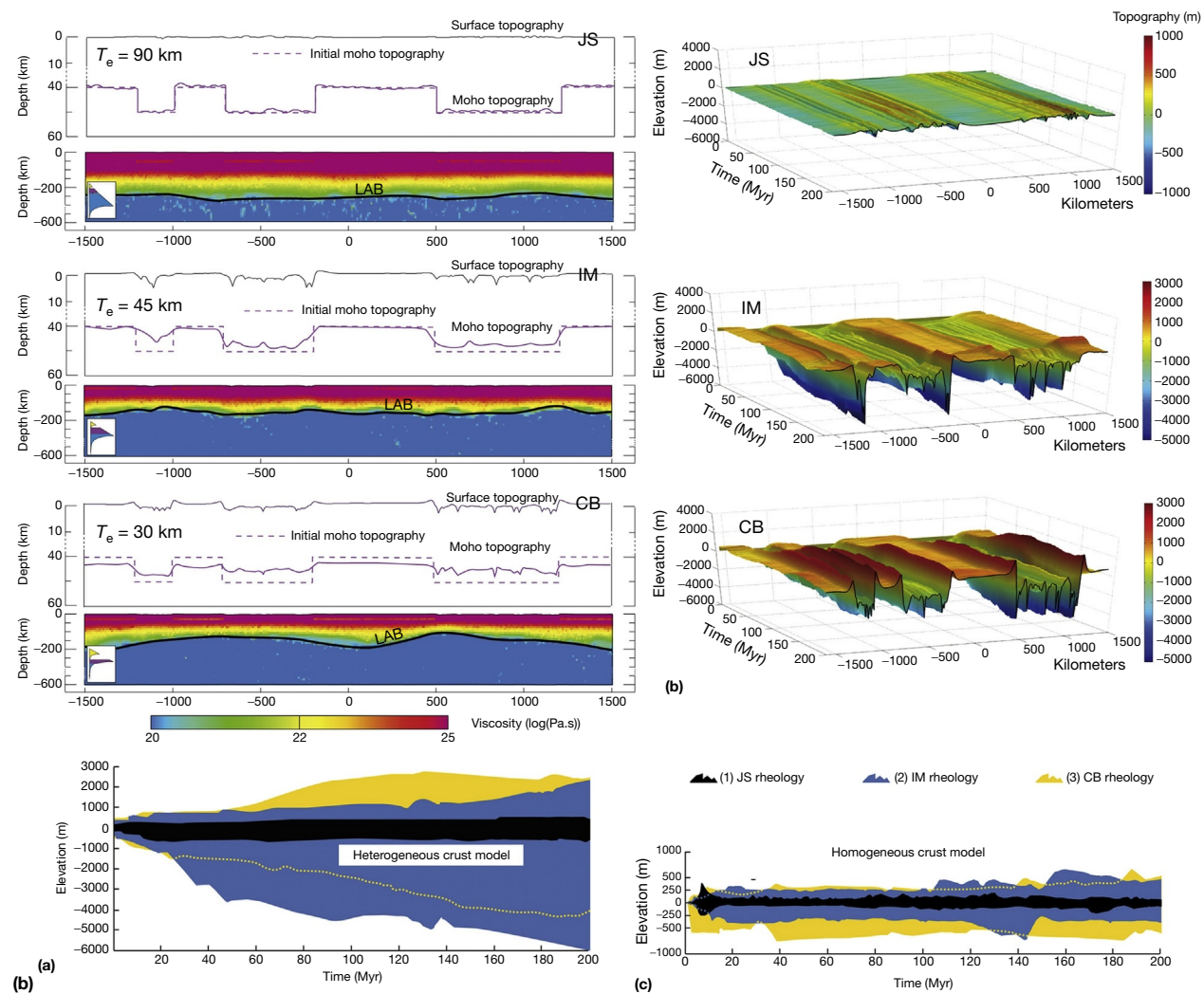


Figure 12 (Continued) (b) Numerical experiments on craton stability corresponding to the settings shown in (a). Top figure displays model setup. (a) Equivalent viscosity and surface and Moho topography evolution for three rheological assumptions: JS; CB, and intermediate case (IM). (b) Predicted surface topography evolution (note that in real cratons, surface topography undulations rarely exceed 100 m in the absence of strong external forcing. Hence, JS model is the most appropriate). (c) Average topography evolution as a function of time.

by a Gaussian-shaped mountain, 3 km high, 200 km wide, of uniform density (2650 kg m^{-3}). As can be seen, for the crème brûlée model, the crust and mantle already become gravitationally and mechanically unstable after 1.5–2.0 My. By 10 My (Figure 13(b) and 13(c)), the lithosphere disintegrates due to

delamination of the sub-Moho mantle followed by its convective removal and replacement with hot asthenosphere. This leads to flattening of the Moho and tectonic erosion of the crustal root that initially supported the topography. The jelly sandwich model, on the other hand, is stable, and there are

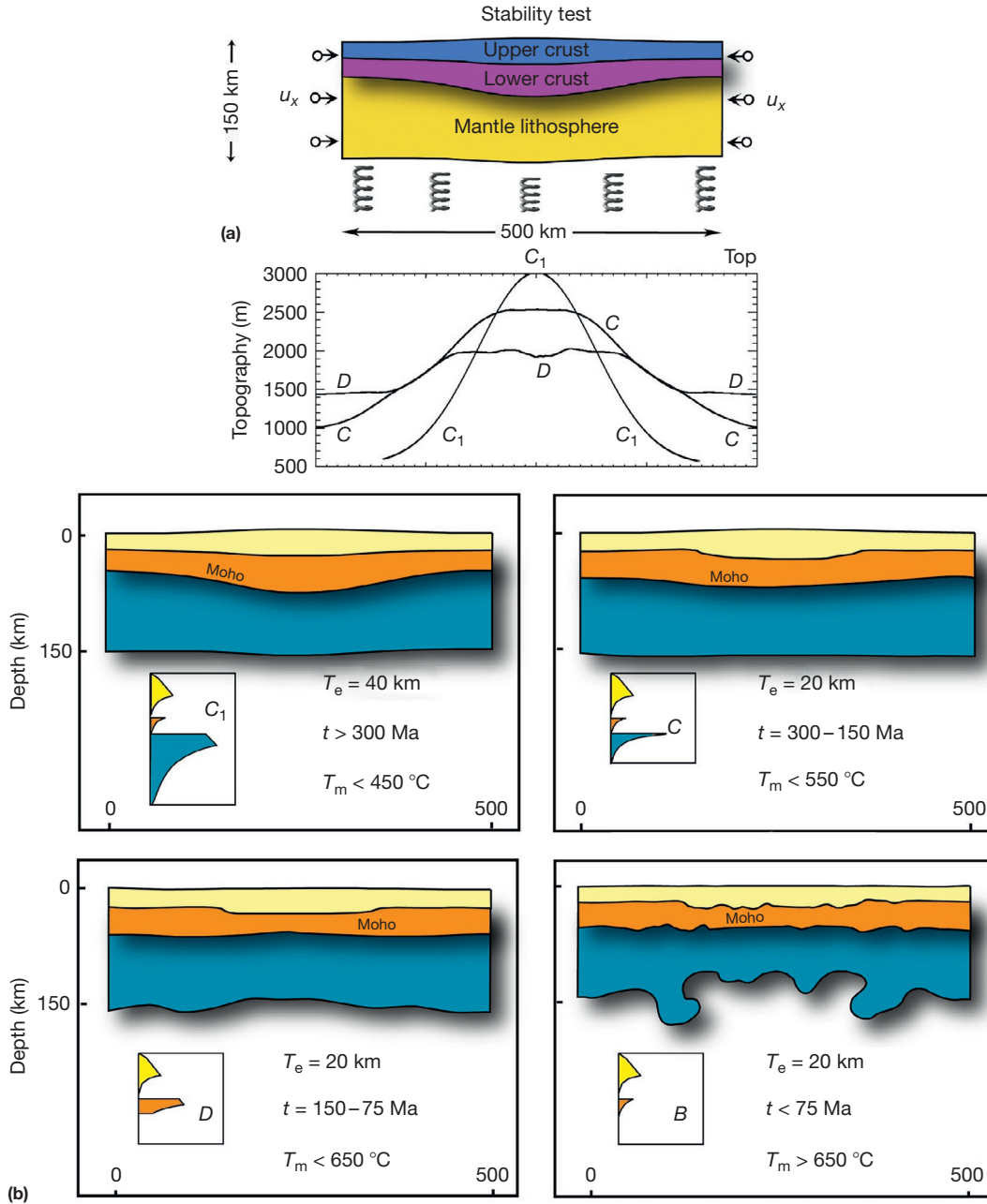


Figure 13 (a) Setup of the numerical thermomechanical model aimed to study gravitational mechanical stability of the lithosphere. Thermomechanical numerical tests of the stability of a mountain range are based on yield stress envelopes corresponding to the ‘jelly sandwich’ and ‘crème brûlée’ rheology models (Figure 4(a) and 4(d); see also Jackson (2002)). The thermal structure is equivalent to that of a 150-My-old plate. The numerical model is based on fully coupled thermomechanical large-strain viscous–elastic–plastic finite element code Paro(a)voz v.9 based on the FLAC algorithm (Cundall, 1989). This code allows for explicit testing of ductile, brittle, and elastic rheology laws. The models assume a free upper surface and a hydrostatic boundary condition at the lower surface (depicted by springs in the figure). The stability test was based on a mountain range of height 5 km and width 200 km that is initially in isostatic equilibrium with a zero elevation 36 km thick crust. The isostatic balance has been disturbed by applying a horizontal compression to the edges of the lithosphere at a rate of 5 mm year^{-1} . The displacements of both the surface topography and Moho were then tracked through time. (b) Crustal and mantle structure after 10 My has elapsed. Middle of the figure shows surface topography evolution for rheologies C_1 , C (jelly sandwich) and D (crème brûlée), left, and effective shear stress distribution for the case C . Note rapid topography collapse in case D , whereas cases C_1 and C are stable.

(Continued)

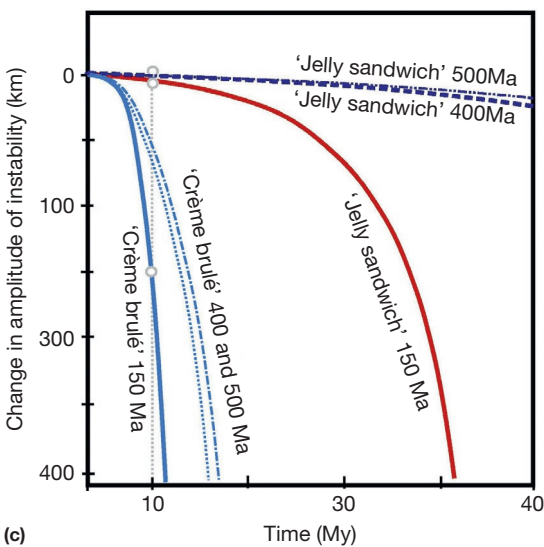


Figure 13 (Continued) (c) The amplitude of the mantle root instability as a function of time. The figure shows the evolution of a marker that was initially positioned at the base of the mechanical lithosphere (i.e., the depth where the strength = 10 MPa). This initial position is assumed to be at 0 km on the vertical plot axis. The solid and dashed lines show the instability for a weak, young (thermotectonic age = 150 My) and strong, old (thermotectonic age = 400- or 500-My-old) plates, respectively.

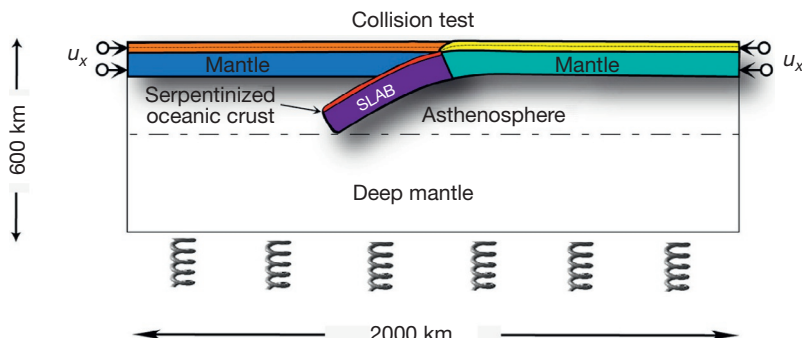


Figure 14 Setup of numerical thermomechanical models aimed to study rheological sensitivities of continental collision mechanisms. The collision test was based on a continent/continent collision initiated by subduction of a dense, downgoing, oceanic plate. Assumed normal thickness of the oceanic crust is 7 km, with serpentinized crust–mantle interface in the slab (Rupke et al., 2002). Total convergence rate of 60 mm year⁻¹. Rheological properties and other parameters are as given in Tables 1–3.

only few signs of crust and mantle instability for the duration of the experiments (10 My).

6.03.6.6 Dynamic Stability Analysis Using Direct Numerical Thermomechanical Models

In order to substantiate the growth times of convective instabilities derived from simple viscous models, and response of the lithosphere to horizontal shortening, Burov and Watts (2006) carried out sensitivity tests using a large-strain thermomechanical numerical model that allows the equations of mechanical equilibrium for a viscous–elastic–plastic plate to be solved for *any* prescribed rheological strength profile (e.g., Cundall, 1989; Poliakov et al., 1993). Similar models have been used by Toussaint et al. (2004), for example, to determine the role that the geotherm, lower crustal composition, and metamorphic changes in the subducting crust may play on the evolution of continental compressional zones. Burov and

Watts (2006) ran separate series of tests (Figure 14) using rheological properties that matched cases with weak mantle rheology (crème brûlée; Figure 4(d)) and strong mantle rheology (jelly sandwich; Figure 4(d)), as well as some intermediate rheology profiles with weak or strong mantle. The goal of these experiments is to test what these and intermediate rheology models imply about the stability of mountain ranges and the structural styles that develop. The next sections show the results of stability tests and continental collision tests.

6.03.6.7 Resistance to Stable Deformation Under Compressional Tectonic Forces ('Simple Shear' Subduction versus 'Pure Shear' Collision)

Figure 15 shows the results of the collision tests for five various YSEs considered in Jackson (2002) and Mackwell et al. (1998) (see also Figure 4(b) and 4(d)). Figure 15(a) shows a snapshot of the deformation after 300 km of shortening, which at

60 mm year⁻¹ takes 5 My. The jelly sandwich models (three cases marked JS1, JS2, and JS3) are stable and subduction occurs by the underthrusting of a continental slab that, with or without the crust, maintains its overall shape. In addition, the predicted deformation style in the accretion prism appears to be highly realistic (Figure 15(b) and 15(c); Burov and Yamato, 2008). The crème brûlée models (two cases in the bottom, one strong and another with weak lower crust), on the other hand, are unstable. There is no subduction and convergence is taken up in the suture zone that separates the two plates. The crème

brûlée model is therefore unable to explain those features of collisional systems that require subduction such as kyanite- and sillimanite-grade metamorphism. The jelly sandwich model, on the other hand, can explain not only the metamorphism and development of fold-and-thrust structures (Figure 15(b) and 15(c)) but also some of the gross structural styles of collisional systems such as those associated with slab flattening (e.g., western North America; Humphreys et al., 2003), crustal doubling (e.g., Alps; Giese et al., 1982), and arc subduction (e.g., southern Tibet; Boutelier et al., 2003).

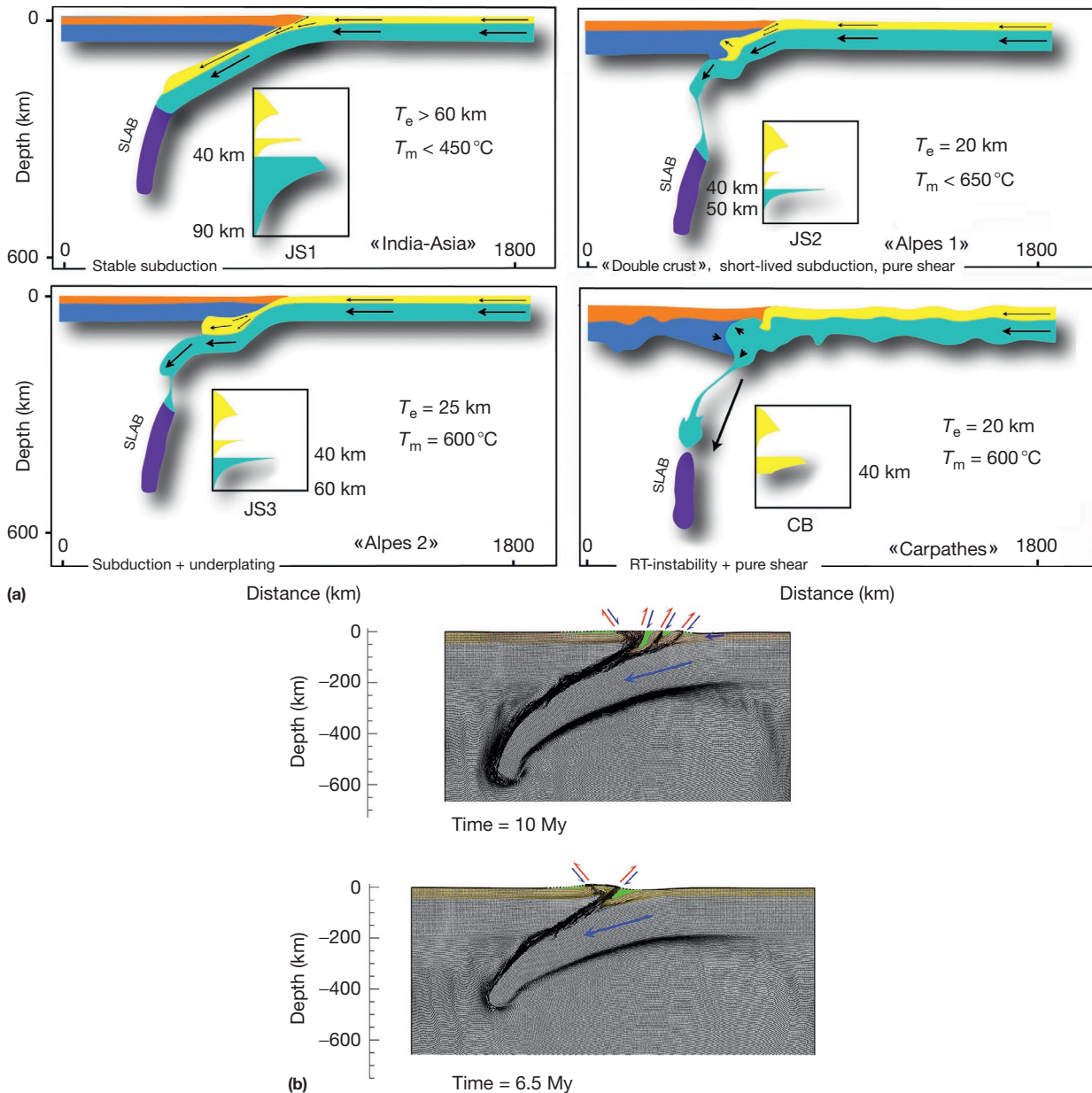


Figure 15 (a) Numerical tests of the stability of a continental collisional system using various failure envelopes. The figure shows a snapshot at 5 My of the structural styles that develop after 300 km of shortening. (b) Deformation of the passive marker grid highlighting multiple thrust-and-fold structures forming at different stages of continental subduction, for the experiment corresponding to the rheology profile 'C₁' from (a). Formation of such structures requires a relatively low strength of the near-Moho zone in the lower crust (possibility of crust–mantle decoupling) and a strong mantle as a sliding surface. This explains the eventual complexity of some of the resulting P – T – t paths. For the sake of space, the image is cut horizontally at 650 km depth (the bottom is not shown). Green color corresponds to sedimentary depots.

(Continued)

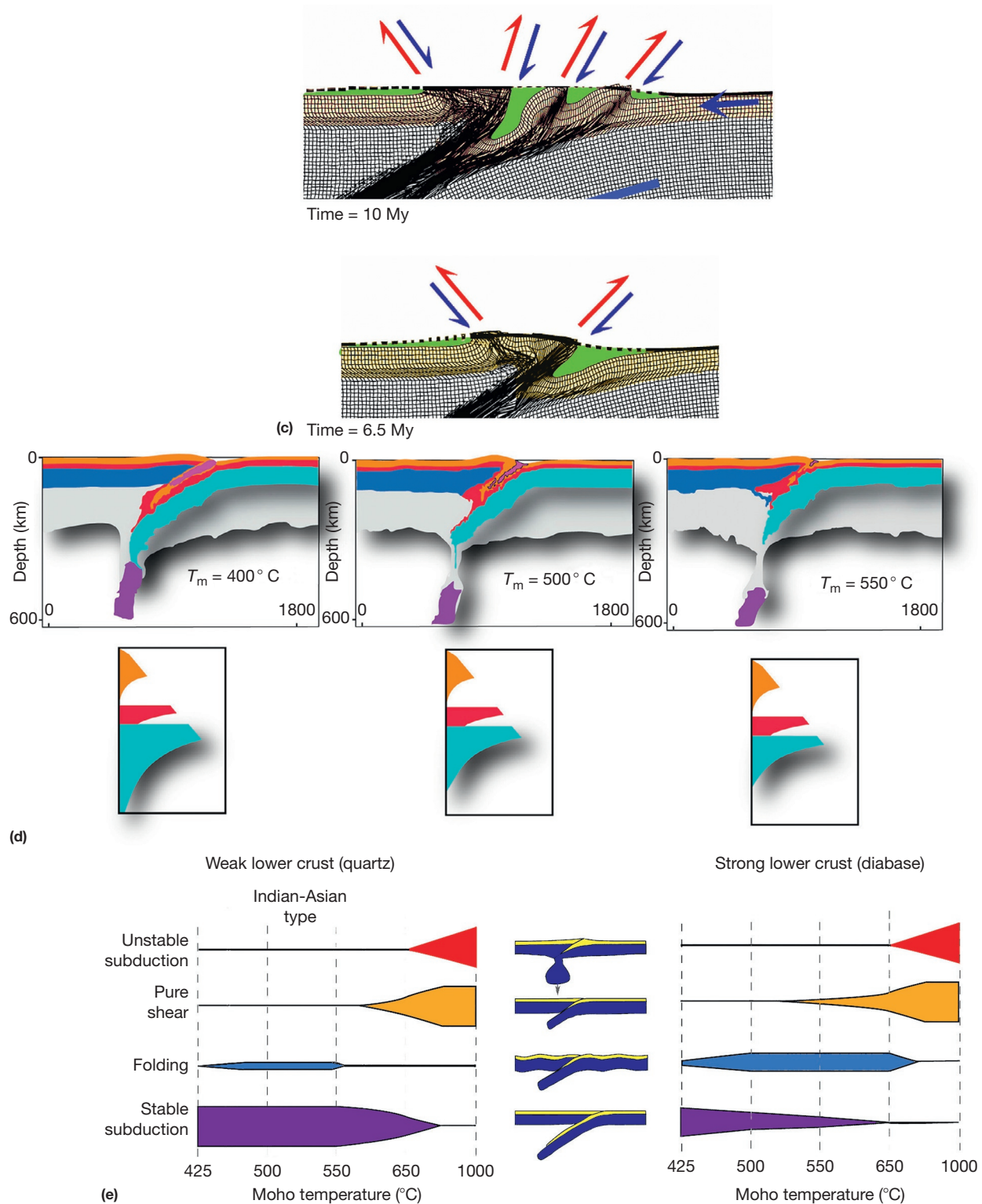


Figure 15 (Continued) (c) Zoom to the central part of (b) (Burov and Yamato, 2008). Purple color corresponds to the created sedimentary matter, orange color marks the upper crustal material, and red color marks the lower crustal material. The gradation of the scale bar is 50 km. (d) Experiments of (a) (profile C_1), (b), and (c) repeated for the case of strong dry diabase lower crust (quartz–diabase–dry olivine rheology) at 5.5 My. Moho temperatures are, respectively, 400, 500, and 550 °C. All other parameters and details are exactly the same as in the experiments from (a). Note important buckling of the plates imposed by the presence of strong diabase crust that results in mechanical coupling between the plates. Purple color corresponds to the sedimentary matter or to the oceanic slab, orange color marks the upper crustal material, and red color marks lower crustal material. Blue (dark or light) color marks mantle lithosphere; gray color marks the asthenosphere. (e) Comparison of shortening styles of continental lithosphere in case of weak lower crust (right) and strong dry diabase lower crust (left, det diabase rheology profile from Figure 4(b)). As also shown in (d), strong lower crust promotes large-scale folding instead of subduction. Similarly to (a), Moho temperature characterizes the geotherm and thus the rheology profile.

Slow-rate continental collision settings such as western Alpine orogeny present a particularly rich context for testing different rheological hypothesis. The continental convergence in the Alpine collision zone goes at rates that are in average smaller than 1 mm year^{-1} (Yamato et al., 2007) and have hardly exceeded $1\text{--}2 \text{ cm year}^{-1}$ at the initial stages of the continent–continent phase of collision. Under these conditions, thermal diffusion strongly competes with thermal advection in the submerging part of the lithosphere. This significantly hampers the chances for stable subduction since high thermal Péclet numbers (ratio of advection rate to diffusion rate) are needed to keep subduction going (Burov et al., 2014a, b, c; Toussaint et al., 2004). In case when thermal diffusion contributes in heat balance as much as thermal advection, the slab heats up at a same rate as it goes down, its buoyancy increases, while its ductile strength decreases. Both factors prevent subduction, whose possibility becomes strongly dependent on subtle peculiarities of the rheological properties and structure of not only the continental mantle lithosphere but also its crust. Or petrology data on exhumation of ultrahigh-pressure metamorphic rocks that where initially buried to depths in excess of 110 km attest that at least at its initial stages, Alpine subduction did take place and continued for at least 5–10 My. Thermomechanical models (Burov et al., 2014a, b, c; Yamato et al., 2007) show that in this case, it is possible to constrain not only the rheological strength of mantle lithosphere but also some fine details of the rheological structure of the crust of both the subducting plate and overriding plate. Figure 16 shows the results of several experiments where different crustal rheological profiles were tested with the goal to determine their compatibility with one-sided continental subduction. Despite the fact that all of the tested profiles are consistent in terms of rock mechanics data, only some of them are compatible with subduction scenario in the Alpine settings. It has been shown that the evolution of the Alpine orogeny can be best explained under the assumption of a three-layer decoupled rheological structure with quartz-dominated upper crust, quartz-diorite lower crust, and dry olivine mantle lithosphere that has a strong mechanical core with effective mechanical thickness of at least 30 km. When this structure is determined, parameterization of the appropriate rheology laws becomes rather straightforward.

6.03.6.8 Response to Large-Scale Compressional Instabilities (Folding)

Analysis of the subsidence and uplift history of sedimentary basins for a number of sites worldwide suggests that lithospheric folding is a primary response of the lithosphere to recently induced compressional stresses (e.g., Burov et al., 1993; Cloetingh et al., 1999; Cloetingh and Ziegler, 2007; Table 5; Figure 7). Despite the widely held view that folding occurs only over a short time interval, it was shown (Cloetingh et al., 1999; Gerbault et al., 1999) that it can persist over very long periods of time ($>10 \text{ My}$) independently of presence of inhomogeneities such as crustal faults (Figure 7(c)). The numerical experiments on brittle–elastic–ductile folding implemented in these studies show that the formation of large-scale faults does not prevent folding. In turn, the localization and spacing of the faults are controlled by the wavelength of folding (faults tend to

localize at the inflection points of folds). As suggested on the base of analytic considerations (eqn [37], section on the oceanic folding), and confirmed by the numerical experiments, the characteristic wavelengths, λ , of small-amplitude folding are proportional to $5\text{--}10 \times$ thickness of the competent layers and thus are indicative of the lithospheric strength:

$$\lambda < 5 - 10h \sim 5T_e - 10T_e \quad [42]$$

These wavelengths are determined by the presence of young lithosphere in large parts of Europe or Central Asia or by that of old lithosphere in the Canadian or Australian craton, as well as by the geometries of the sediment bodies acting as a load on the lithosphere in basins. The proximity of some of these sites to the areas of active tectonic compression suggests that the tectonically induced horizontal stresses are responsible for the large-scale warping of the continental lithosphere. The persistence of periodical undulations in Central Australia (700 Ma since onset of folding) or in the Paris Basin (60 Ma) long after the end of the initial tectonic compression requires a strong rheology compatible with the effective elastic thickness values of about 100 km in the first case and 50–60 km in the second case (Cloetingh and Burov, 2010; Cloetingh et al., 1999). Figure 7(b) and Table 5 show recent compilation of the observed wavelength of continental folding (Cloetingh et al., 1999) compared to the predictions of analytic models (e.g., Burov et al., 1993). In continental lithosphere, there may be several competent layers that yield different folding wavelengths. In such cases, observed folding wavelengths allow one to separate between strong crustal and mantle layers. For example, in the case of Central Asian lithosphere, two wavelengths can be depicted: crustal (50–100 km) and mantle (300–350 km). These wavelengths suggest the existence of roughly 10 km thick strong crustal ‘core’ and 30–50 km thick strong mantle layer. In case of cratons (Central Australia), the folding wavelength reaches 600–700 km indicating a 60 km thick competent layer. In both cases, the thickness of the strongest folded layer appears to be higher than the crustal thickness, confirming the idea that plates maintain considerable strength concentrated in their mantle part. The observations of folding suggest thicknesses of competent layers comparable with the corresponding T_e estimates (Figures 5 and 8). It is noteworthy, however, that there are some cases when λ/T_e ratios are abnormally high (>10) or low (<4). The high ratios mostly correspond to very weak lithospheres loaded by large amounts of sediment, which increases the wavelength of folding. The linear folding theory (eqn [37] or [42]) also does not apply in case of high amplitude-to-wavelength ratios (basically small λ/T_e), because in this case, plastic hinging at the weakened inflection points results in transition from unstable-to-stable folding, for which the wavelength is a simple function of the amount of shortening and does not depend on h or T_e . Wavelength of folding may be additionally influenced by superposition of various geodynamic events, for example, post-compressional extension and mantle dynamics.

As an illustration, Figure 17 shows the results of thermo-mechanical modeling experiments for a 250-Ma-old lithosphere shortened at a slow rate of $1.25 \text{ cm year}^{-1}$ (Smit et al., 2013). In this case, some strongly decoupled low-amplitude short-wavelength (50–100 km) folding superimposed on large-wavelength mantle folding (300–400 km) develops, leading to crustal thickening above synclinal mantle folds.

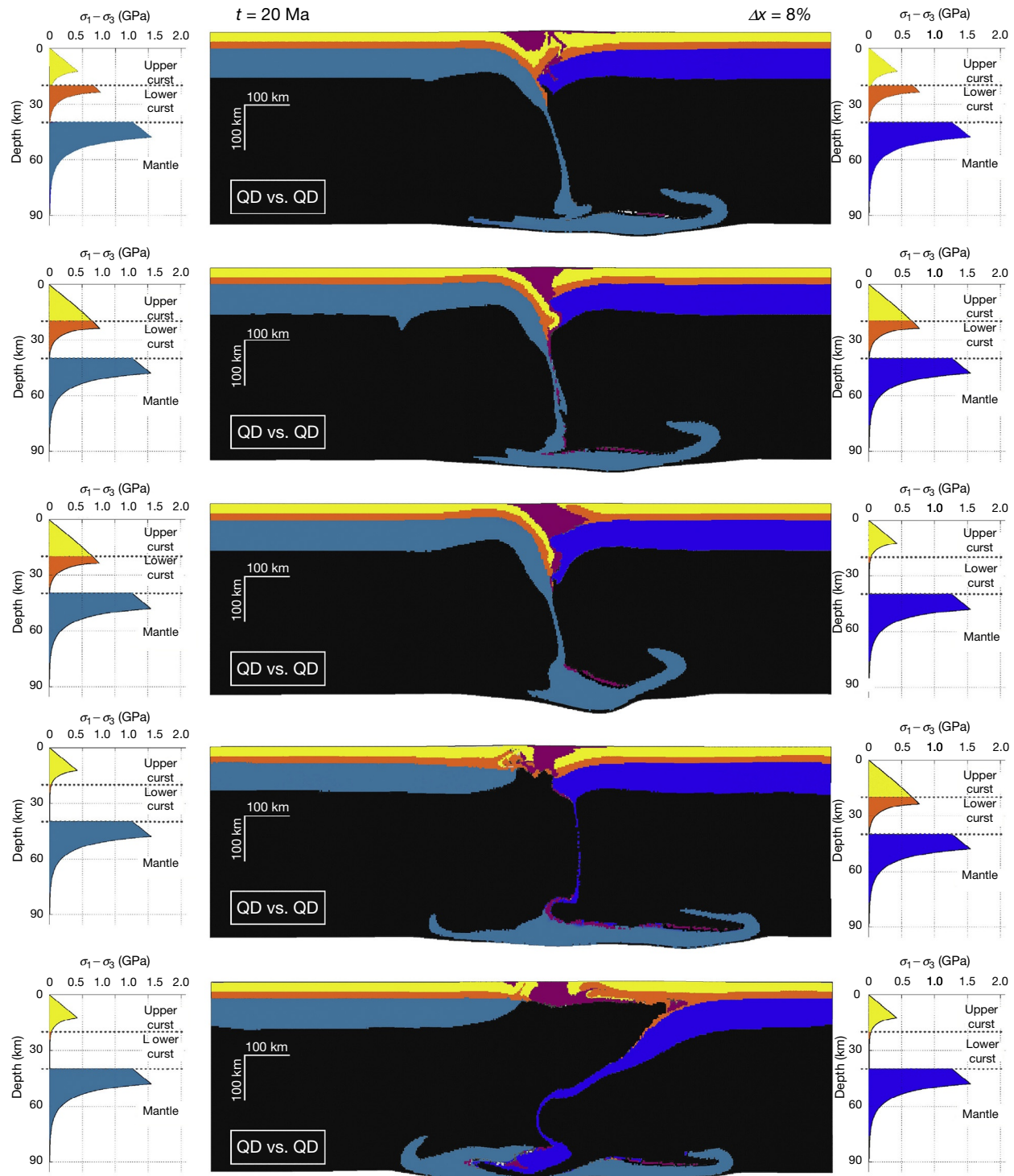


Figure 16 Influence of crustal rheology on the collision style in case of slow (6 mm year^{-1}) Alpine-type collision (weak lithosphere; Burov et al., 2012). Shown are morphologies for the models at 20 My for different crustal strength profiles. QD, quartz–diabase double-layer crustal structure (upper and lower crust, respectively); QQ, quartz–quartz double-layer crustal structure; DD, strong single-layer structure simulated by diabase. Color code: blue, mantle; orange, lower crust; yellow, upper crust; dark, asthenosphere and sublithosphere mantle.

The experiments shown in **Figure 17** put further emphasis on the effect of rheological decoupling on the observed surface topography wavelengths, specifically in case of 500-Ma-old lithosphere. For small convergence rates, mantle folding may not develop or will occur with reduced wavelength due to low Péclet number of the system, which leads to heat diffusion and weakening of the folds. The observed folding wavelengths are directly related to the thickness of the mechanical cores in the crust and mantle. Hence, it becomes possible to parameterize leading crustal and mantle rheologies by varying tested rheological profiles until the model-predicted wavelength spectra start to match the observations.

6.03.6.9 Response to Extensional Tectonic Loading (Rifting)

A number of authors (e.g., Bassi, 1995; Buck, 2007; Huismans et al., 2005) have studied possible rifting modes as a function of the rheological profile. The results show that the narrow rifting mode is only possible in case of substantial mantle strength. If the lithospheric mantle is weak, the system switches to the wide rifting mode (e.g., Basin and Range) that may be characterized by periodic instabilities such as boudinage. These models suggest that not only narrow rifting mode but also other rifting styles (wide rifting mode and metamorphic core complex mode), except very wide delocalized rifts, require at

least a 20–30 km thick competent mantle layer. Application of common dry olivine flow laws in the direct numerical models of tectonic deformation yields generally coherent results for predicted rifting styles (**Figure 18**). Certainly, strength in the mantle may not always be needed to form metamorphic core complexes. In this case, rather thick, weak lower crust may be required (Block and Royden, 1990; Buck, 1988, 1991). In this case, it is suggested that the lack of a pronounced basin, associated with the large extension inferred for core complexes, may indicate that crust has flowed into the extending region. The crust in such cases would decouple the mantle from the surface so mantle strength would have very little effect on core complex development.

6.03.7 Relations Between Short-Term and Long-Term Properties

6.03.7.1 Seismicity and Long-Term Deformation

Handy and Brun (2004) argued that seismicity is an ambiguous indicator of strength, that is, it is an indicator of mechanical weakness of the relevant layer that is not capable of sustaining tectonic or bending stress. The models of previous sections show that T_s is also an indicator of current stress level (eqn [36]) and probably reflects the thickness of the uppermost weak

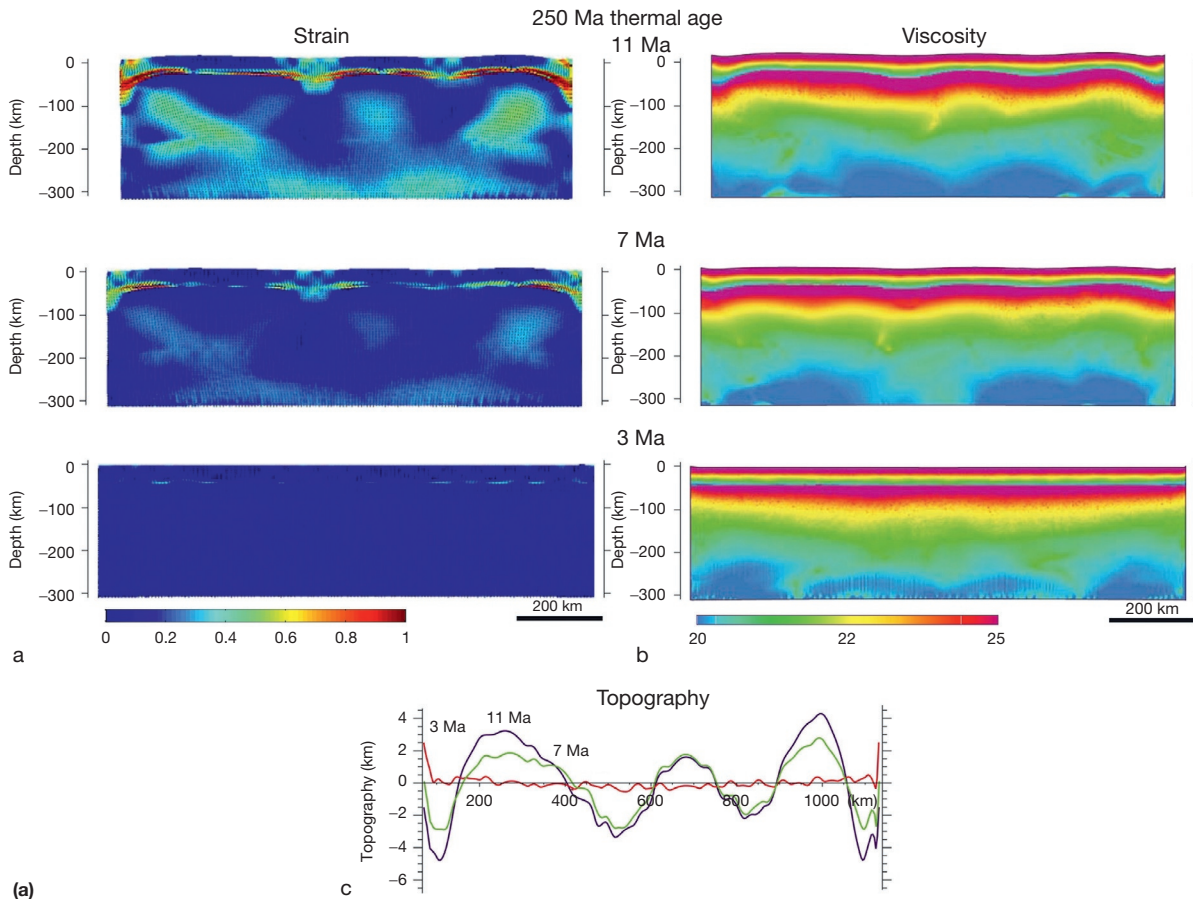


Figure 17 (a) Example of continental folding models for thermotectonic age of 250 Ma. Shown are finite strain, effective viscosity, and surface topography (Smit et al., 2012). Shortening at $1.25 \text{ cm year}^{-1}$. The horizontal scale of the model is identical to the vertical scale.

(Continued)

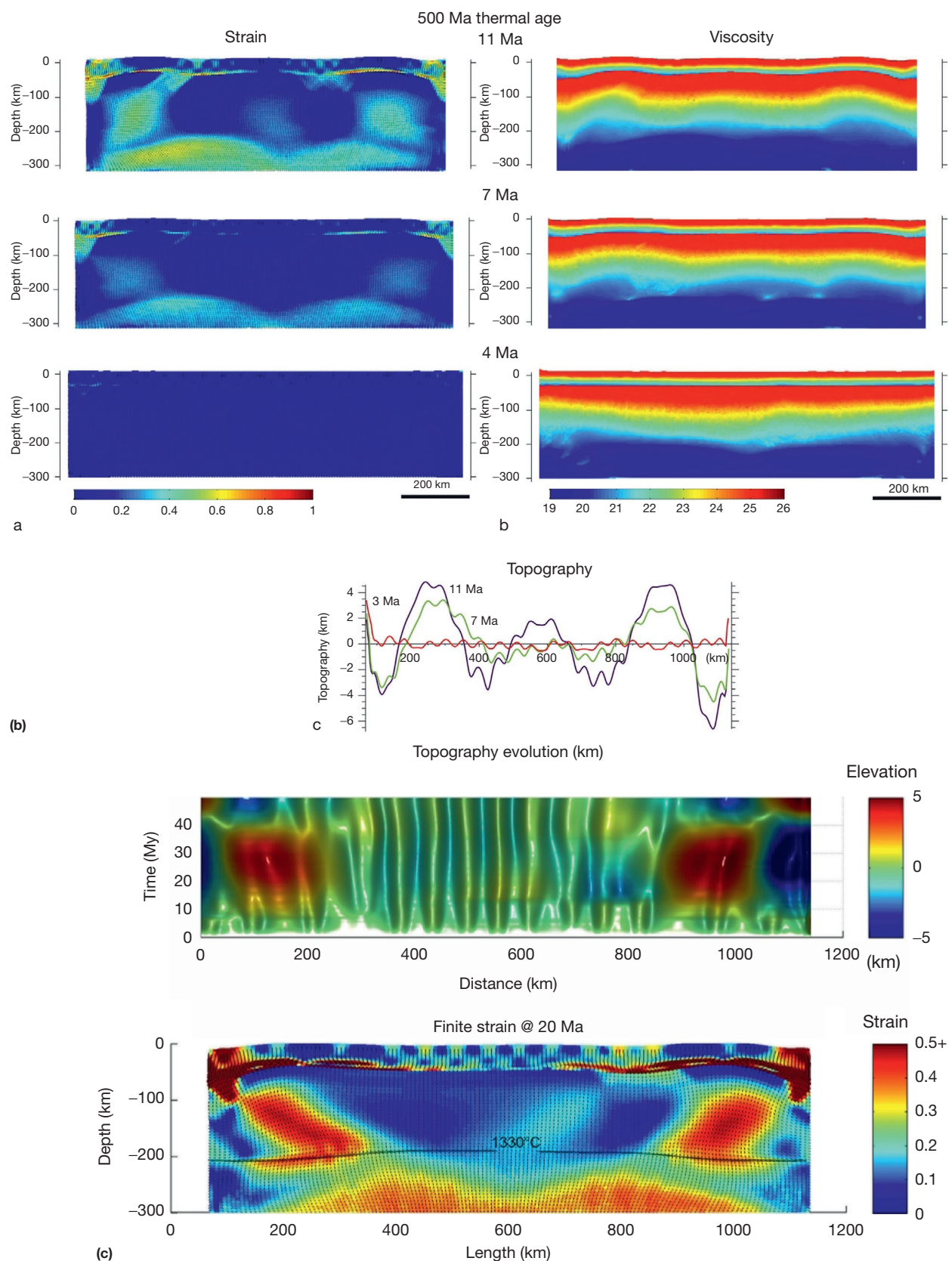


Figure 17 (Continued) (b) Numerical models of continental folding models for thermotectonic age of 500 Ma. Shown are finite strain, effective viscosity, and surface topography (Smit et al., 2012). Shortening at $1.25 \text{ cm year}^{-1}$. The horizontal scale of the model is identical to the vertical scale. (c) Surface topography evolution at 20 Ma for the experiment shown in [Figure 16\(a\)](#) (Smit et al., 2012). The horizontal scale of the model is identical to the vertical scale.

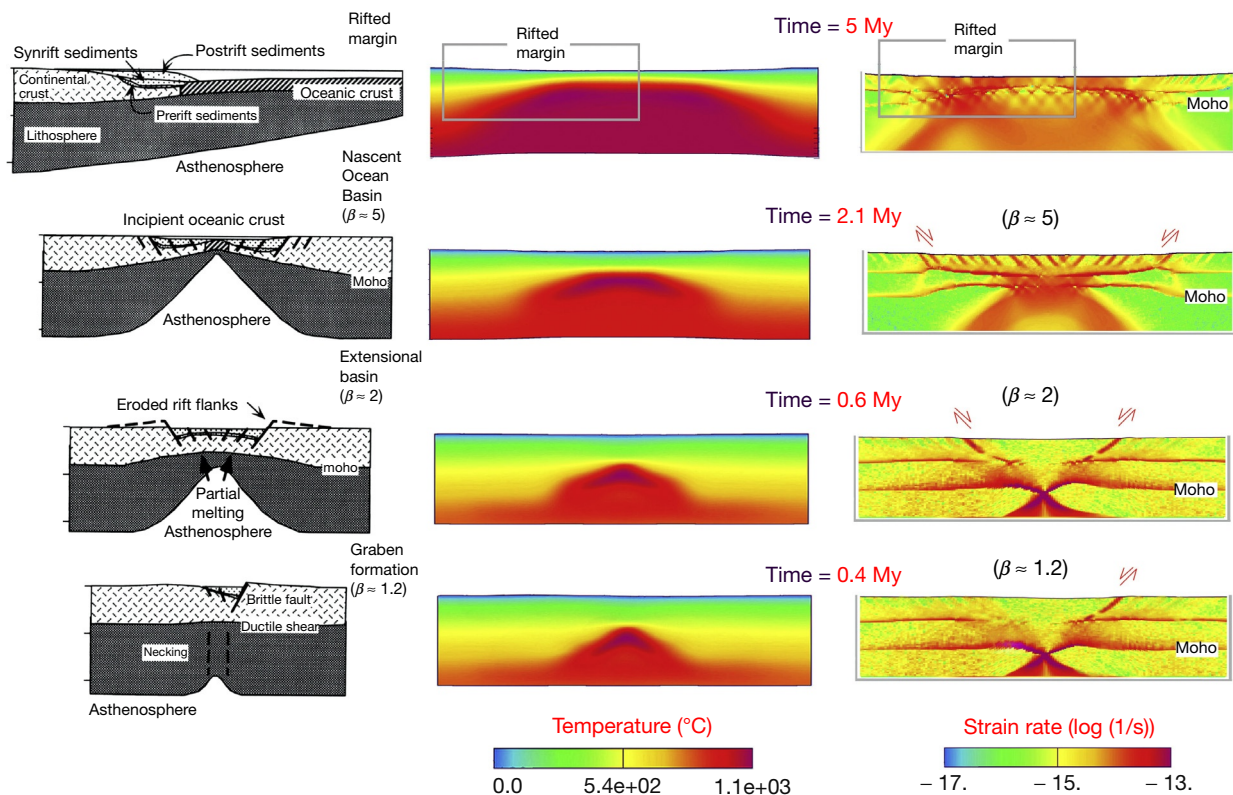


Figure 18 Stable and unstable extension styles predicted from direct numerical viscous–elastic–plastic thermomechanical models (Burov and Poliakov, 2001) and compared with the typically observed extension styles. Application of common dry olivine flow laws for mantle lithosphere yields generally coherent results for predicted styles of rifting. (right) Rifting styles as a function of the amount of extension (factor β) according to the geologic observations (Salveson, 1978). (left) Model predicted rifting styles (log strain rate) computed from the viscous–elastic–plastic numerical model based on ‘jelly sandwich’ rheology with strong upper crust (quartz) and upper mantle (olivine) (reproduced from Burov EB and Poliakov ANB (2001) Erosion and rheology controls on synrift and postrift evolution: Verifying old and new ideas using a fully coupled numerical model. *Journal of Geophysical Research* 106: 16,461–16,481). The rheology profile used for thermomechanical modeling corresponds to 150–200 My profile 3 from Figure 9(a).

brittle layers that respond on historical timescales to stresses by faulting and earthquakes. T_e , in contrast, is proxy for the integrated strength of the entire lithosphere that responds to long-term ($>10^5$ year) geologic loads by flexure. A number of seismic tomography studies (e.g., Soureau et al., 2001) have also demonstrated that when compared with the distribution of seismicity, tomography reveals that earthquake depths are often limited by density or compositional boundaries, specifically those between the upper and lower crust. This may be related to stress drops caused by mechanical inconsistencies between these layers.

Seismic patterns do not allow for discrimination between the brittle and hypothetical nonbrittle–ductile earthquakes. Although the absence of earthquakes beneath the seismic Moho remains enigmatic, the simplest explanation refers to the insufficiency of tectonic and bending stresses to reach high brittle strength at Moho depth and below, healing of microfractures, and dominance of GBS shear strain localization that is specific for mantle in temperature range of 500–800 °C. As shown in Figure 10, for continental crust of typical thickness and a crust–mantle detachment, the bending stresses at the crust–mantle boundary are lower than the yielding strength, whereas the weight of the thickened crust increases the brittle strength of the mantle lithosphere.

From field observations, it is argued (Handy and Brun, 2004; see also Section 112.5.5) that earthquakes can be reasonably interpreted as a manifestation of a transient mechanical instability within shear zones. According to observations of outcropping fault surfaces, most shear zones have very specific rheological properties that distinguish them from normal rocks. For example, in these zones, ductile mylonitic creep is punctuated by ephemeral high-stress events involving fracture, frictional melting, and episodic local loss of cohesion.

6.03.7.2 Postseismic Relaxation Data and Long-Term Deformation

A number of studies interpret postseismic relaxation data in terms of the long-term viscosity of the crust or mantle (e.g., DallaVia et al., 2005; Pollitz et al., 2001; Sabadini and Vermeersen, 2004). Most of these studies yield ‘subsurface’ viscosities of 5×10^{16} to 2×10^{19} Pa s. These values are smaller than the estimates of asthenospheric viscosity derived from post-glacial rebound data but considerably higher (8 orders of magnitude) than predictions of rock mechanics for seismic timescale (Figure 3). They are also 3–6 orders of magnitude lower than what can be inferred for long-term deformation from the data of rock mechanics, except for some quartz-dominated lower

crustal compositions. We conclude that postseismic viscosity values are either not indicative of the long-term behavior, referring to early Kelvin reaction according to Burger's rheology model (eqn [29]), or indicative of highly nonlinear behavior, which yields disproportionately small viscosities at high deformation rates. Several mechanisms may be considered, for example, preferential deformation due to cavitation in fine-grained mylonitic shear zones that results in porosity increase and major ductile weakening of the shear zone (Bürgmann and Dresen, 2008). Such deformation may only occur at seismic and postseismic timescales. Since postseismic deformation rates may vary with time, the effective Kelvin viscosities might be also nonlinear. For example, one of the alternative explanations of the low postseismic viscosity values refers to strain rate-dependent deformation caused by postseismic equilibration of fluid pressure in seismically modified fracture networks. In all cases, postseismic data are most probably not related to the long-term behavior.

6.03.7.3 Field Observations and Geophysical Data

Geophysical transects of plate margins and structural studies of exhumed fault rocks generally validate the rheology laws derived from experimental rock mechanics (Handy and Brun, 2004; Mouthereau et al., 2013) assuming 'jelly sandwich' parameters. Seismically observed crustal and mantle lithosphere structures are largely indicative of cases of ductile lower crust and stronger mantle lithosphere. In particular, this refers to the geophysical traverses NFP20 and ECORS-CROP across the Alps (Bayer et al., 1989; ECORS-CROP group, 1989; Frei et al., 1990; Kissling and Spakman, 1996) and DEKORP-ECORS across the Rhine Graben (Brun et al., 1991, 1992; Meissner and Bortfeld, 1990). The Alpine part of the transects shows that the lower crust of the Apulian Plate is detached from its underlying mantle and forms a north-tapering wedge between the downgoing European lithosphere and partly exhumed nappe edifice of the Alpine orogen (Handy and Brun, 2004). Burov et al. (1999) had studied the mechanical stability of this structure to find that high mantle resistance compatible with a 30 km thick competent mantle lithosphere layer is required to ensure its long-term stability. Similar considerations concerning the presence of strong mantle can be derived from seismic cross sections of the Rhine Graben and those across the Altyn Tagh fault system (Wittlinger et al., 1998) and Ferghana basin (Central Asia; Burov and Molnar, 1998), across the Abitibi-Wawa belts and Kapuskasing uplift system in the Canadian craton (LITHOPROBE). In the case of the Altyn Tagh fault system, oblique convergence of the bounding plates is accommodated by the Altyn Tagh strike-slip and thrust system, indicating that the lithospheric mantle was displaced along the fault as a rigid media. Remarkable direct evidence of high mantle strength is based on the data on the Kapuskasing uplift (Burov et al., 1998). The Kapuskasing structural zone cuts structures of the Superior Province in the Canadian Shield: the Abitibi-Wawa granite-greenstone belts to the south and Quetico-Opatica metasedimentary belts to the north. The geophysical and seismic transect LITHOPROBE reveals enormous volumes of dense granulites thrust upward along the ancient Kapuskasing thrust fault that was active about 2700 My ago. Despite the load of the granulite body, which exceeds that of an 'average'

mountain belt, Moho boundary shows a small depression with an amplitude of just a few kilometers, which implies T_e of 100 km and viscosities $>10^{24}$ Pa s. It was concluded that independently of crustal strength, the mantle part of the lithosphere of the Canadian craton should include a strong layer with a minimum thickness of 60 km and thus rheology corresponding to strongest of the dry olivine rheologies (Table 2). This conclusion has been drawn (Burov et al., 1998) from the results of thermomechanical numerical models testing the mechanical stability of the Kapuskasing structure for a wide spectrum of rheology laws. It is also noted that in the collision zones (e.g., Himalaya), the lower crust is practically never exposed at the surface. Since the lower crust is lighter than the mantle, the simplest explanation would be that it is dragged down by the downgoing mantle lithosphere, which requires high mantle strength.

6.03.8 Conclusions and Future Perspectives

Although rheology laws based on experimental data of rock mechanics may be partly representative for long-term and large-scale deformation, they need validation and re-parameterization for geologic temporal and spatial scales. This particularly refers to the flow laws for crustal rocks, due to the diversity of mineralogical composition of continental crust (Burov, 2002). Long-term rheological properties can be scaled on the basis of observations of long-term/large-scale deformation such as the deformation of the lithosphere under known geologic loads (flexure, collision–subduction, folding, boudinage, and rifting), tectonic deformation styles, seismic and geodetic data, postglacial rebound data, and so on. The laboratory data serve as a 'first guess' for construction of long-term rheological models. Parameterization of these data requires better constraints on some major structural parameters such as the equilibrium thermal thickness of continents, $a=z(1330^\circ\text{C})$, and density contrasts between the lithospheric mantle and asthenosphere. The data on the equivalent elastic thickness (T_e) and other large-scale data confirm that the rheology of the oceanic lithosphere is in acceptable agreement with rock mechanics data for dislocation creep in dry olivine. For continents, rock mechanics data are largely compatible with the observation that T_e varies from 0–10 km in young plates to 110–120 km in cratons. If $T_e > T_c$, the strongest rheological layer refers to the mantle and fits dry olivine rheology. If $T_e < T_c$, the strength is likely to be shared between crust and mantle. 'Jelly sandwich' (decoupled) or 'dried jelly sandwich' (coupled) rheology models appear to be the most applicable for continents. The data and models suggest that for equivalent conditions, the integrated strength of continental mantle does not significantly differ from that of the oceanic lithosphere. After the thermal structure, the second major control on the mechanical behavior of continental plates refers to the diverse structure and rheology of their crusts. Depending on the crustal strength and thickness, continents may be either stronger or weaker than the oceanic plates. 'Weak or moderate' continental plate strength ($T_e < 1-1.5T_c$) refers to the cases of 'generalized jelly sandwich' rheology with ductile lower or intermediate crust (most orogenic belts and some cratons, plateaus, and most post rift basins). Strong 'dried jelly sandwich' applies to old cratons ($T_e=1.5-2.5T_c$) where the lower crust is strong

and thus crust and mantle are mechanically coupled. ‘Crème brûlée’ rheology ($T_e < T_c$, strong crust–weak mantle) is extremely weak and may apply only for young or rejuvenated lithospheres or some active rift zones (e.g., Salton Sea, Southern California, and Taupo Volcanic Zone, North Island New Zealand).

The primary question related to the interpretation of the T_s data is ‘why is there little or no microseismicity below the depth to 500 °C or at most 40–50 km, in both the oceans and continents?’ The T_s data, we believe, are indicative of limited tectonic stress levels in the lithosphere and of small brittle strength of its upper layers compared to that of the deeper mantle. Since Byerlee’s brittle failure becomes less probable with growing pressure (depth) and with healing of the pre-existing fractures due to increasing pressure–temperature, it is highly probable that aseismic (e.g., grain size-dependent GBS creep; Drury, 2005) deformation replaces Byerlee’s brittle failure in the mantle at temperatures above 500–600 °C. GBS creep is specific for mantle olivine and is efficient in the ‘cold’ sub-Moho temperature range (500–600–700 °C), which explains why the probability of earthquakes in the continental mantle is lower than in the crust. T_s is thus not a proxy for the integrated strength of the lithosphere or T_e . T_s anticorrelates with T_e if intraplate force $F < B$ (integrated plate strength). If $F = B$, the entire plate is in the yield state and T_e has no mechanical meaning, while T_s equals BDT depth. The only possible relation between T_s and T_e is related to the influence of T_e on the mean intraplate stress level: for a given value of normal load or tectonic force $F < B$, T_s decreases with increasing T_e . In most cases, simple consideration suggests, as a rule of thumb, $T_s \leq \gamma(F/T_e + \sigma_{xx}^f)/\rho g \leq \gamma T_e$ (eqn [36]). In oceans, the only possibility for $T_s = T_e$ refers to nearly broken plates having equally strong brittle and ductile parts. This invalidates the proposition that plate strength is concentrated in the brittle part. In continents, $T_s = T_e$ may happen in ‘thermally young’ plates because there, in contrast to oceans, T_s and T_e may refer to different lithologic layers, upper crust, lower crust, and mantle (e.g., broken brittle crust supported by strong ductile mantle).

Even provided that rheology laws based on experimental rock mechanics are robust, continental YSEs based on these laws are subject to large uncertainties due to differing assumptions on the geotherm, background strain rate, hydrous conditions, and crustal structure. It is largely these factors that mainly determine the long-term mechanical properties of the lithosphere. Hence, future investigations should focus on finding better observational and model constraints on these key conditions. In particular, the cross compatibility of estimates of continental plate strength obtained from the observations of (1) flexure (for T_e values coming from the models accounting for all surface and subsurface loads), (2) folding, (3) mechanical stability models, and (4) field and indirect geophysical data supports YSE profiles derived for dry olivine and (with more reservations) granite upper crust assuming plate cooling model for 200–250 km thick lithosphere.

There is almost certainly no one type of strength profile that characterizes all continental lithosphere. It was shown that jelly sandwich rheology models (and their variants that include strong mantle and various crustal structures) are mechanically compatible with long-term support of tectonic loads and major structural styles, whereas crème brûlée models, or any models with weak mantle, are mechanically unstable. Thermomechanical modeling

of lithospheric deformation suggests that the persistence of surface topographic features and their compensating roots requires that the subcrustal mantle is strong and able to act as both a stress guide and a support for surface loads. It might be thought that it would not matter which competent layer in the lithosphere is the strong one. However, the models show that the density contrast between the crust and mantle is sufficient to ensure that it is the mantle, rather than the crust, which provides both the stress guide and support. In our view, subduction, orogenesis, or narrow to normal rifting *requires* a strong mantle layer. We have found this to be true irrespective of the actual strength of the crust. Weak mantle is mechanically unstable and tends to delaminate from the overlying crust because it is unable to resist forces of tectonic origin. Once it does delaminate, hotter and lighter mantle asthenosphere can flow upward to the Moho. The resulting increase in Moho temperature would lead to extensive partial melting and magmatic activity as well as further weakening (e.g., Karato, 1986) such that, for example, subduction is inhibited and surface topography collapses in a relatively short interval of time.

Appendix A Flexure of Continental Lithosphere with Multilayered Nonlinear Rheology

The rheology-independent form of 2-D plate bending equation is

$$-\frac{\partial^2 M_x}{\partial x^2} + \frac{\partial}{\partial x} \left(T_x \frac{\partial w}{\partial x} \right) + p_- = p_+ \quad [\text{A.1}]$$

$$M = - \int_{h_m} \sigma_{xx} y dy$$

where M_x is bending moment, h_m is the total thickness of the plate, F_x is horizontal fiber force, w is the vertical deflection of the plate (bathymetry, geometry of Moho), and p_- and p_+ are negative and positive normal loads, respectively. The equivalent elastic thickness T_e of a plate with arbitrary rheology (yet compatible with static bending) is

$$M = -D \frac{\partial^2 w}{\partial x^2} = -E \frac{T_e^3}{12(1-v^2)} \frac{\partial^2 w}{\partial x^2}$$

or

$$T_e = \sqrt[3]{-M \frac{12(1-v^2)}{E} \left(\frac{\partial^2 w}{\partial x^2} \right)^{-1}} = \sqrt[3]{MK^{-1}G} \quad [\text{A.2}]$$

where E and v are the assumed elastic parameters, K is plate curvature, and $G = 12(1-v^2)E^{-1}$.

For a single-layer plate (e.g., oceanic lithosphere, $T_e \leq h_m$) composed of n mechanically coupled rheological layers of thickness h_i , $i=1,\dots,n$,

$$T_e \approx h_1 + h_2 + \dots = \sum_n h_i \quad [\text{A.3}]$$

For a lithosphere composed of n mechanically decoupled layers,

$$T_e \approx (h_1^3 + h_2^3 + \dots) = \sqrt[3]{\sum_n h_i^3} < \sum_n h_i \quad [\text{A.4}]$$

In case of equally thick decoupled layers ($h_1 \approx h_2 \approx h_3 \dots = h$), $T_e \approx n^{1/3}h$ instead of $T_e = nh$ for a coupled plate (eqn [A.3]). Layer decoupling thus reduces T_e by a factor

of $n\%$, that is, by 40–50% for $n < 4$. The effective rigidity $D(x, w'' \dots)$ of a plate with nonlinear rheology can be estimated as

$$D(\phi) \frac{\partial^2 w(x)}{\partial x^2} \approx -D(\phi) R_{xy}^{-1} = -M_x(\phi) \quad [A.5]$$

Accordingly, $T_e = T_e(x, w'' \dots)$ of such a plate is

$$T_e = \left(\frac{D(\phi)}{D_0} \right)^{\frac{1}{3}} = \left(-\frac{M_x(\phi) R_{xy}}{D_0} \right)^{\frac{1}{3}} \approx \left(\frac{M_x(\phi)}{D_0} \left(\frac{\partial^2 w(x)}{\partial x^2} \right)^{-1} \right)^{\frac{1}{3}} \quad [A.6]$$

where $D_0 = E(12(1-v^2))^{-1}$ and $\phi = (x, w'' \dots)$. R_{xy} is local radius of bending $R_{xy} \approx -(w'')^{-1}$. For a multilayer plate composed of $i=1 \dots n$ lithologic layers with $j=1 \dots m_i$ rheological zones (brittle, elastic, ductile, etc.) per each layer, D and T_e can be obtained from the following system:

$$\begin{cases} M_x(\phi) \\ \frac{\partial^2}{\partial x^2} \left(D_0 T_e^3(\phi) \underbrace{\frac{\partial^2 w(x)}{\partial x^2}}_K \right) + \frac{\partial}{\partial x} \left(F_x(\phi) \frac{\partial w(x)}{\partial x} \right) + p_-(\phi) w(x) = p_+(x) \\ T_e(\phi) = \left(\frac{M_x(\phi)}{D_0} \left(\frac{\partial^2 w(x)}{\partial x^2} \right)^{-1} \right)^{\frac{1}{3}} \\ M_x(\phi) = - \sum_{i=1}^n \sum_{j=1}^{m_i} \int_{z_{ij}^-(\phi)}^{z_{ij}^+(\phi)} \sigma_{xx}^{(j)}(\phi) z_i^*(\phi) dz \\ F_x(\phi) = - \sum_{i=1}^n \sum_{j=1}^{m_i} \int_{z_{ij}^-(\phi)}^{z_{ij}^+(\phi)} \sigma_{xx}^{(j)}(\phi) dz \end{cases} \quad [A.7]$$

The boundaries of the rheological zones z_{ij} are not predefined *a priori* but are computed, using an iterative procedure, as function of ϕ . Mechanical decoupling of rheological layers has three major consequences:

Up to 50% reduction of the flexural resistance, T_e
Maintenance of high resistance to cutting loads
 T_e mainly controlled by thickness of the strongest layer

Appendix B Thermal Model of the Lithosphere

The thermal structure of the oceanic lithosphere is described in detail in [Section 6.03.5.1](#). The thermal structure of multi-layer continental lithosphere is estimated using a similar half-space cooling model that is subdivided on three layers (upper and lower crust, and mantle) and incorporates radiogenic heat sources:

$$\begin{cases} \dot{T} - \chi_{c1} \Delta T = \chi_{c1} \rho_{c1} H_s k_{c1}^{-1} e^{-zh_r^{-1}}, & 0 \leq z \leq h_{c1} \\ \dot{T} - \chi_{c2} \Delta T = H_{c2} C_{c2}^{-1}, & h_{c1} \leq z \leq T \\ \dot{T} - \chi_m \Delta T = 0, & T_c \leq z \leq a \end{cases} \quad [B.1]$$

where the overdot means differentiation with respect to time. h_{c1} is thickness of the upper crust, and T_c is total crustal thickness (see [Table 4](#) for other parameters). The boundary and initial conditions are

$T(0, t) = 0$ (surface temperature),

$T(a, t) = T_m = 1350^\circ\text{C}$ ($a \approx 250$ km is the depth to the thermal bottom, or *equilibrium thermal thickness*),

$T(z, 0) = T_m$ (homogeneous temperature distribution at the beginning).

The solution of the system (eqn [B.1]) is obtained under assumption of heat flux and temperature continuity across the upper and lower crust and mantle lithosphere.

Acknowledgments

A large part of this review study has benefited from author's collaboration with A. B. Watts. I am very much thankful to Mary Ford, Roger Buck, and Antony Watts for their many helpful discussions and comments on initial versions of the manuscript. I also thank P. Molnar, C. Jaupart, L. Jolivet, Y. Podladchikov, and S. Cloetingh for their many helpful discussions. The first edition of this study was funded by the ANR EGEO program and by ISTEP internal project funding. The second edition is supported by the Advanced ERC Grant RHEOLITH.

References

- Afonso JC and Ranalli G (2004) Crustal and mantle strengths in continental lithosphere: Is the jelly sandwich model obsolete? *Tectonophysics* 394: 221–232.
- Aldersons F, Ben-Avraham Z, Hofstetter A, Kissling E, and Al-Yazjeen T (2003) Lower-crustal strength under the Dead Sea basin from local earthquake data and rheological modelling. *Earth and Planetary Science Letters* 214: 129–142.
- Angiboust S, Wolf S, Burov E, Agard Ph, and Yamato P (2012) Effect of fluid circulation on subduction interface tectonic processes: Insights from thermo-mechanical numerical modelling. *Earth and Planetary Science Letters* 357–358: 238–248.
- Artemieva IM (2009a) Are xenoliths representative of the "intact" cratonic mantle? A geophysical perspective. *Geophysical Research Abstracts* 11, EGU2009–1717, 2009, EGU General Assembly.
- Artemieva IM (2009b) The continental lithosphere: Reconciling thermal, seismic, and petrologic data. *Lithos* 109: 23–46.
- Artyushkov EV (1973) Stresses in the lithosphere caused by crustal thickness inhomogeneities. *Journal of Geophysical Research* 78: 7675–7708.
- Ashby MF and Verall RA (1978) Micromechanisms of flow and fracture, and their relevance to the rheology of the upper mantle. *Philosophical Transactions of the Royal Society of London* 288: 59–95.
- Audet P and Burgmann R (2011) Dominant role of tectonic inheritance in supercontinent cycles. *Nature Geoscience* 4(3): 184–187. <http://dx.doi.org/10.1038/NGEO1080>.
- Austrheim H and Boundy T (1994) Pseudotachylites generated during seismic faulting and eclogitization of the deep crust. *Science* 265: 82–83.
- Avoauc J-P (2007) Mountain building. In: *Treatise on Geophysics*. Amsterdam: Elsevier.
- Barrell J (1914) The strength of the Earth's crust. I. Geologic tests of the limits of strength. *Journal of Geology* 22: 28–48.
- Bassi G (1995) Relative importance of strain rate and rheology for the mode of continental extension. *Geophysical Journal International* 122: 195–210.
- Bayer R, Carozzo MT, Lanza R, Miletto M, and Rey D (1989) Gravity modelling along the ECORS-CROP vertical seismic reflection profile through the Western Alps. *Tectonophysics* 162: 203–218.
- Beuchert MJ and Podladchikov YY (2010) Viscoelastic mantle convection and lithospheric stresses. *Geophysical Journal International* 183(1): 35–63. <http://dx.doi.org/10.1111/j.1365-246X.2010.04708.x>.
- Beuchert MJ, Podladchikov YY, Simon NSC, and Ruepke LH (2010) Modeling of craton stability using a viscoelastic rheology. *Journal of Geophysical Research* 115: B11413. <http://dx.doi.org/10.1029/2009JB006482>.
- Bills BG, Adams KD, and Wesnousky SG (2007) Viscosity structure of the crust and upper mantle in western Nevada from isostatic rebound patterns of Lake Lahontan shorelines. *Journal of Geophysical Research* 112: B08411.

- Bills BG, Currey D, and Marshall GA (1994) Viscosity estimates for the crust and upper mantle from patterns of lacustrine shoreline deformation in the Eastern Great Basin. *Journal of Geophysical Research* 99(B11): 22,059–22,086.
- Biot MA (1961) Theory of Folding of Stratified viscoelastic media and its implications in tectonics and orogenesis. *Geological Society of America Bulletin* 72: 1595–1620.
- Bird P (1991) Lateral extrusion of lower crust from under high topography in the isostatic limit. *Journal of Geophysical Research* 96: 10275–10286.
- Block L and Royden LH (1990) Core complex geometries and regional scale flow in the lower crust. *Tectonics* 9: 557–567.
- Bos B and Spiers CJ (2002) Frictional-viscous flow in phyllosilicate-bearing fault rock: Microphysical model and Implications for crustal strength profiles. *Journal of Geophysical Research* 107(B2): 2028. <http://dx.doi.org/10.1029/2001JB000301>.
- Bott MHP (1993) Modelling the plate-driving mechanism. *Journal of the Geological Society of London* 150: 941–951.
- Boutelier D, Chemenda A, and Burg J-P (2003) Subduction versus accretion of intra-oceanic volcanic arcs: Insight from thermo-mechanical analogue experiments. *Earth and Planetary Science Letters* 212: 31–45.
- Brace WF and Kohlstedt DL (1980) Limits on lithospheric stress imposed by laboratory experiments. *Journal of Geophysical Research* 85: 6248–6252.
- Brun J-P (2002) Deformation of the continental lithosphere: Insights from brittle-ductile models. In: De Meer S, Drury MR, De Bresser JHP, and Pennoch GM (eds.) *Deformation Mechanisms, Rheology and Tectonics: Current Status and Future Perspectives*, pp. 355–370. Spec. Publ.-Geol. Soc. Lond., 200.
- Brun J-P and Gutscher MADEKORP-ECORS teams (1992) Deep crustal structure of the Rhine Graben from DEKORP-ECORS seismic reflection data: A summary. *Tectonophysics* 208: 139–147.
- Brun J-P and Wenzel Fthe ECORS-DEKORP Team (1991) Crustal structure of the southern Rhine Graben from ECORS-DEKORP seismic reflection data. *Geology* 19: 758–762.
- Buck WR (1988) Flexural rotation of normal faults. *Tectonics* 7: 959–973.
- Buck WR (1991) Modes of continental extension. *Journal of Geophysical Research* 96: 20161–20178.
- Buck WR (2007) Continental break-up and building. In: *Treatise on Geophysics*. New York: Elsevier.
- Buck WR and Toksöz MN (1983) Thermal effects of continental collisions: Thickening a variable viscosity lithosphere. *Tectonophysics* 100: 53–69.
- Bürgmann R and Dresen G (2008) Rheology of the lower crust and upper mantle: Evidence from rock mechanics, geodesy, and field observations. *Annual Review of Earth and Planetary Sciences* 36: 531–567. <http://dx.doi.org/10.1146/annurev.earth.36.031207.124326>.
- Burov E (2002) The upper crust is softer than dry quartzite. *Tectonophysics* 361: 321–326.
- Burov EB (2007) Plate rheology and mechanics. In: Watts AB and Schubert G (eds.) *Treatise on Geophysics. Crust and Lithosphere Dynamics*, vol. 6, pp. 99–152. Elsevier, ISBN: 978-0-444-51928-3, TOGP00102. 611 pp.
- Burov E (2010) The equivalent elastic thickness (T_e), seismicity and the long-term rheology of continental lithosphere: Time to burn-out “crème brûlée”? Insights from large-scale geodynamic modeling. *Tectonophysics* 484(4): 26.
- Burov E (2011) Rheology and strength of the lithosphere. *Marine and Petroleum Geology* 28(8): 1402–1443. <http://dx.doi.org/10.1016/j.marpetgeo.2011.05.008>. Invited paper.
- Burov E and Cloetingh S (2010) Plume-like upper mantle instabilities drive subduction initiation. *Geophysical Research Letters* 37, L03309.
- Burov EB and Cloetingh S (1997) Erosion and rift dynamics: New thermomechanical aspects of post-rift evolution of extensional basins. *Earth and Planetary Science Letters* 150: 7–26.
- Burov EB and Diamant M (1992) Flexure of the continental lithosphere with multilayered rheology. *Geophysical Journal International* 109: 449–468.
- Burov EB and Diamant M (1995) The effective elastic thickness (T_e) of continental lithosphere: What does it really mean? *Journal of Geophysical Research* 100: 3895–3904.
- Burov EB and Diamant M (1996) Isostasy, effective elastic thickness (EET) and inelastic rheology of continents and oceans. *Geology* 24: 419–423.
- Burov E, Francois T, Yamato P, and Wolf S (2014a) Mechanisms of continental subduction and exhumation of HP and UHP rocks. *Gondwana Research* 25: 464–493. <http://dx.doi.org/10.1016/j.gr.2012.09.010>.
- Burov E, Francois T, Agard P, et al. (2014b) Mechanisms of subduction and HP/UHP exhumation of continental crust: Rheological and geodynamic controls. *Tectonophysics* 631: 212–250. <http://dx.doi.org/10.1016/j.tecto.2014.04.033>.
- Burov E, Francois T, Yamato P, and Wolf S (2014c) Advances and challenges in geotectonic modeling. *Société Géologique de France* 185: 147–168. <http://dx.doi.org/10.2113/gssgbull.185.3.147>.
- Burov EB, Kogan MG, Lyon-Caen H, and Molnar P (1990) Gravity anomalies, the deep structure, and dynamic processes beneath the Tien Shan. *Earth and Planetary Science Letters* 96: 367–383.
- Burov EB, Lobkovsky LI, Cloetingh S, and Nikishin AM (1993) Continental lithosphere folding in Central Asia (part 2), constraints from gravity and topography. *Tectonophysics* 226: 73–87.
- Burov EB, Mareschal J-C, and Jaupart C (1998) Large scale crustal inhomogeneities and lithospheric strength in cratons. *Earth and Planetary Science Letters* 164: 205–219.
- Burov EB and Molnar P (1998) Gravity anomalies over the Ferghana Valley (central Asia) and intracontinental deformation. *Journal of Geophysical Research* 103: 18,137–18,152.
- Burov EB and Molnar P (2008) Rayleigh-Taylor instability of a viscoelastic (Maxwell solid): Dependence of growth rates on wave number and elastic constants. *Earth and Planetary Science Letters* 275(3–4): 370–381.
- Burov E, Podladchikov Y, Grandjean G, and Burg J-P (1999) Validation of multidisciplinary data using thermo-mechanical modelling: Application to the Western and Northern Alps. *Terra Nova* 11: 124–131.
- Burov EB and Poliakov ANB (2001) Erosion and rheology controls on synrift and postrift evolution: Verifying old and new ideas using a fully coupled numerical model. *Journal of Geophysical Research* 106: 16,461–16,481.
- Burov E and Watts AB (2006) The long-term strength of continental lithosphere: “jelly-sandwich” or “crème-brûlée”? *GSA Today* 16: 4–10.
- Burov E and Yamato P (2008) Continental plate collision, P-T-t-z conditions and unstable vs. stable plate dynamics: Insights from thermo-mechanical modelling. *Lithos* 103: 178–204.
- Byerlee JD (1978) Friction of rocks. *Pure and Applied Geophysics* 116: 615–626.
- Caristan Y (1982) The transition from high temperature creep to fracture in Maryland diabase. *Journal of Geophysical Research* 87: 6781–6790.
- Carter NL and Tsenn MC (1987) Flow properties of continental lithosphere. *Tectonophysics* 136: 27–63.
- Chandrasekhar S (1961) *Hydrodynamic and Hydromagnetic Stability*, p. 704. Oxford: Oxford University Press.
- Chapman Y (1986) Thermal gradient in the continental crust. In: Dawson JB, et al. (eds.) *The Nature of the Continental Crust*, pp. 63–70. Spec. Publ. Geol. Soc. London, 24.
- Chen S, Hiraga K, and Kohlstedt DL (2006) Water weakening of clinopyroxene in the dislocation creep regime. *Journal of Geophysical Research* 111: B08203.
- Chen W-P and Molnar P (1983) Focal depths of intracontinental and intraplate earthquakes and their implications for the thermal and mechanical properties of the lithosphere. *Journal of Geophysical Research* 88: 4183–4214.
- Chester FM (1988) The brittle-ductile transition in a deformation-mechanism map for halite. *Tectonophysics* 154: 125–136.
- Chester FM (1995) A rheologic model for wet crust applied to strike-slip faults. *Journal of Geophysical Research* 100(B7): 13,033–13,044.
- Chopra PN and Paterson MS (1981) The experimental deformation of dunite. *Tectonophysics* 78: 453–473.
- Chopra PN and Paterson MS (1984) The role of water in the deformation of dunite. *Journal of Geophysical Research* 89: 7861–7876.
- Cloetingh S and Banda E (1992) Europe's lithosphere – Physical properties. Mechanical structure. In: Blundell D, Freeman R, and Mueller S (eds.) *A Continent Revealed: The European Geotraverse*, pp. 80–91. New York: Cambridge University Press/European Science Foundation.
- Cloetingh S and Burov EB (1996) Thermomechanical structure of the European continental lithosphere: Constraints from rheological profiles and EET estimates. *Geophysical Journal International* 124: 695–723.
- Cloetingh S and Burov E (2010) Lithospheric folding and sedimentary basin evolution: A review and analysis of formation mechanisms. *Basin Research* 23: 257–290. <http://dx.doi.org/10.1111/j.1365-2117.2010.00490.x>.
- Cloetingh S, Burov E, and Poliakov A (1999) Lithosphere folding: Primary response to compression? (from central Asia to Paris Basin). *Tectonics* 18: 1064–1083.
- Cloetingh S and Wortel R (1986) Stress in the Indo-Australian plate. *Tectonophysics* 132: 49–67.
- Cloetingh S and Ziegler P (2007) Tectonic models of sedimentary basins. In: Watts AB (ed.) *Treatise on Geophysics*, vol. 6, pp. 485–611. Amsterdam: Elsevier.
- Cloetingh S, et al. (1982) Evolution of passive continental margins and initiation of subduction zones. *Nature* 297: 139–142.
- Cochran JR (1980) Some remarks on isostasy and the long-term behavior of the continental lithosphere. *Earth and Planetary Science Letters* 46: 766–2711.
- Conrad CP and Molnar P (1997) The growth of Rayleigh-Taylor-type instabilities in the lithosphere for various rheological and density structures. *Geophysical Journal International* 129: 95–112.
- Cundall PA (1989) Numerical experiments on localization in frictional materials. *Archive of Applied Mechanics* 59: 148–159.

- Dahlen FA (1981) Isostasy and the ambient state of stress in the oceanic lithosphere. *Journal of Geophysical Research* 86: 7801–7807.
- DallaVia G, Sabadini R, DeNatale G, and Pingue F (2005) Lithospheric rheology in southern Italy inferred from postseismic viscoelastic relaxation following the 1980 Irpinia earthquake. *Journal of Geophysical Research* 110: B06311. <http://dx.doi.org/10.1029/2004JB003539>.
- DeMets C, Gordon RG, Argus DF, et al. (1990) Current plate motions. *Geophysical Journal International* 101: 425–478.
- Deverchere J, Houdy F, Diamant M, Solonenko NV, and Solonenko AV (1991) Evidence for a seismogenic upper mantle and lower crust in the Baikal rift. *Geophysical Research Letters* 18(6): 1099–1102.
- Deverchere J, Houdy F, Solonenko NV, Solonenko AV, and Sankov VA (1993) Seismicity, active faults and stress field of the North Muya Region, Baikal Rift: New insights on the rheology of extended continental lithosphere. *Journal of Geophysical Research* 98: 19895–19912.
- Doin M and Fleitout L (1996) Thermal evolution of the oceanic lithosphere: An alternative view. *Earth and Planetary Science Letters* 142: 121–136.
- Doser D and Yarwood DR (1994) Deep crustal earthquakes associated with continental rifts. *Tectonophysics* 229: 123–131.
- Drury MR (2005) Dynamic recrystallization and strain softening of olivine aggregates in the laboratory and the lithosphere. *Geological Society London Special Publications* 243: 143–158.
- Durham WB, Meib S, Kohlstedt DL, Wang L, and Dixon NA (2009) New measurements of activation volume in olivine under anhydrous conditions. *Physics of the Earth and Planetary Interiors* 172: 67–73.
- ECORS-CROP Deep Seismic Sounding Group (1989) A new picture of the Moho under the western Alps. *Nature (London)* 337: 249–251.
- England PC and Houseman GA (1989) Extension during continental convergence, with application to the Tibetan Plateau. *Journal of Geophysical Research* 94: 17561–17579.
- England P and Molnar P (1997) Active deformation of Asia: From kinematics to dynamics. *Science* 278: 647–650.
- England PC and Molnar P (2005) Late Quaternary to decadal velocity fields in Asia. *Journal of Geophysical Research* 110: B12401. <http://dx.doi.org/10.1029/2004JB003541>.
- England P and Richardson SW (1980) Erosion and age dependence of continental heat flow. *Geophysical Journal of the Royal Astronomical Society* 62: 421–437.
- Evans B (2005) Creep constitutive laws for rocks with evolving structure. *Geological Society London Special Publications* 245: 329–346.
- Evans B and Goetze C (1979) The temperature variation of hardness of olivine and its implication for polycrystalline yield stress. *Journal of Geophysical Research* 84: 5505–5524.
- Evans B and Kohlstedt DL (1995) Rheology of rocks. In: Ahrens TJ (ed.) *Rock Physics and Phase Relations: A Handbook of Physical Constants*. AGU Reference Shelf, vol. 1, pp. 149–165. Washington, DC: AGU.
- Faccenda M, Gerya TV, and Burlini L (2009) Deep slab hydration induced by bending related variations in tectonic pressure. *Nature Geoscience* 2: 790–793.
- Fleitout L and Froidevaux C (1983) Tectonic stresses in the lithosphere. *Tectonics* 3: 315–334.
- Forsyth DW (1985) Subsurface loading and estimates of the flexural rigidity of continental lithosphere. *Journal of Geophysical Research* 90: 12,623–12,632.
- Francois T, Burov E, Meyer B, and Agard P (2013) Survival and rheological structure of cratons: Key constraints from surface topography. *Tectonophysics* 602: 106–223. <http://dx.doi.org/10.1016/j.tecto.2012.10.009>.
- Freed AM, Burgmann R, and Herring TA (2007) Far-reaching transient motions after Mojave earthquakes require broad mantle flow beneath a strong crust. *Geophysical Research Letters* 34: L19302.
- Frei W, Heitzmann P, and Lehner P (1990) Swiss NFP20 research program of the deep structure of the Alps. *Mémoires de la Société géologique de France* 156: 29–46.
- Fuchs K, Bonjer K-P, Gajewski D, et al. (1987) Crustal evolution of the Rhinegraben area, I. Exploring the lower crust in the Rhinegraben rift by unified geophysical experiments. *Tectonophysics* 141: 261–275.
- Gerbault M, Burov EB, Poliakov A, and Dagnieres M (1999) Do faults trigger folding in the lithosphere? *Geophysical Research Letters* 26: 2271–2274.
- Giese P, Nicolich R, and Reutter K-J (1982) Explosion crustal seismic studies in the Alpine-Mediterranean region and their implications to tectonic processes. In: Berckhemer H and Hsu KJ (eds.) *Alpine-Mediterranean Geodynamics*, pp. 347–376. Washington, DC: American Geophysical Union.
- Gleason GC and Tullis J (1995) A flow law for dislocation creep of quartz aggregates determined with the molten salt cell. *Tectonophysics* 247: 1–23.
- Goetze C and Evans B (1979) Stress and temperature in bending lithosphere as constrained by experimental rock mechanics. *Geophysical Journal of the Royal Astronomical Society* 59: 463–478.
- Govers R, Wortel MJR, Cloetingh SAPL, and Stein CA (1992) Stress magnitude estimates from earthquakes in oceanic plate interiors. *Journal of Geophysical Research* 97: 11749–11759.
- Gratier J, Guiguet R, Renard F, and Jenatto L (2006) Experimental pressure solution creep of quartz by indenter technique. *Eos, Transactions of the American Geophysical Union* 87(52). Fall Meet. Suppl., Abstract T23D-0525.
- Green HW II (2007) Shearing instabilities accompanying high-pressure phase transformations and the mechanics of deep earthquakes. *PNAS* 104(22): 9133–9138.
- Handy MR and Brun JP (2004) Seismicity, structure and strength of the continental lithosphere. *Earth and Planetary Science Letters* 223: 427–441.
- Hier-Majumder S, Mei S, and Kohlstedt DL (2005) Water weakening of clinopyroxenite in diffusion creep. *Journal of Geophysical Research* 110: B07406. <http://dx.doi.org/10.1029/2004JB003414>.
- Hirth G and Kohlstedt DL (1996) Water in the oceanic upper mantle: Implications for rheology, melt extraction and the evolution of the lithosphere. *Earth and Planetary Science Letters* 144: 93–108.
- Hirth G and Kohlstedt DL (2003) Rheology of the upper mantle and the mantle wedge: A view from the experimentalists. In: Eiler J (ed.) *Inside the Subduction Factory*, pp. 83–105, American Geophysical Union Monograph.
- Houseman GA, McKenzie DP, and Molnar P (1981) Convective instability of a thickened boundary layer and its relevance for the thermal evolution of continental convergent belts. *Journal of Geophysical Research* 86: 6135–6155.
- Huet B, Le Pourhet L, Labrousse L, Burov E, and Jolivet L (2011) Post-orogenic extension and metamorphic core complexes in a heterogeneous crust: The role of crustal layering inherited from collision. Application to the Cyclades (Aegean domain). *Geophysical Journal International* 184(2): 611–625.
- Huismans RS, Butier S, and Beaumont C (2005) Effect of plastic-viscous layering and strain softening on mode selection during lithospheric extension. *Journal of Geophysical Research* 110: B02406. <http://dx.doi.org/10.1029/2004JB003114>.
- Hull D and Bacon DJ (1984) *Introduction to Dislocations*, 3rd edn., p. 255. Oxford: Pergamon Press.
- Humphreys ED, Hessler E, Dueker K, Farmer GL, Erslov E, and Atwater T (2003) How Laramide-age hydration of North American lithosphere by the Farallon slab controlled subsequent activity. *International Geology Review* 45: 575–595.
- Jackson J (2002) Strength of the continental lithosphere: Time to abandon the jelly sandwich? *GSA Today September*: 4–10.
- Jaeger JC and Cook NGW (1976) *Fundamentals of Rock Mechanics*, 2nd edn, p. 585. NY: Chapman and Hall.
- Jaupart C and Mareschal JC (1999) The thermal structure and thickness of continental roots. *Lithos* 48: 93–114.
- Jaupart C and Mareschal JC (2007) Heat flow and thermal structure of the lithosphere. In: *Treatise on Geophysics*. Amsterdam: Elsevier.
- Ji S, Wirth R, Rybacki E, and Jiang Z (2000) High-temperature plastic deformation of quartz-plagioclase multilayers by layer-normal compression. *Journal of Geophysical Research* 105(B): 16,651–16,664.
- Jin D, Karato S, and Obata M (1998) Mechanisms of shear localization in the continental lithosphere: Inference from the deformation microstructures of peridotites from the Ivrea zone, northwestern Italy. *Journal of Structural Geology* 20: 195–209.
- John T, Medvedev S, Rüpke LH, Andersen TB, Podladchikov Y, and Austrheim H (2009) Generation of intermediate-depth earthquakes by self-localizing thermal runaway. *Nature Geoscience* 2: 137–140.
- Jolivet L, Faccenna C, Goffé B, et al. (1998) Mid-crustal shear zones in post-orogenic extension: The northern Tyrrhenian Sea case. *Journal of Geophysical Research* 103: 12123–12160.
- Jordan TA and Watts AB (2005) Gravity anomalies, flexure and the elastic thickness structure of the India-Eurasia collisional system. *Earth and Planetary Science Letters* 236: 732–750.
- Judge A and McNutt MK (1991) The relationship between plate dip and elastic plate thickness: A study of the Peru-Chile Trench. *Journal of Geophysical Research* 96: 16,625–16,639.
- Kachanov LM (1971) *Foundations of the Theory of Plasticity*, p. 324. Amsterdam: North-Holland Publications.
- Karato S-I (1986) Does partial melting reduce the creep strength of the upper mantle? *Nature* 319: 309–310.
- Karato S-I (1998) Effects of pressure on plastic deformation of polycrystalline solids: Some geological applications. *Materials Research Society Symposium Proceedings* 499: 3–14.
- Karato S (1998) Effects of pressure on plastic deformation of polycrystalline solids: Some geological applications. *Materials Research Society Symposium Proceedings* 499: 3–14.
- Karato S-I and Jung H (2003) Effects of pressure on high-temperature dislocation creep in olivine. *Philosophy Magazine* 83: 401–414.

- Karato S-I, Paterson MS, and FitzGerald JD (1986) Rheology of synthetic olivine aggregates: Influence of the grain size and water. *Journal of Geophysical Research* 91: 8151–8176.
- Katayama I, Karato S-I, and Brandon M (2005) Evidence for high water content in the deep upper mantle inferred from deformation microstructures. *Geology* 33(7): 613–616.
- Katz RF, Spiegelman M, and Langmuir CH (2003) A new parameterization of hydrous mantle melting. *Geochemistry, Geophysics, Geosystems* 4(9): 1073. <http://dx.doi.org/10.1029/2002GC000433>.
- Kaufmann G and Amelung F (2000) Reservoir-induced deformation and continental rheology in the vicinity of Lake Mead, Nevada. *Journal of Geophysical Research* 105: 16341–16358.
- Keefner JW, Mackwell SJ, Kohlstedt DL, and Heidelbach F (2011) Dependence of dislocation creep of dunite on oxygen fugacity: Implications for viscosity variations in Earth's mantle. *Journal of Geophysical Research* 116: B05201. <http://dx.doi.org/10.1029/2010JB007748>.
- Kenis J, Urai JL, van der Zee W, Hilgers C, and Sintubin M (2005) Rheology of fine-grained siliciclastic rocks in the middle crust – Evidence from structural and numerical analysis. *Earth and Planetary Science Letters* 233: 351–360.
- Kirby SH (1983) Rheology of the lithosphere. *Reviews of Geophysics* 21: 1458–1487.
- Kirby SH, Durham W, and Stern L (1991) Mantle phase changes and deep-earthquake faulting in subducting lithosphere. *Science* 252: 216–225.
- Kirby SH and Kronenberg AK (1987) Rheology of the lithosphere: Selected topics. *Reviews of Geophysics* 25: 1219–1244, correction 1680–1681.
- Kirby SH, Stein S, Okal EA, and Rubie DC (1996) Metastable mantle phase transformations and deep earthquakes in subducting oceanic lithosphere. *Reviews of Geophysics* 34: 261–306.
- Kirby JF and Swain CJ (2009) A reassessment of spectral T_e estimation in continental interiors: The case of North America. *Journal of Geophysical Research* (114): B08401. <http://dx.doi.org/10.1029/2009JB006356>.
- Kirby JF and Swain CJ (2011) Improving the spatial resolution of effective elastic thickness estimation with the fan wavelet transform. *Computers & Geosciences* 37(9): 1345–1354. <http://dx.doi.org/10.1016/j.cageo.2010.10.008>.
- Kissling E and Spakman W (1996) Interpretation of tomographic images of uppermost mantle structure: Examples from the Western and Central Alps. *The Journal of Geodynamics* 21: 97–111.
- Klemperer S and Hobbs R (1991) *The BIRPS Atlas*, p. 124. Cambridge: Cambridge University Press.
- Kohlstedt DL (2007) Constitutive equations, rheological behavior, and viscosity of rocks. In: Schubert G and Schubert G (eds.) *Treatise on Geophysics*. Miner. Phys., vol. 2.14, pp. 389–417. Amsterdam: Elsevier.
- Kohlstedt DL, Evans B, and Mackwell SJ (1995) Strength of the lithosphere: Constraints imposed by laboratory experiments. *Journal of Geophysical Research* 100: 17587–17602.
- Kruse S and Royden L (1994) Bending and unbending of an elastic lithosphere: The Cenozoic history of the Apennine and Dinaride foredeep basins. *Tectonics* 13: 278–302.
- Kusznir NJ (1991) The distribution of stress with depth in the lithosphere: Thermo-rheological and geodynamic constraints. *Philosophical Transactions of the Royal Society of London* A337: 95–110.
- Kusznir NJ and Matthews DH (1988) Deep seismic reflections and the deformational mechanics of the continental lithosphere. *Journal of Petrology Special_Volume* (1): 63–87.
- Kuznir NL and Park RG (1986) Continental lithosphere strength: The critical role of lower crustal deformation. In: Dawson JB, Carswell DA, Hall J, and Wedepohl KH (eds.) *The Nature of the Lower Continental Crust*, pp. 79–94, Special Publication-Geological Society, 24.
- Lachenbruch AH and Morgan P (1990) Continental extension, magmatism and elevation: formal relations and rules of thumb. *Tectonophysics* 174: 39–62.
- Lambeck K (1983) Structure and evolution of intracratonic basins in central Australia. *Geophysical Journal of the Royal Astronomical Society* 74: 843–886.
- Larsen CF, Motyka RJ, Freymueller JT, Echelmeyer KA, and Ivins ER (2005) Rapid viscoelastic uplift in southeast Alaska caused by post-Little Ice Age glacial retreat. *Earth and Planetary Science Letters* 237: 548–560.
- Lavier LL, Buck WR, and Poliakov ANB (2000) Factors controlling normal fault offset in ideal brittle layer. *Journal of Geophysical Research* 105: 23,431–23,442.
- Le Pichon X, Francheteau J, and Bonnin J (1973) *Plate Tectonics*, p. 300. New York: Elsevier Scientific.
- Le Pourtier L, Burov E, and Moretti I (2004) Rifting through a stack of inhomogeneous thrusts (the dipping pie concept). *Tectonics* 23(4): TC4005. <http://dx.doi.org/10.1029/2003TC001584>.
- Lenardic A, Moresi LN, and Muhlhaus H (2003) Longevity and stability of cratonic lithosphere: Insights from numerical simulations of coupled mantle convection and continental tectonics. *Journal of Geophysical Research* 108(B6). <http://dx.doi.org/10.1029/2002JB001859>.
- Lobkovsky LI and Kerchman VI (1992) A two-level concept of plate tectonics: Application to geodynamics. *Tectonophysics* 199: 343–374.
- Lokhner DA (1995) Rock failure. In: Ahrens TJ (ed.) *Rock Physics and Phase Relations: A Handbook of Physical Constants*, AGU Reference Shelf 1, pp. 127–147. Washington, DC: AGU.
- Lowry AR and Smith RB (1994) Flexural rigidity of the Basin and Range–Colorado Plateau–Rocky Mountain transition from coherence analysis of gravity and topography. *Journal of Geophysical Research* 99: 20,123–20,140.
- Mackwell SJ, Zimmerman ME, and Kohlstedt DL (1998) High-temperature deformation of dry diabase with applications to tectonics on Venus. *Journal of Geophysical Research* 103: 975–984.
- Maggi A, Jackson JA, Priestley K, and Baker C (2000) A re-assessment of focal depth distributions in southern Iran, the Tien Shan and northern India: Do earthquakes occur in the continental mantle? *Geophysical Journal International* 143: 629–661.
- McAdoo DC, Martin CF, and Polouze S (1985) Seasat observations of flexure: Evidence for a strong lithosphere. *Tectonophysics* 116: 209–222.
- McKenzie D and Bickle MJ (1988) The volume and composition of melt generated by extension of the lithosphere. *Journal of Petrology* 29: 342–532.
- McKenzie DP and Fairhead D (1997) Estimates of the effective elastic thickness of the continental lithosphere from Bouguer and free-air gravity anomalies. *Journal of Geophysical Research* 102: 27,523–27,552.
- McNutt MK and Menard HW (1982) Constraints on yield strength in the oceanic lithosphere derived from observations of flexure. *Geophysical Journal of the Royal Astronomical Society* 71: 363–395.
- Meissner R and Bortfeld RK (eds.) (1990) *DEKOPR-Atlas, Results of Deutsches Kontinentales Reflexionsseismisches Programm*. Berlin, Heidelberg, New York: Springer Verlag, 18 and 80 plates.
- Melosh HJ (1990) Mechanical basis for low-angle normal faulting in the Basin and Range province. *Nature* 343: 331–335.
- Molnar P and Houseman GA (2004) The effects of buoyant crust on the gravitational instability of thickened mantle lithosphere at zones of intracontinental convergence. *Geophysical Journal International* 158: 1134–1150.
- Molnar P and Lyon-Caen H (1988) Some simple physical aspects of the support, structure, and evolution of mountain belts. *Geological Society of America Special Paper* 218: 179–207.
- Molnar P and Tapponnier (1981) A possible dependence of the tectonic strength on the age of the crust in Asia. *Earth and Planetary Science Letters* 52: 107–114.
- Monsalve G, Sheehan A, Schulte-Pelkum V, Rajaure S, Pandey MR, and Wu F (2006) Seismicity and one-dimensional velocity structure of the Himalayan collision zone: Earthquakes in the crust and upper mantle. *Journal of Geophysical Research* 111: B10301. <http://dx.doi.org/10.1029/2005JB004062>.
- Montesi LGJ (2004) Controls of shear zone rheology and tectonic loading on post-seismic creep. *Journal of Geophysical Research* 109: B10404. <http://dx.doi.org/10.1029/2003JB002925>.
- Morley CK (1989) Extension, detachments, and sedimentation in continental rifts (with particular reference to East Africa). *Tectonics* 8: 1175–1192.
- Mouhounou F, Watts AB, and Burov E (2013) Collisional orogens, structural inheritance and the long-term strength of continental lithosphere. *Nature Geoscience* 6(9): 785–789.
- Müller B, Zoback ML, Fuchs K, et al. (1992) Regional patterns of stress in Europe. *Journal of Geophysical Research* 97: 11783–11803.
- Nadai A (1963) *Theory of Flow and Fracture of Solids*, vol. 2, p. 705. New York: McGraw-Hill.
- Okaya N, Cloetingh S, and Mueller St (1996) A lithospheric cross section through the Swiss Alps – II. Constraints on the mechanical structure of a continent-continent collision zone. *Geophysical Journal International* 127: 399–414.
- Parsons BE and Sclater JG (1977) An analysis of the variation of ocean floor bathymetry and heat flow with age. *Journal of Geophysical Research* 82: 803–827.
- Passeys QP (1981) Upper mantle viscosity derived from the difference in rebound of the Provo and Bonneville shorelines, Lake Bonneville basin. *Journal of Geophysical Research* 86: 11701–11708.
- Peltier WR (1974) The impulse response of a Maxwell Earth. *Reviews of Geophysics and Space Physics* 12: 649–669.
- Peltier WR and Andrews JT (1976) Glacial-isostatic adjustment – I. The forward problem. *Geophysical Journal of the Royal Astronomical Society* 46: 605–646.
- Pérez-Gussinyé M and Watts AB (2005) The long-term strength of Europe and its implications for plate-forming processes. *Nature* 436(7049): 381–384. <http://dx.doi.org/10.1038>.
- Petrini K and Podladchikov Yu (2000) Lithospheric pressure-depth relationship in compressive regions of thickened crust. *Journal of Metamorphic Geology* 18: 67–78.

- Pinet C, Jaupart C, Mareschal J-C, Gariepy C, Bienfait G, and Lapointe R (1991) Heat flow and lithospheric structure of the eastern Canadian shield. *Journal of Geophysical Research* 96: 19,923–19,941.
- Poirier JP (1985) *Creep of Crystals*, p. 260. Cambridge: Cambridge University Press.
- Poliakov ANB, Cundall P, Podladchikov Y, and Laykhovsky V (1993) An explicit inertial method for the simulation of visco-elastic flow: An evaluation of elastic effects on diapiric flow in two- or three-layers models. In: Stone DB and Runcorn SK (eds.) *Flow and Creep in the Solar System: Observations, Modelling and Theory, Dynamic Modelling and Flow in the Earth and Planets Series*, pp. 175–195.
- Politz FF, Wicks C, and Thatcher W (2001) Mantle flow beneath a continental strike-slip fault: Postseismic deformation after the 1999 Hector mine earthquake. *Science* 293: 1814–1818.
- Précigout J and Gueydan F (2009) Mantle weakening and strain localization: Implications for the long-term strength of the continental lithosphere. *Geology* 37(2): 147–150. <http://dx.doi.org/10.1130/G25239A.1>.
- Precigout J, Gueydan F, Gapais D, Garrido CJ, and Essaifi A (2007) Strain localisation in the subcontinental mantle – A ductile alternative to the brittle mantle. *Tectonophysics* 445: 318–336.
- Ranalli G (1995) *Rheology of the Earth*, 2nd edn., p. 413. London: Chapman and Hall.
- Regenauer-Lieb K, Yuen DA, and Branhurst J (2001) The initiation of subduction: Criticality by addition of water? *Science* 294(5542): 578–580.
- Rice JR and Tse ST (1986) Dynamic motion of a single degree of freedom system following a rate and state dependent friction law. *Journal of Geophysical Research* 91: 521–530.
- Rupke LH, Morgan JP, Hort M, and Connolly JAD (2002) Are the regional variations in Central American arc lavas due to differing basaltic versus peridotitic slab sources of fluids? *Geology* 30: 1035–1038.
- Rutter EH and Brodie KH (1991) Lithosphere rheology – A note of caution. *The Journal of Structural Geology* 13: 363–367.
- Rutter EH and Brodie KH (2004) Experimental grain size-sensitive flow of hot-pressed Brazilian quartz aggregates. *Journal of Structural Geology* 26: 2011–2023.
- Rybacki E, Gottschalk M, Wirth R, et al. (2006) Influence of water fugacity and activation volume on the flow properties of fine-grained anorthite aggregates. *Journal of Geophysical Research* 111: B03203. <http://dx.doi.org/10.1029/2005JB003663>.
- Sabatini R and Vermeersen LLA (2004) Global dynamics of the earth: Applications of normal mode relaxation theory to solid-earth geophysics. *Modern Approaches Geophys*, vol. 30. New York: Springer.
- Salvesen JO (1978) Variations in the geology of rift basins: A tectonic model. In: *Conf. Proc. Los Alamos Natl. Lab.*, 7487, Los Alamos, N.M., pp. 82–86.
- Schmeling H, Babeyko AY, Enns A, et al. (2008) A benchmark comparison of spontaneous subduction models – Toward a free surface. *Physics of the Earth and Planetary Interiors* 171: 198–223.
- Scholz CH (1990) Mechanics of faulting. *Annual Review of Earth and Planetary Sciences* 17: 309–334.
- Scholz CH (2002) *The Mechanics of Earthquakes and Faulting*, 2nd edn. Cambridge, England: Cambridge University Press.
- Slater JG, Jaupart C, and Galson D (1980) The heat flow through oceanic and continental crust and the heat loss of the Earth. *Journal of Geophysical Research* 85: 269–311.
- Seno T and Seito A (1994) Recent East African earthquakes in the lower crust. *Earth and Planetary Science Letters* 121: 125–135.
- Seno T and Yamanaka Y (1996) Double seismic zones, compressional deep trench-outer rise events and superplumes. In: Bebout GE, Scholl DW, Kirby SH, and Platt JP (eds.) *Subduction Top to Bottom, Geophysical Monograph Series*, vol. 96, pp. 347–355. Washington, D.C.: AGU.
- Shelton G and Tullis JA (1981) Experimental flow laws for crustal rocks. *Eos, Transactions, American Geophysical Union* 62: 396.
- Shudofsky GN (1985) Source mechanisms and focal depths of east African earthquakes using Rayleigh-wave inversion and body-wave modelling. *Geophysical Journal of the Royal Astronomical Society* 83: 563–614.
- Shudofsky GN, Cloetingh S, Stein S, and Wortel R (1987) Unusually deep earthquakes in east Africa: Constraints on the thermo-mechanical structure of a continental rift system. *Geophysical Research Letters* 14(7): 741–744.
- Sibson RH (1980) Transient discontinuities in ductile shear zones. *Journal of Structural Geology* 2: 165–171.
- Smit J, Cloetingh S, Burov E, et al. (2013) Interference of lithospheric folding in western Central Asia by simultaneous Indian and Arabian plate indentation. *Tectonophysics* 602: 176–193. <http://dx.doi.org/10.1016/j.tecto.2012.05.030>.
- Souriau A, Chevrot S, and Olivera C (2008) A new tomographic image of the Pyrenean lithosphere from teleseismic data. *Tectonophysics* 460: 206–214.
- Stacey FD (1992) *Physics of the Earth*, p. 513. Brisbane: Brookfield Press.
- Stephenson RA and Cloetingh S (1991) Some examples and mechanical aspects of continental lithospheric folding. *Tectonophysics* 188: 27–37.
- Terry M and Heidelbach F (2004) Superplasticity in garnet from eclogite facies shear zones in the Haram Gabbro, Håramsvøya, Norway. *Geology* 32(4): 281–284. <http://dx.doi.org/10.1130/G20157.1>.
- Tesauro M, Burov E, Kaban M, and Cloetingh S (2011) Ductile crustal flow in Europe's lithosphere. *Earth and Planetary Science Letters* 312(1–2): 254–265.
- Tesauro M, Kaban MK, and Cloetingh SAPL (2008) EuCRUST-07: A new reference model for the European crust. *Geophysical Research Letters* 35: LXXXX. <http://dx.doi.org/10.1029/2007GL032244>.
- Tesauro M, Kaban MK, and Cloetingh S (2009a) How rigid is Europe's lithosphere? *Geophysical Research Letters* 36, L16303.
- Tesauro M, Kaban MK, and Cloetingh SAPL (2009b) A new thermal and rheological model of the European lithosphere. *Tectonophysics* 476: 478–495.
- Tesauro M, Kaban MK, Cloetingh SAPL, Hardebol NJ, and Beekman F (2009c) 3D strength and gravity anomalies of the European lithosphere. *Earth and Planetary Science Letters* 263: 56–73.
- Tirel C, Brun J-P, and Burov E (2004) Thermo-mechanical modeling of extensional gneiss dome. In: *Gneiss Domes and Orogeny*, pp. 67–78 Geological Society of America Special Paper, 380.
- Toussaint G, Burov E, and Jolivet J (2004) Continental plate collision: Unstable vs. stable slab dynamics. *Geology* 32: 33–36.
- Tse ST and Rice JR (1986) Crustal earthquake instability in relation to the depth variation of friction slip properties. *Journal of Geophysical Research* 91: 9452–9472.
- Turcotte DL and Schubert G (2002) *Geodynamics*, 2nd edn., p. 456. Cambridge: Cambridge University Press.
- Van Hunen J, Zhong S, Shapiro N, and Ritzwoller HR (2005) New evidence for dislocation creep from 3-D geodynamic modelling of the Pacific upper mantle structure. *Earth and Planetary Science Letters* 238: 146–155.
- Vermeer PA (1990) The orientation of shear bands in biaxial tests. *Geotechnique* 40(2): 223–236.
- Vermeer PA and de Borst R (1984) Non-associated plasticity for soils, concrete and rocks. In: *Heron*, pp. 1–75. Rijswijk, The Netherlands: Stevin-laboratory of Civil Engineering, University of Technology, Delft Institute TNO for Building Materials and Building Structures, 29(3a).
- Walcott RI (1970) Isostatic response to loading of the crust in Canada. *Canadian Journal of Earth Sciences* 7: 716–727.
- Watremez L, Burov E, d'Acremont E, et al. (2013) Buoyancy and localizing properties of continental mantle lithosphere: Insights from thermomechanical models of the eastern Gulf of Aden. *Geochemistry, Geophysics, Geosystems* 14: 2800–2817. <http://dx.doi.org/10.1029/ggge.2019>, ISSN: 15252027.
- Watts AB (1978) An analysis of isostasy in the world's oceans: 1. Hawaiian-Emperor Seamount Chain. *Journal of Geophysical Research* 83: 5,989–6,004.
- Watts AB (1992) The elastic thickness of the lithosphere and the evolution of sedimentary basins. *Basin Research* 4: 169–178.
- Watts AB (2001) *Isostasy and Flexure of the Lithosphere*, p. 458. Cambridge: Cambridge University Press.
- Watts AB and Burov E (2003) Lithospheric strength and its relationship to the elastic and seismogenic layer thickness. *Earth and Planetary Science Letters* 213: 113–131.
- Wei W, Unsworth M, Jones A, et al. (2001) Detection of widespread fluids in the Tibetan crust by magnetotelluric studies. *Science* 292(5517): 716–719. <http://dx.doi.org/10.1126/science.1010580>.
- Weinberg RF and Podladchikov Y (1995) The rise of solid state diapirs. *The Journal of Structural Geology* 17: 1183–1195.
- Weissel J, Anderson RN, and Geller C (1980) Deformation of the Indo-Australian plate. *Nature* 287: 284–291.
- Wever T (1989) The Conrad discontinuity and the top of the reflective lower crust – Do they coincide? *Tectonophysics* 157: 39–58.
- Wilks KR and Carter NL (1990) Rheology of some continental lower crustal rocks. *Tectonophysics* 182: 57–77.
- Willinghofer E and Cloetingh S (2003) The present-day lithospheric strength of the Eastern Alps and its relationship to neotectonics. *Tectonics* 22: 1075. <http://dx.doi.org/10.1029/2002TC001463>.
- Wittlinger G, Tapponnier P, Poupinet G, et al. (1998) Tomographic evidence for localized lithospheric shear along the Altyn Tagh fault. *Science* 282: 74–76.
- Yamato P, Agard P, Burov E, Le Pourhiet L, Jolivet L, and Tiberi C (2007) Burial and exhumation in a subduction wedge: Mutual constraints from thermo-mechanical modelling and natural p-t-t data (sch. Lustres, w. Alps). *Journal of Geophysical Research* 112, B07410.
- Zoback ML (1992) First- and second-order patterns of stress in the lithosphere: The World Stress Map project. *Journal of Geophysical Research* 97: 11,703–11,728.
- Zoback MD, Apel R, Baumgartner J, et al. (1993) Upper-crustal strength inferred from stress measurements to 6 km depth in the KTB borehole. *Nature* 365: 633–635.
- Zoback MD and Townend J (2001) Implication of hydrostatic pore pressures and high crustal strength for the deformation of intraplate lithosphere. *Tectonophysics* 336: 19–30.